



**Universidad de Investigación de Tecnología Experimental Yachay**

**Escuela de Ciencias Químicas e Ingeniería**

**TITULO:**

**Spin-orbit coupling as a strategy to improve the photoactivity of metallic complexes**

Trabajo de integración curricular presentado como requisito para la obtención de título como Química

**Autor:**

Andrea Carolina Chimarro Contreras

**Tutor:**

Thibault Terencio, PhD.

**Co-tutor:**

Juan Pablo Saucedo, PhD.

Urcuqui, August 2023

## AUTORÍA

Yo, **ANDREA CAROLINA CHIMARRO CONTRERAS**, con cédula de identidad 172401555-5, declaro que las ideas, juicios, valoraciones, interpretaciones, consultas bibliográficas, definiciones y conceptualizaciones expuestas en el presente trabajo; así como, los procedimientos y herramientas utilizadas en la investigación, son de absoluta responsabilidad de el/la autora (a) del trabajo de integración curricular, ensayo o artículo científico. Así mismo, me acojo a los reglamentos internos de la Universidad de Investigación de Tecnología Experimental Yachay.

Urcuquí, agosto 2023.



---

Andrea Carolina Chimarro Contreras

CI: 172401555-5

## AUTORIZACIÓN DE PUBLICACIÓN

Yo, **ANDREA CAROLINA CHIMARRO CONTRERAS**, con cédula de identidad 172401555-5, cedo a la Universidad de Tecnología Experimental Yachay, los derechos de publicación de la presente obra, sin que deba haber un reconocimiento económico por este concepto.

Asimismo, autorizo a la Universidad que realice la digitalización y publicación de este trabajo de integración curricular, en el repositorio virtual, de conformidad a lo dispuesto en el Art. 144 de la Ley Orgánica de Educación Superior. En caso que el ensayo o artículo se encuentre aprobado para publicación en bases indexadas, únicamente se publicará el resumen del mismo.

Urcuquí, agosto 2023.



---

Andrea Carolina Chimarro Contreras

CI: 172401555-5

## DEDICATORIA

A mis padres,

a mis abuelos,

a mis hermanas del alma,

por siempre creer en mí y darme fuerzas para luchar por mis sueños.

Andrea Carolina Chimarro Contreras

## AGRADECIMIENTOS

En primer lugar, quisiera agradecer a mis padres, por tenerme tanta paciencia en el proceso de descubrir mi camino profesional, por guiarme y aconsejarme con amor, por enseñarme a ser valiente y por apoyarme siempre; sin su ejemplo y su amor incondicional, no sería la persona que soy hoy. También me gustaría agradecer a mis abuelos, por alegrarme el día con sus videollamadas sin aviso, por estar siempre pendientes de que haya dormido y de que haya comido; su amor me dio fuerzas muchas veces para seguir adelante. Gracias también a toda mi familia, que ha sido un apoyo incondicional y fuente de amor durante todo este tiempo.

Así mismo me gustaría agradecer a las hermanas que me dio la Universidad: Monse, Dianita y Daya. Gracias por ser mi familia, por tanto amor, por tantas cosas vividas. También agradezco a Juan Diego, Alex y a los amigos que hice en este camino. Les agradeceré siempre por hacer de la Universidad la etapa más bonita de mi vida. Gracias también a Paúl por hacerme tan feliz, eres el amor más bonito que he tenido en mi vida.

También quisiera agradecer a mis profesores. En primer lugar, gracias al profe Thibault, por darme a conocer la especialidad más bonita de la Química; gracias por enseñarme tanto, por motivarme a que cumpla mis sueños y por ayudarme tanto a que se hagan realidad. Y gracias infinitas por ayudarme tanto en la aventura de graduarme antes de septiembre. Sin duda todo lo que sé y lo que he logrado ha sido gracias a su ayuda. También quiero agradecer al profe Juan Pablo, por todo lo que me enseñó en la carrera y en la tesis; su ejemplo me motiva a diario a ser una buena profesional. Gracias también a la profe Flor y Sandra y a Mariela, por ayudarme tanto para tener lista la tesis a tiempo. Finalmente, gracias a la profe Lola y a Zaillmar por ayudarme cada vez que parecía que no salía nada bien en la tesis.

Andrea Carolina Chimarro Contreras

## Resumen

El cáncer es una de las mayores causas de muerte en el mundo. Debido a que existen varios tipos de cáncer, actualmente existen también diferentes tipos de tratamientos que son usados dependiendo del tipo y qué tan avanzado está la enfermedad. Uno de estos tipos de tratamiento es la fototerapia. Este tipo de terapia llama bastante la atención debido a que tiene ciertas ventajas en comparación a otros tipos de tratamiento convencionales como la quimioterapia, por ejemplo, tiene mínima invasión y es bastante selectiva. Este tipo de terapia tiene dos tipos: la terapia fotodinámica y la fotoactivación. Esta última consiste en un proceso independiente de oxígeno en el que una droga fotosensible inactiva se activa al ser irradiada con un tipo de luz específica, generando, por ejemplo, especies reactivas que actúan contra los tumores.

El uso en aumento de la fototerapia ha llevado a la búsqueda de nuevas estrategias que mejoren la actividad fotosensible. Una de estas estrategias es el aumento del cruce intersistema aumentando el acoplamiento spin-órbita para mejorar la fotosensibilidad. El aumento del acoplamiento spin-órbita permite transiciones que antes estaban prohibidas, por lo que podría promover que una molécula absorba en el rango de longitud de onda deseado para fotoactivación (620-850 nm) y al mismo tiempo podría incrementar los canales disociativos disponibles, favoreciendo el carácter disociativo de la molécula fotosensible.

El presente trabajo es un estudio teórico y experimental para determinar qué estrategias podrían favorecer el acoplamiento spin-órbita para favorecer la absorción de complejos metálicos en el rango de longitud de onda deseado para fotoactivación (620-850 nm) y para plantear una potencial droga para fotoactivación. En primer lugar, se realizó una búsqueda computacional de un complejo de  $\text{Co}^{3+}$  que absorba luz en el rango de longitud de onda deseado para fotoactivación gracias al efecto de acoplamiento spin-órbita. Este complejo fue sintetizado y caracterizado. Luego, se realizaron varias modificaciones computacionales en este complejo (cambio de metal, substituciones aromáticas y cambio de solventes) para estudiar cómo estas estrategias favorecen el acoplamiento spin-órbita. Finalmente, se añadieron computacionalmente ligantes salientes en el complejo para estudiar una posible droga para fotoactivación.

**Palabras clave:** fotoactivación, acoplamiento spin-órbita, complejo metálico

## Abstract

Cancer is one of the principal causes of death worldwide. Given the fact that there are several types of cancer, nowadays there are different types of treatments that are used depending on the type and on the advance of the disease. One of the cancer treatments is phototherapy. This therapy attracts attention given that it has some advantages over other traditional treatments such as chemotherapy, for instance, it has less invasiveness and is very selective. Phototherapy has 2 types: photodynamic therapy and photoactivation. This last is an oxygen-independent process in which an inactive photosensitizer is activated upon irradiation with a specific type of light, producing for example, reactive species that act against tumors.

The increasing use of phototherapy has augmented the search for new strategies that enhance photosensitivity. One strategy is to increase intersystem crossing by increasing Spin-Orbit Coupling in order to enhance photosensitivity. Spin-Orbit Coupling allows transitions that were forbidden before, so, it could favor the absorption of a molecule in the desired range for photoactivation (620-850 nm) and at the same time it could increase the available dissociative channels, enhancing the dissociative character of the photosensitizer.

This work is a theoretical and experimental study to determine which strategies could favor Spin-Orbit Coupling to favor metallic complexes absorption in the desired range for photoactivation (620-850 nm) and present a potential drug for photoactivation. First of all, a computational search for a  $\text{Co}^{3+}$  complex that absorbs in the desired range for photoactivation due to Spin-Orbit Coupling effects was done. This complex was then synthesized and characterized. Then, several computational modifications were done to this complex (change of metal, aromatic substitutions and solvent change) to study how these strategies could favor Spin-Orbit Coupling. Finally, leaving ligands were added computationally to the complex to study a potential drug for photoactivation.

**Key word:** photoactivation, Spin-Orbit Coupling, metallic complex

## Tabla de contenido

Chapter 1: Introduction.....	1
1.1 Introduction.....	1
1.2 Problem Statement.....	2
1.3 General and Specific Objectives.....	2
1.3.1 General Objective.....	2
1.3.2 Specific Objectives.....	3
Chapter 2: Theoretical Framework.....	4
2.1 Coordination Complexes.....	4
2.2 Electronic Transitions and Electronic Spectra of Coordination Complexes.....	5
2.3 Phototherapy.....	6
2.4 Improving photosensitizer efficiency.....	11
2.5 Spin-Orbit Coupling.....	11
Chapter 3: Methodology.....	16
3.1 General procedure.....	16
3.2 Theoretical approach.....	16
3.3 Experimental approach.....	16
3.3.1 Synthesis.....	16
3.3.2 Characterization.....	16
Chapter 4: Results and Discussion.....	18
4.1 Search for a $\text{Co}^{3+}$ complex with Spin-Orbit Coupling effect.....	18
4.1.1 $\text{Co}^{3+}$ with cyanide ligands.....	18
4.1.2 $\text{Co}^{3+}$ with azide ligands.....	19
4.1.3 $\text{Co}^{3+}$ with diphenylcarbazide.....	22
4.2 Synthesis of a cobalt complex with diphenylcarbazide.....	29
4.2.1 Characterization results.....	29
4.2.2 Elucidation of the complex.....	39
4.3 Strategies to enhance Spin-Orbit Coupling effect in the metallic complexes with diphenylcarbazide.....	45
4.3.1 Study of metallic-diphenylcarbazide complexes.....	45
4.3.2 Study the complex with aromatic ring substitutions.....	51
4.3.3 Study the complex in different solvents.....	53
4.4 Addition of leaving ligands to the $\text{Co}^{3+}$ complex with diphenylcarbazide.....	55
4.5 Discussion.....	59



4.5.1	Obtention of a $\text{Co}^{3+}$ complex with SOC effects .....	59
4.5.2	Strategies to enhance SOC effects in the $\text{Co}^{3+}$ complex with diphenylcarbazide.....	60
4.5.3	Addition of a leaving ligand to the $\text{Co}^{3+}$ complex with diphenylcarbazide 64	
	Chapter 5: Conclusions.....	66
	Chapter 6: Bibliography .....	67

## Chapter 1: Introduction

---

### 1.1 Introduction

Cancer is one of the main causes of death worldwide (1). In these terms, cancer is a disease in which some of the body's cells grow uncontrollably and spread to different parts of the body (2). Cancerous tumors can invade nearby tissues and do metastasis, which is the formation of new tumors in other parts of the body (2). Due to the different types of cancer, there are different treatments proposed depending on its type and on how advanced it is (2). There are several treatments such as chemotherapy (use of drugs to kill cancer cells), hyperthermia (body tissue is heated to help damage and kill cancer cells), immunotherapy (enhancement of the immune system), radiation therapy (use of high doses of radiation to kill cancer cells), etc. Several other treatments have been proposed for this disease, with the objective of alleviating critical side effects caused by conventional treatments such as chemotherapy (1). For instance, phototherapy has attracted attention in the treatment of this disease due to its high spatial-temporal controllability and minimal invasiveness (3). In addition, phototherapy consists of two types: photodynamic therapy and photoactivation therapy.

Photodynamic therapy consists of the use of a drug (photosensitizer) that is activated by light, generating highly reactive species that lead to tumor cell death by causing damage on various cellular components (2,4,5). This therapy has been approved by FDA for the treatment of actinic keratosis, advanced cutaneous T-cell lymphoma, Barrett esophagus, basal cell skin cancer, esophageal cancer, non-small cell lung cancer and squamous cell skin cancer (2). The therapy is a two-step process: first, the patient receives a photosensitizer (by mouth, spread on skin or intravenously) and after 24 to 72 hours the tumor is exposed to the light source (2). One of the most important benefits of this therapy is that the damage is limited to sick cells, given that the photosensitizers tend to build up in abnormal cells, and then, the light is focused directly on them (2). On the other hand, photoactivation therapy is oxygen-independent, and it involves the activation of a prodrug upon irradiation with a specific light. The activation generates cytotoxic species or heat that act against the tumor cells (3). It is important to mention that photoactivation has advantages over photodynamic therapy; the former depends highly on oxygen, so its efficacy is limited in tumors with low levels of oxygen (3,6).

Due to the increased use of phototherapy, the search for new prodrugs has gained importance, as well as the search for strategies to improve photosensitizer's activity. It has been reported previously that intersystem crossing, a non-radiative electronic transition between two states of different multiplicity, can be enhanced, and its enhancement can improve photoactivation activity (7). In these terms, one of the strategies to improve intersystem crossing is the enhancement of Spin-Orbit Coupling, which happens to be important for the photoactivation mechanism of several platinum-based photoactivated drugs (7). Moreover, the enhancement of Spin-Orbit Coupling (SOC) effect could enhance the complex absorption at the specific wavelength of activation (620-850 nm) and favor dissociative character by making more dissociation channels available.

In this work, a cobalt complex with Spin-Orbit Coupling effect will be proposed theoretically and then synthesized and characterized. In addition, several strategies to improve the photoactivation properties of this cobalt complex will be studied, including the use of different solvents, the addition of several functional groups to the ligand's structure and the change of the metal, to determine which strategies are better to improve Spin-Orbit Coupling, and therefore, to improve photoactivation. Finally, a potential cobalt prodrug for photoactivation will be proposed.

## **1.2 Problem Statement**

Phototherapy is nowadays a promising cancer treatment that replaces conventional strategies such as chemotherapy. Several benefits in comparison to other treatments is its high spatial-temporal controllability and minimal invasiveness. Phototherapy can be of two types: photoactivation and photodynamic therapy. The first one has the advantage over the second that its mechanism of action doesn't depend highly on oxygen, so, its application is less limited. For this type of therapy, it is needed an inactive molecule (photosensitizer) that becomes an active agent upon irradiation with a specific light.

As photoactivation is more used, there has been a constant search of new prodrugs, and in this search, metallic complexes have been suggested as potential candidates due to the interesting electronic properties that they show, especially when d-block metals are used. Several metallic complexes have been proposed as potential photosensitizers, principally platinum complexes. As recently suggested, the photosensitizing activity can be enhanced by improving Spin-Orbit Coupling effect. This effect contributes with new transitions that were forbidden before, so, systems that are not expected to have certain transitions will have them thanks to this effect. Therefore, a particularly promising route to improve photoactivation properties is a molecular design including Spin-Orbit Coupling, which could enhance the complex absorption in the specific wavelength of activation (620-850 nm, maximum depth penetration into mammalian tissue) and favor dissociative character by making more dissociation channels available.

Consequently, a theoretical and experimental study is proposed in order to determine which strategies can enhance Spin-Orbit Coupling to favor absorption of a metallic complex in the specific wavelength of activation for phototherapy purposes and introduce a potential cobalt prodrug for photoactivation.

## **1.3 General and Specific Objectives**

### **1.3.1 General Objective**

Determine which strategies can increase Spin-Orbit Coupling in order to favor absorption of a metallic complex in the specific wavelength of activation (620-850 nm) and introduce a potential cobalt prodrug for photoactivation. This wavelength of activation must be taken into account given that this range is the maximum depth penetration into mammalian tissue.

### 1.3.2 Specific Objectives

- Computational search for a  $\text{Co}^{3+}$  complex with SOC effect (Geometry optimization and TD-DFT calculation).
- Synthesis and characterization of a cobalt complex that presents the more useful SOC effect for photoactivation purposes.
- Computational study of strategies that could modify SOC effect using different metals, substituents and solvents (Geometry optimization and TD-DFT calculation).
- Computational study of a potential cobalt prodrug for photoactivation (Geometry optimization and TD-DFT calculation).

## Chapter 2: Theoretical Framework

### 2.1 Coordination Complexes

A coordination complex is a system in which a metal ion is attached to coordinated groups through coordinate bonds (8). These coordinated groups are called ligands and they are neutral molecules or ions that have at least one pair of electrons available to donate to the metal ion. In the coordinate bonds the ligands act as Lewis bases, so they donate a lone pair of electrons to the metal ion, which acts as a Lewis acid. Coordination complexes have a variety of geometries, such as tetrahedral, square plane and octahedral, which are the most common. The main metal ions involved in coordination complexes are transition-metals in their different oxidation states. Transition metals have their d subshell available, so, coordination complexes have a variety of d-shell configurations. The different possible electronic configurations lead to coordination complexes presenting interesting magnetic properties, so they can be diamagnetic (no unpaired electrons) or paramagnetic (one or more unpaired electrons), and that they present color, which is mainly due to d-d transitions that occur in the visible spectrum (9).

To describe the orbitals of coordination complexes, Crystal Field Theory is mainly used (8,9). This theory considers that the 5 metal d orbitals are split into different energy levels due to the presence of point metal charges (lone pair of electrons of the ligands) (9). This split depends on the geometry of the complex, giving different electronic configurations. The difference between the energy levels is called splitting energy, and it is obtained by measuring the energy absorbed when an electron is excited from the lower energy state to a higher energy state (9). The magnitude of the splitting energy depends on the charge of the metal ion, transition series, geometry, and ligand to which metals are bonded to; some ligands favor Low-Spin configurations (bigger split energy, strong field) while others favor High-Spin configurations (lower split energy, weak field). Different electronic configurations are obtained for these 2 cases, as it is observed in Figure 1, which shows an octahedral crystal field diagram for a low (Figure 1.a.) and high spin complex (Figure 1.b.).

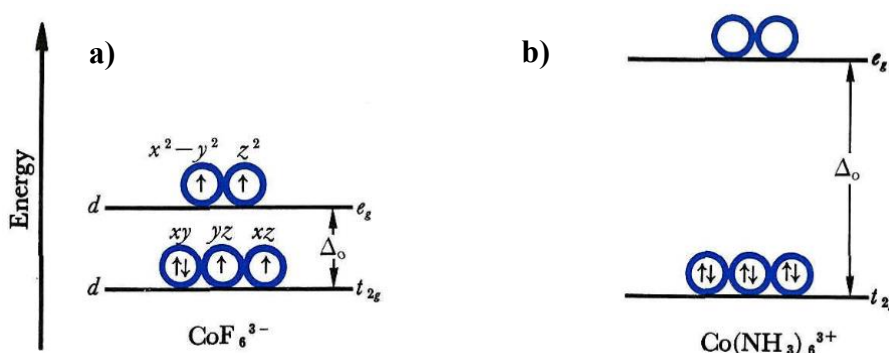


Figure 1

Crystal field diagram for an octahedral complex in a) low-spin configuration and b) high-spin configuration. Taken from (9)

The chemical behavior of metals can be significantly changed by the coordination to the ligands, for example, the coordination of magnesium to chlorin in chlorophyll changes its electronic properties, making chlorophyll able to absorb visible light, which the metal

alone cannot (9). In these terms, transition-metal complexes are very interesting since properties such as spin/oxidation state or electronic/optical properties can be tuned through ligand design and metal selection (10).

## 2.2 Electronic Transitions and Electronic Spectra of Coordination Complexes

A distinctive characteristic of coordination complexes is that they present color. The color that is observed is the complementary to the color absorbed. The energy of electromagnetic radiation that is absorbed by the complex during the excitation of an electron to a higher energy state is described by equation 1 (9).

$$E = h\nu = hc/\lambda \quad \text{(Equation 1)}$$

From equation 1, the wavelength  $\lambda$  of the light absorbed by the coordination complex can be calculated. The transitions responsible of the complexes color can be of different types:

- a. Ligand transitions
- b. Charge transfer transitions
- c. d-d transitions
- d. Counter-ion transitions

If these transitions fall into the visible region, they will be responsible for the color exhibited by complexes. The ligand transitions correspond to  $\pi \rightarrow \pi^*$  or  $n \rightarrow \pi^*$  transitions that occur in the UV region when the ligands of the complex have a  $\pi$ -electron system (11). These bands usually correspond to. The first are observed for molecules that have double or triple bonds without atoms that have non-bonding electrons, and the second are observed for molecules that have a lone pair of electrons and a  $\pi$ -bond (11). In addition, charge transfer absorptions can happen in two ways: ligand to metal charge transfer (LMCT) and metal to ligand charge transfer (MLCT) (11,12). Also, d-d transitions are mainly d-electron excitations from a lower energy state to a higher energy state. Finally, many ions have high intensity absorption bands in the UV region. The different types of transitions have an associated molar extinction coefficient  $\epsilon$ , which is related to the intensity observed in the spectrum. For instance, the charge transfer transitions have a molar extinction coefficient of 1 000 to 55 000  $\text{L}\cdot\text{mol}^{-1}\text{cm}^{-1}$ , ligand transitions have a coefficient on the order of 10 000  $\text{L}\cdot\text{mol}^{-1}\text{cm}^{-1}$  and d-d transitions have a coefficient of 0,5 to 20  $\text{L}\cdot\text{mol}^{-1}\text{cm}^{-1}$ . This difference in intensity is observed in Figure 2.

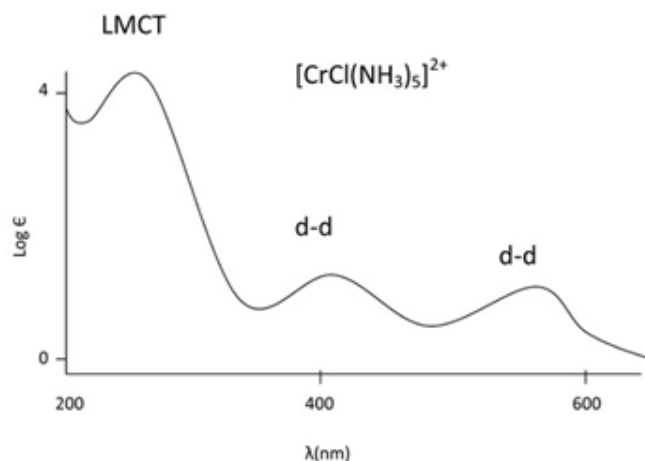


**Figure 2**

UV-Vis spectrum of a coordination complex. Taken from (13)

It is important to mention that the intensity of the absorption bands depends on whether the transition is allowed or forbidden (higher and lower intensity, respectively). The selection rules that govern transitions between electronic energy levels are (11,12,14,15):

- a. Spin selection rule: only transitions between states with the same spin multiplicity are allowed ( $\Delta S = 0$ )
- b. Laporte selection rule: only transitions between states with different symmetry with respect to an inversion center (gerade or ungerade) are allowed.

$d \rightarrow d$  transitions are Laporte forbidden, but they can be observed in a UV-Vis spectrum because of an exception to this rule. Moreover, relaxation of the Laporte and Spin selection rules that allow forbidden transitions to be observed in the UV-Vis spectrum can occur due to (14):

- a. Vibronic coupling: bonds vibrate and this can distort the molecular geometry, thus, can cause temporary loss in symmetry, allowing the Laporte forbidden transitions.
- b. Orbital mixing: hybrid orbitals can allow transitions that would otherwise be forbidden in pure orbitals.
- c. Spin-Orbit Coupling: spin forbidden transitions occur by the shift in the electron's atomic energy levels. The strength of the transitions increases with the size of the Spin-Orbit Coupling (16)

The  $d-d$  transitions of coordination complexes can be determined using the Tanabe-Sugano diagrams. These are the energy plots of various electronic states of every electron configuration of coordination complexes for both high and low spin configuration cases (15). In these diagrams, the ground state is set as reference and the energy of all the other states are plotted with respect to it (15). The transitions expected in the UV-Vis spectrum are those between states with the same multiplicity.

### 2.3 Phototherapy

Phototherapy is the treatment of a disease that involves certain types of light. This kind of therapy offers selectivity, at least for locally confined tumors, that can be achieved by

activating an anticancer agent with light in a particular body area (3,17). It focuses on the different decays pathways that follows photoexcitation, which can be radiative energy release, loss of ligands or transfer of energy to other species, such as triplet oxygen (18). Phototherapy can be of two types: photoactivated and photodynamic therapy (3).

On one hand, photoactivated therapy is oxygen-independent, it involves light-mediated chemical changes of prodrugs, which means that an inactive prodrug is transformed into an active agent upon irradiation (3). The processes in which prodrugs are activated can be (3,18):

- a. Photoreduction: the complex is reduced upon irradiation to release cytotoxic species and ligands.
- b. Photosubstitution: a complex with photolabile ligands undergo ligand dissociation followed by solvent substitution.
- c. Photocleavage of ligand: cleavage of organic bonds occurs after photon absorption by the metal center.
- d. Photoswitching: complexes bridged by a ligand that change their geometry or chemical properties upon irradiation to alter the cytotoxic properties.
- e. Photothermal reaction: conversion of excited state energy to thermal energy (heat), which can destroy the tumor.

An example of metal-based photoactivated drugs are platinum-based drugs (3,17). Since the discovery of cisplatin and its approval to be used as anticancer treatment in 1978, several platinum-based drugs have been proposed. Due to the notable photodecomposition feature of  $Pt^{4+}$  complexes, it was suggested that this metal is a potential photoactivated chemotherapy prodrug (3). In addition, since transition metal azido complexes are light sensitive, azido-platinum complexes have been proposed for photoactivation therapy (3). Therefore, there are photoactive  $Pt^{4+}$  complexes that act by the release of cytotoxic  $Pt^{2+}$  species and radicals upon irradiation (3).  $Pt^{4+}$ -azide complexes are very promising photoactivated drug candidates as they are stable in the absence of light but release cytotoxic products upon irradiation (17). For example, when diazido  $Pt^{4+}$  drugs are irradiated with visible light, they release cytotoxic azidyl radicals and reactive oxygen species, as well as DNA-binding  $Pt^{2+}$  species (3). It is important to remark that photoactive drugs contain axial, non-leaving and leaving ligands: axial ligands are used to tune the physical and chemical properties of the complexes, while the leaving ligands will be the cytotoxic released components of the drug (3). Figure 3 shows several action modes for platinum-based anticancer drugs.



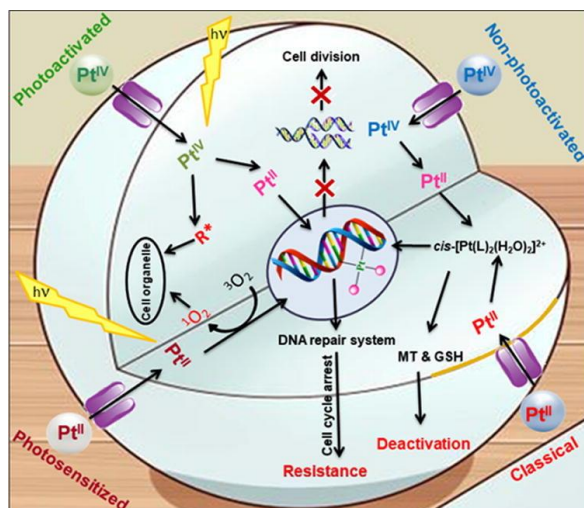


**Figure 3**

Different action modes for platinum-based anticancer drugs. Taken from (19)

In this kind of process, electronic transitions that contribute to the dissociative character of the leaving ligands are fundamental. These electronic transitions can be singlet or triplet. Upon excitation to higher energy levels, internal conversion and intersystem crossing can occur to other states, singlet or triplet (17,20). These states can favor dissociative character as they make many more dissociation channels available, and even if these states are not dissociative, they can act as intermediate doorway states toward dissociation channels (17). Spin-Orbit Coupling favors this process by inducing large energy splitting, which allows ultrafast intersystem crossing shortly after photoexcitation (17).

On the other hand, in photodynamic therapy it is involved a photosensitizer, light and oxygen. In this type of therapy, photosensitizers excited by light produce electronically excited species that can react with  $O_2$  present in the medium and generate highly reactive species (ROS) such as singlet oxygen  $^1O_2$  and superoxide anion  $O_2^{\cdot-}$  (4,5,6). ROS can cause an imbalance of the redox state of tumor cells and lead to cell death by causing damage on various cellular components (4). More precisely, the mode of action of this therapy is as follows: a photosensitizer is irradiated with light of a specific wavelength, it absorbs energy and goes from a ground state  $S_0$  to an excited singlet state  $S_1$ , then, through intersystem crossing, this  $S_1$  state passes to an excited triplet state  $T_1$  that has a longer lifetime, allowing to transfer electrons to different molecules, and then, return to its basal state  $S_0$  (4,6). At this point, there are 2 different pathways (4,6). In Type II Redox Reactions, the oxygen that is in a ground triplet state  $^3O_2$  accepts this energy and forms a singlet oxygen  $^1O_2$ . In Type I Redox Reactions, transfer reactions of hydrogen atoms or electrons with  $O_2$  or with different substrates occur, so, free radicals and other ROS will be formed, for instance, superoxide ions. A scheme of this process is shown in Figure 4. These two processes happen simultaneously, and their proportion depends on the type of photosensitizer as well as the concentration of substrates and oxygen (4). It is important to mention that the radiative transition from  $S_1 \rightarrow S_0$  with the emission of photon is known as fluorescence and from the  $T_1 \rightarrow S_0$  is known as phosphorescence (4).

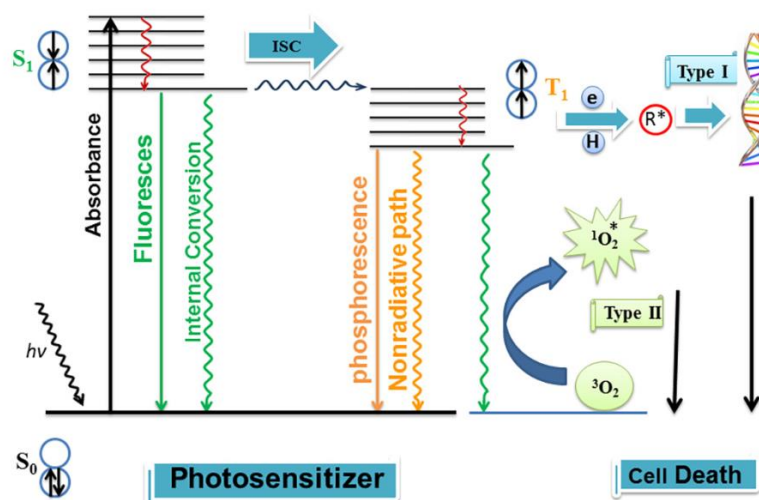


**Figure 4**

Molecular mechanism of photosensitizers. Taken from (19)

Some examples of photosensitizers used for medical purposes are shown next:

- Photofrin<sup>®</sup>: is a mixture of oligomeric hematoporphyrin derivatives used to treat bladder cancer with red light (630 nm).
- Foscan<sup>®</sup>: derivate from chlorin. It has been approved for clinical photodynamic therapy with red light (652 nm) and is used for head and neck and lung cancer.
- Redaporfin: derivate from bacteriochlorin. It can be activated with infrared light (749 nm) and used for head and neck cancer.

These photosensitizers can be classified in protoporphyrin IX precursors, porphyrin derivatives, chlorin derivatives, bacteriochlorin derivatives and phthalocyanine derivatives (4,6). Most of them have in their structure highly electron delocalized systems and they absorb wavelengths between 500 and 700 nm. Some examples of FDA approved anticancer photosensitizers are shown in Figure 5.

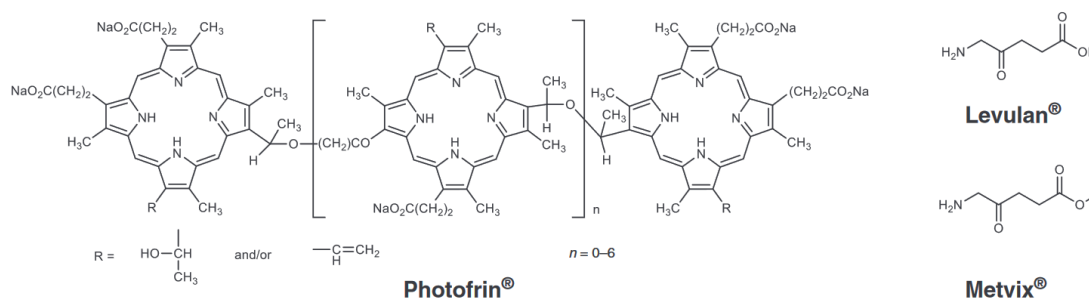


**Figure 5**

Some commercial anticancer photosensitizers. Taken from (6)

Also, metal-based complexes are widely used in photodynamic therapy. These complexes have advantages in the design of photosensitizers due to the fact that they can improve stability, photocytotoxicity and also they allow their quantification and localization by techniques such as ICP-MS (6). Some examples of metal-based photosensitizers under development are shown in Figure 6.

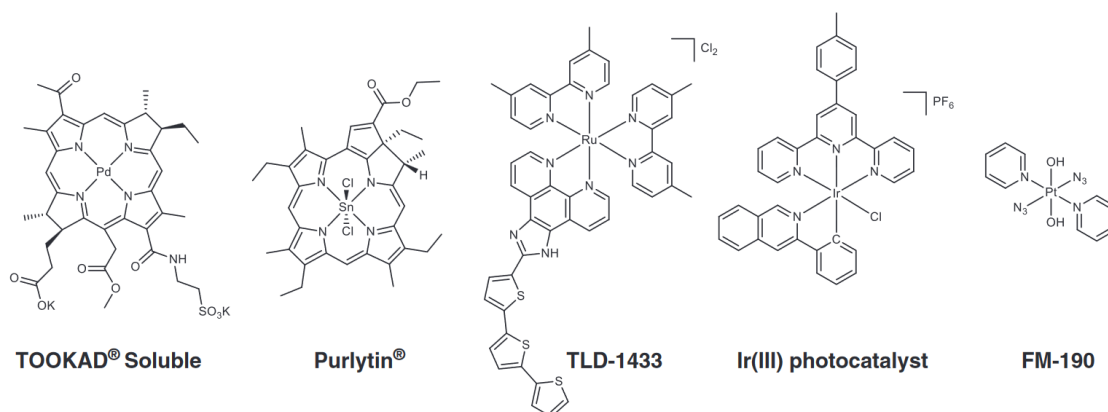


**Figure 6**  
Metal-based photosensitizers. Taken from (6)

An important difference between the two types of phototherapy is that photoactivated agents generally decompose upon irradiation, while photodynamic agents are photostable (20). However, an important problem of photodynamic therapy is that the mechanism of action depends highly on oxygen, which limits the efficacy in tumors with low levels of oxygen. In these cases, photoactivation therapy might be better (6). Nevertheless, it is important to remark that in general, phototherapy has the advantage that the treatment is highly controllable, spatially and temporally with minimal invasiveness (3,6,18).

It is also important to mention that d-block metals complexes are promising prodrug agents for phototherapy. Metals have excited states that are easily accessible by irradiation with visible and UV light. Among metals,  $d^3$  and  $d^6$  electronic configurations are very promising due to the favorable photophysical properties and the relative non-lability of the complexes with this configuration (18). For instance, Cr, Co, Ru, Rh, Re, Os, Ir, Pt and Au have well-documented photochemical activity, and Rh, Pt and Au have also anticancer activity (18,47,48).

When a metal complex is photoexcited, photochemical reactions such as ligand dissociation or redox processes, can happen at any stage during the decay back to the ground state, so, it is important not only the nature of the excited state, but the energy and nature of closely-lying states that determine the population and depopulation of reactive states (18). In these terms, the excited state reactivity of metal complexes can be described by the following transitions (18):

- Metal-centered (d-d) transitions: they usually populate antibonding orbitals, leading to bond lengthening and favoring ligand substitution. These transitions can favor the release of a bioactive molecule for example.
- Charge-transfer transitions: they can lead to redox reactions.
- Ligand-centered transitions

In metallic complexes in which the charge-transfer absorption band is separated from the d-d transitions, selective irradiation can control the type of photoreaction.

Important features of potential metal-based drugs for phototherapy are that they must be aqueous soluble and stable in biological media. Also, they must show low dark

cytotoxicity, tumor-specific accumulation, high photocytotoxicity (large difference between cytotoxicity in the presence and absence of irradiation), low skin photosensitivity and easy administration, combined with long wavelength fluorescence emission, large molar absorption coefficient and photostability (6,7,18). Also, the wavelength of activation should be ideally within 620 and 850 nm, given that this range has the maximum depth penetration into mammalian tissue (6,18).

## 2.4 Improving photosensitizer efficiency

It has been reported previously that the photosensitizing efficiency of photosensitizers can be improved by raising the intersystem crossing from states of different multiplicity (7). This can be achieved by different methods:

- a. Reducing the energy gap between singlet and triplet states: this is achieved by integrating enhanced electron donating-accepting interaction to conjugated chromophores (7).
- b. Improving the Spin-Orbit Coupling process: this is achieved by integrating heavy atoms or carbonyl with n and  $\pi$  orbital to the photosensitizers (7). It is important to mention that the rate constant of intersystem crossing ( $k_{ISC}$ ) is correlated to the Hamiltonian for Spin-Orbit Coupling, which means that the Spin-Orbit Coupling values is of superior influence on the intersystem crossing efficiency (7). Carbonyl groups are known to show high Spin-Orbit Coupling effects due to their hybrid singlet-triplet transition electronic configuration that contains both n and  $\pi$  orbitals (7).
- c. Using photosensitizers with aggregation-induced emission (AIE): these materials have good photostability, high concentration tolerance, low dark toxicity, and high fluorescence quantum yield in aggregate state. Also, they promote energy transfer from singlet to triplet states due to the inhibition of non-radiative transition in the aggregation state (7).

Therefore, a good strategy for improving intersystem crossing is to find a strong electron donating-accepting group that presents large Spin-Orbit Coupling simultaneously.

## 2.5 Spin-Orbit Coupling

At the nonrelativistic level of theory, the nonrelativistic interaction Hamiltonian doesn't have spin-dependent terms, so, transitions between states of different spin multiplicities are strictly forbidden (21). In the relativistic theory, Spin-Coupling Hamiltonians are considered, being the Spin-Orbit Coupling the most important of the spin-dependent terms (21). The most widespread SOC Hamiltonian is an operator that incorporates the screening of the one-electron terms due to the two-electron interactions by an effective charge. This Hamiltonian is shown in equation 2.

$$\hat{\mathcal{H}}_{SO}^{eff} = \frac{e^2 \hbar^2}{2m_e^2 c^2} \sum_i^n \sum_v^N \frac{Z_v^{eff}}{r_{iv}^3} \hat{\ell}_{iv} \hat{S}_i, \quad \text{(Equation 2)}$$

Therefore, Spin-Orbit Coupling is a fully relativistic one-particle theory for spin  $\frac{1}{2}$  systems (20). In general, Spin-Orbit Coupling is a relativistic effect that is observed when

a particle with non-zero spin moves around a region with a finite electric field (22), as seen in Figure 7. The orbital motion of the electron around a positively charged nucleus (based on the Bohr atomic model) is the responsible of the presence of this finite electric field. When the electron's spin interacts with this electric field, Spin-Orbit Coupling causes a shift in the electron's atomic energy levels, therefore affecting the electronic transitions (23). Then, Spin-Orbit Coupling give rise to exotic electronic and magnetic states, principally in transition metals (24). However, the nature of the metal must be discussed, as some metals can be described reasonably accurate with the spin-only model (Heisenberg Model), which assumes that the orbital angular momentum of the d orbitals is quenched by their splitting by the crystal field effect, ruling out any orbital effects. This approximation is enough for 3d systems, but there are some exceptions such as Ni, Cu and Co. Therefore, some metals with small Spin-Orbit Coupling interaction are Li, Al, V, Cr, Mn, Ni and Cu (25). For 4d and 5d, orbital effects are more significant (24). Moreover, electronic and magnetic properties of f-electron systems are heavily influenced by strong Spin-Orbit Coupling (24). It is important to mention that not only metals present Spin-Orbit Coupling, but also high Z-elements such as Pb or Bi.

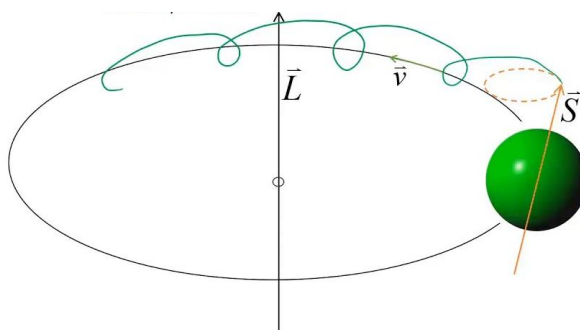


**Figure 7**

Representation for Spin-Orbit Coupling. Taken from (26)

The Spin-Orbit Coupling scales approximately with the fourth power of the nuclear charge  $Z^4$  due to the  $Z/r^3$  dependence of its leading one-electron term, as seen in equation 2 (20, 24). The values of the Spin-Orbit Coupling strength can vary from a few tenths of a milli eV in 2p elements to several eV in 6p elements. However, this doesn't mean that Spin-Orbit Coupling should only be considered when dealing with heavy metals; on the contrary, it is only necessary that two electronic states of different multiplicity are close in energy, and in these cases, a small coupling matrix element is enough to induce an efficient transition between the states (20). An example of this behavior is formaldehyde; as it is a simple small organic molecule, no luminescent properties are expected. However, phosphorescence is observed in this molecule as the result of the transition  ${}^1A_1 \leftarrow {}^3A_2$  ( $n \leftarrow \pi^*$ ) that is forbidden by spin selection rules, but that gains intensity due to the spin-orbit interaction of the  ${}^3A_2$  state with singlet states (27). This behavior is rarely observed in electronic ground-state reactions, but it is more present in processes involving electronically excited states. Also, Spin-Orbit Coupling in organic molecules are crucial for determining mechanisms of chemical reactions that occur via triplet states. Molecules that often present Spin-Orbit Coupling interaction are many-atomic conjugated molecules and the responsible are the singlet-triplet pairs  $\pi\pi^*$  and  $\sigma\pi^*$ ,  $\pi\pi^*$  and  $n\pi^*$  or  $\sigma\pi^*$  and  $\sigma\sigma^*$  (28). Also, the presence of sulfur and nitrogen can provide  $n\pi^*$  transition character for efficient Spin-Orbit Coupling (39).

An important process that occurs due to Spin-Orbit Coupling effects is intersystem crossing. When a molecule is photo-excited, there are two possible processes: radiative and nonradiative deactivation processes. Within the nonradiative processes there can be mentioned the internal conversion and the intersystem crossing. Figure 8 shows a representation of these processes by the Jablonski diagram.

- Internal conversion (IC): is the nonradiative transition between two states of equal spin multiplicity (20).
- Intersystem crossing (ISC): is the nonradiative transition between two states of different multiplicity (20). This process is forbidden in non-relativistic quantum theory.

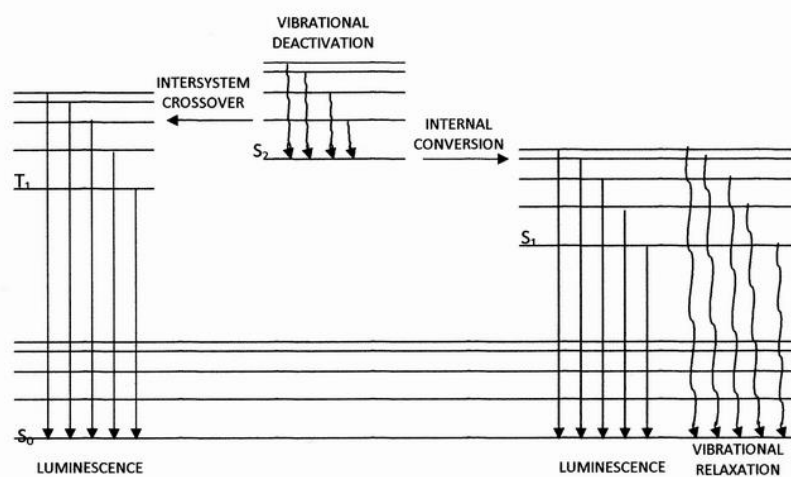


**Figure 8**  
Jablonski diagram. Taken from (29)

Intersystem crossing is an example of spin-forbidden transitions, as they occur between electronic states that have different spin multiplicities. The intersystem crossing between singlets and triplets arises from spin-orbit interaction and it is the main contributor to the creation of spin polarization (30,31). In this process, a singlet excited electronic state makes a transition to a triplet excited state at the point where the potential energy curves for the singlet and triplet excited state intersect; this transition is forbidden in the absence of Spin-Orbit Coupling (32). Typically, a vibrational level of an excited singlet state is spin-orbit coupled to the dense manifold of vibrational levels of a lower-lying triplet state, or a triplet vibrational level is coupled to the dense manifold of vibrational levels of a lower-lying singlet state (usually the ground state) (31). Spin-mixed states can gain access to spin-forbidden states, so that for example, it is possible to transfer spontaneous fluorescence intensity from a short wavelength  $S_1 \rightarrow S_0$  transition to the longer wavelength of a  $S_1 \sim T_n \rightarrow T_1$  transition (31). The triplet state can reach its lowest vibrational state by collisions with other molecules; the transition from this state to the singlet state is forbidden in the absence of Spin-Orbit Coupling and results in the slow emission of phosphorescence (32). Metal complexes generally emit from triplet states, so, phosphorescence dominates (18). Due to the efficient intersystem crossing promoted by the metal ion, the lifetime of these triplets can be between 50 ns and 1  $\mu$ s, and their emission quantum yield is relatively high (18).

It is important to mention that there are some strategies that can modulate intersystem crossing:

a. Heavy-atom effect

The presence of an atom of high atomic number, which can be part of or external to the excited molecular entity, can enhance the rate of a spin-forbidden process. This is due to the linear dependence of the one-electron SOC Hamiltonian on the effective nuclear charge and its inverse cubic dependence on the orbital radius, as seen in equation 2. So, Spin-Orbit Coupling constants of the atoms increase strongly when they move from left to right or from top to bottom in the periodic table (21). Two types are possible:

i. Internal heavy-atom effect

It means the replacement of a constituent element by a heavier homologue. For example, halogenation is known to enhance radiative and non-radiative singlet-triplet transitions. However, indirect effects such as energy shifts or changes in the composition of the wavefunctions must also be considered, so, heavier atoms do not always present higher SOC constants (21).

ii. External heavy-atom effect

It means an enhancement of singlet-triplet transitions if a system is embedded in a matrix, for example, in alkyl halide matrices or solutions, the effectiveness of the perturbation increases in the order  $\text{Cl} < \text{Br} \ll \text{I}$  (21).

b. Environment effects

Two types are possible:

i. Solvent polarity and reorganization

Solvatochromic response of the solute can tune the wavelength of absorption and emission spectra, and it can have a large impact on the rates or mechanisms of nonradiative transitions (21). This phenomenon depends strongly on the magnitude and the orientation of the solute's static dipole moments in the ground and excited states (21). Therefore, the solvent-solute interaction can stabilize a state over the other, for instance, solvent reorganization can stabilize the charge distribution in the excited state, destabilizing the ground state (21). The favorable or non-favorable interaction in polar solvents can cause bathochromic or hypsochromic shifts respectively (21).

ii. Hydrogen bonding

Hydrogen bonding between a specific state and the solvent can favor some transitions over others. For instance, in a polar protic environment, flavin molecules in the singlet state 1 no longer have access to the triplet state 2, which mediates a fast ISC passage to the triplet 1 in nonpolar environments (21).

However, it is important to mention that even if the factors that control the probability of intersystem crossing are known, the modulation will not be easy, since side effects on the electronic structure and the energetics of the excited states can be observed.



## Chapter 3: Methodology

---

### 3.1 General procedure

- i. Three  $\text{Co}^{3+}$  complexes were studied computationally to select one in which SOC effects favor a transition in the specific wavelength of activation (620-850 nm)
- ii. The selected cobalt complex was synthesized and characterized.
- iii. Three strategies were studied computationally to determine if they can increase the SOC effects in the  $\text{Co}^{3+}$  complex: change of the metal, substitutions of the aromatic ring and change of solvent.
- iv. Leaving ligands were added to the  $\text{Co}^{3+}$  complex and it was studied computationally to determine if it could be a potential prodrug for photoactivation.

### 3.2 Theoretical approach

The complexes were studied computationally by the following procedure:

- i. An initial structure was outlined in Avogadro software.
- ii. The structure was optimized using the orca program with the following parameters: B3LYP, def2-SVP and D3BJ
- iii. The optimized structure with the lowest energy was selected. If other structures are less than 15 kJ/mol different from the lowest energy structure, they were selected.
- iv. The excited states of the optimized structure(s) were calculated using TD-DFT with the following parameters: CAM-B3LYP, def2-TZVP, D3BJ and CPCM with the respective solvent.
- v. The excited states with SOC contributions of the optimized structure/s were calculated using TD-DFT with the following parameters: CAM-B3LYP, def2-TZVP, D3BJ and CPCM with the respective solvent.
- vi. The calculated UV-Vis spectra with and without SOC effects were plotted.

### 3.3 Experimental approach

The complex selected was synthesized experimentally and characterized by different techniques. The one selected was a complex of cobalt with diphenylcarbazide.

#### 3.3.1 Synthesis

0.2482 g (1.024 mmol) of diphenylcarbazide was first dissolved in 10 mL methanol at 20 °C and a pale rose solution was obtained. On the other hand, 0.2390 g (1.004 mmol) of  $\text{CoCl}_2 \cdot 6\text{H}_2\text{O}$  was dissolved in 10 mL methanol at 70 °C and a blue solution was obtained. Then, the solution of diphenylcarbazide was slowly added to the metal solution and the solution was held stirring under reflux at 80 °C for 4 hours. During the reaction was observed a notable change in color, from pale rose (diphenylcarbazide alone) to dark violet at the end of the reaction. After 4 hours of reaction the mixture was let to cool. The mixture was vacuum filtered and the solvent was let to evaporate for 24 hours. The remaining solid (0.3679 g) was then recovered.

#### 3.3.2 Characterization

- i. The melting point of the reagents and the complex were measured.

- ii. The reagents and the complex were characterized using FT-IR between 400 and 4000  $\text{cm}^{-1}$ . The vibrations were assigned using infrared correlation tables (44).
- iii. The reagents and the complex dissolved in ethanol were characterized using UV-Vis between 200 and 1000 nm.
- iv. The reagents and the complex were studied in the paramagnetic balance. The magnetic susceptibility calculation was done using the Pascal's Constants for Diamagnetic Corrections (45).
- v. The complex was studied by atomic absorption in order to determine its stoichiometry: a 10 ppm standard using  $\text{CoCl}_2 \cdot 6\text{H}_2\text{O}$  dissolved in water was used to plot a 5-point calibration curve to determine the mass of cobalt in the sample. It is important to mention that 4 measurements of the sample were taken.
- vi. A study on conductivity of the complex dissolved in ethanol was carried.
- vii. The solid complex was characterized using UV-Vis between 200 and 800 nm.

## Chapter 4: Results and Discussion

---

### 4.1 Search for a $\text{Co}^{3+}$ complex with Spin-Orbit Coupling effect

$\text{Co}^{2+}$  and  $\text{Co}^{3+}$  have well-documented photochemical activity and they are expected to have SOC effect (18). Due to the high availability of this metal in the laboratory, cobalt was proposed as a starting point. It is important to mention that  $\text{Co}^{2+}$  is a  $d^7$  species, whereas  $\text{Co}^{3+}$  is a  $d^6$  species, so,  $\text{Co}^{3+}$  was chosen given the fact that singlet-to-triplet transitions are possible to study (no singlet configuration is possible for  $\text{Co}^{2+}$ ). In addition, it is reported that  $d^6$  electronic configurations are very promising complexes for photoactivation purposes due to their favorable photophysical properties and the relative non-lability.

#### 4.1.1 $\text{Co}^{3+}$ with cyanide ligands

The cyanide ligand is used to improve the SOC effects in organic molecules (7); therefore, it is expected that a complex of  $\text{Co}^{3+}$  with cyanide ligands presents SOC effect. Consequently, the study of this complex is used to determine if the behavior of SOC effects in organic and inorganic systems is similar.

The complex  $[\text{Co}(\text{CN})_6]^{3-}$  was simulated and one optimized structure was obtained considering the singlet multiplicity as the ground state. In the structure, cobalt has an oxidation state of +3 and each ligand has a charge of -1. The metal is complexed to the ligands by the carbon, and the complex has an octahedral geometry. With the optimized structure, the corresponding UV-Vis spectra was calculated, as well as the SOC spectrum. The optimized structures, as well as their corresponding spectra are shown in Figures (9-10).

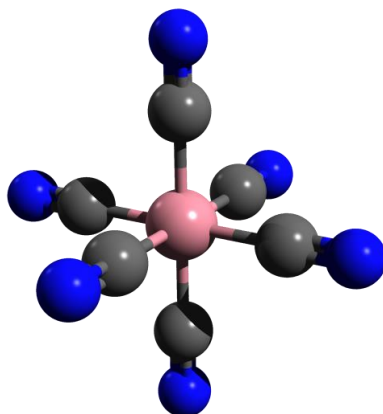


**Figure 9**  
Optimized structure of  $[\text{Co}(\text{CN})_6]^{3-}$

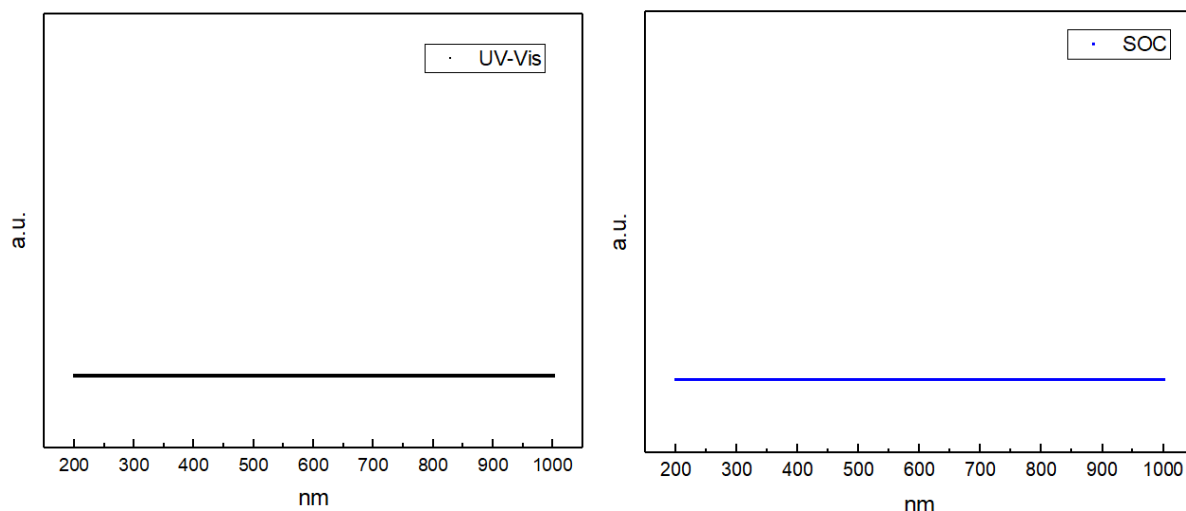


**Figure 10**  
UV-Vis and SOC spectra of  $[\text{Co}(\text{CN})_6]^{3-}$

The complex has Co(III), which is a  $d^6$  species, so, d-d transitions are expected. However, no transitions are observed in the UV-Vis spectrum nor in the UV-Vis spectrum considering the SOC contributions. Therefore, contrary to what was expected, no SOC effect was observed after the complexation of cyanide ligands to the metal.

#### 4.1.2 $\text{Co}^{3+}$ with azide ligands

Several azide platinum complexes are potential photoactivated drugs, an example is the complex  $\text{trans,trans,trans-}[\text{Pt}(\text{N}_3)_2(\text{OH})_2(\text{Py})(\text{MA})]$ . This complex is a potential photoactive drug due to its capacity to release azide ligands under irradiation and it has known SOC effects that contribute to its photoactivation properties (3, 33). Consequently, the same ligands of a known azido platinum complex were used to simulate an azido cobalt complex. The study of this complex is useful to understand the ligand contribution to the SOC effects.

The complex  $[\text{Co}(\text{N}_3)_2(\text{OH})_2(\text{Py})(\text{MA})]^-$  was simulated and one optimized structure was obtained, considering the singlet multiplicity as the ground state. In the complex, cobalt has an oxidation state of +3, the azide ligand has a charge -1 as well as the hydroxyl groups; the pyridine and the methylamine don't have charge. The complex has an octahedral geometry. For the optimized structure, the corresponding UV-Vis spectrum was calculated, as well as the UV-Vis spectrum considering the Spin-Orbit Coupling contributions. The optimized structure, as well as their corresponding spectra, are shown in Figures (11-12). Also, the bands of the spectra (between 300 and 850 nm) will be described in detail and the orbitals involved in these transitions will be shown as well (Tables 1-3).

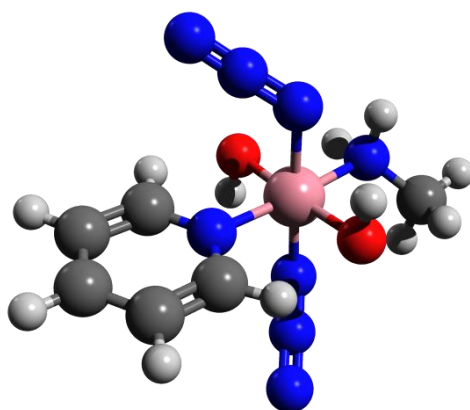


**Figure 11**  
Optimized structure of  $[\text{Co}(\text{N}_3)_2(\text{OH})_2(\text{Py})(\text{MA})]^-$

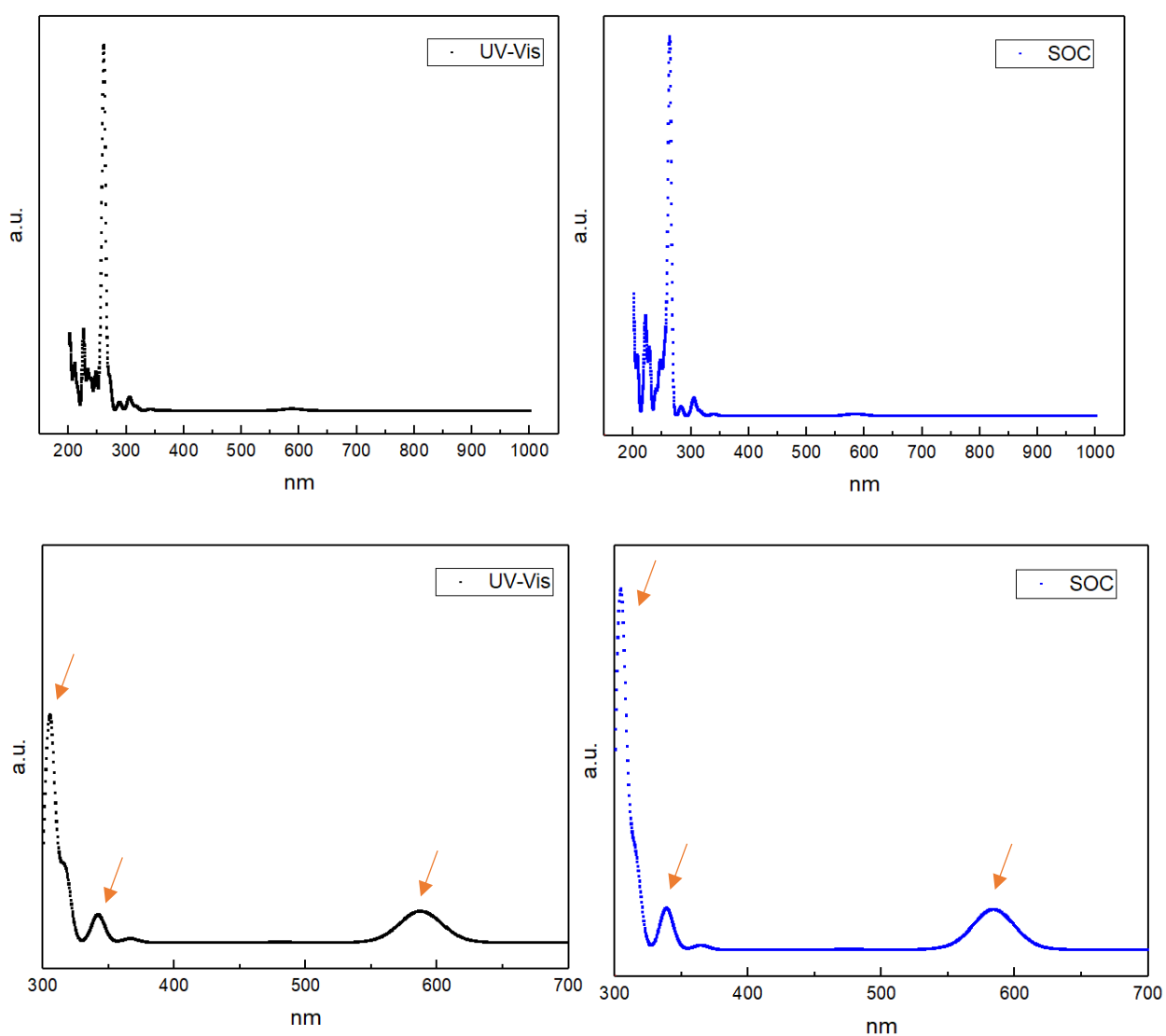


**Figure 12**  
UV-Vis and SOC spectra of  $[\text{Co}(\text{N}_3)_2(\text{OH})_2(\text{Py})(\text{MA})]^-$

There are 3 peaks in the UV-Vis spectrum (Figure 12) at 305, 341 and 588 nm. The fact that there are 3 peaks (maybe another one more at lower wavelengths) suggests that  $\text{Co}^{3+}$  ( $d^6$  species) favors low spin (4 transition expected).

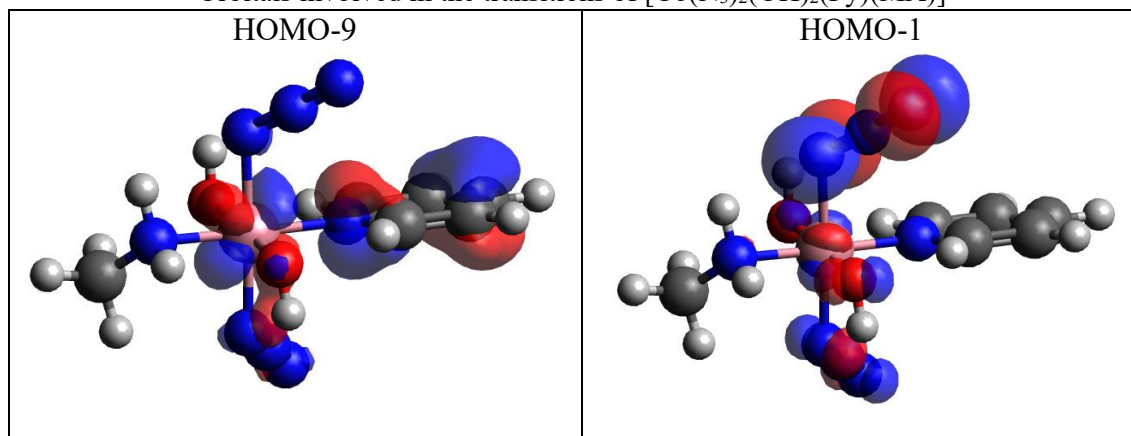
**Table 1**  
Description of the UV-Vis spectrum transitions of  $[\text{Co}(\text{N}_3)_2(\text{OH})_2(\text{Py})(\text{MA})]^-$

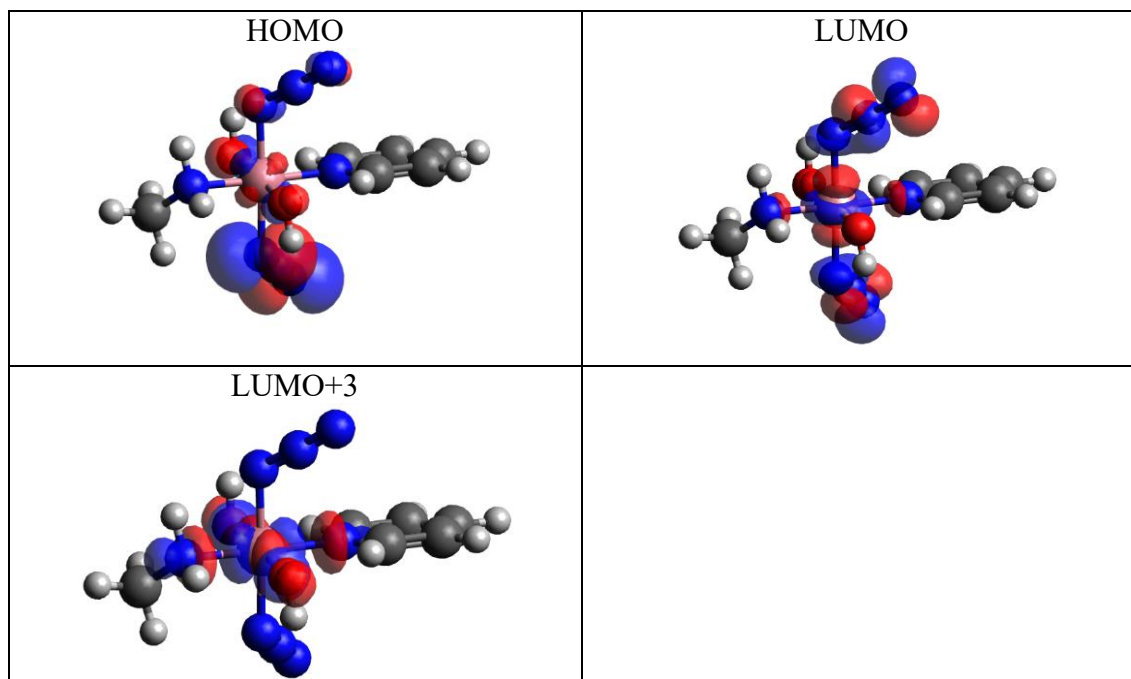
State	Energy (eV)	Wavelength (nm)	Major Contributions	Oscillator Strength
8	4.066	304.9	HOMO $\rightarrow$ LUMO (26.88%) HOMO-9 $\rightarrow$ LUMO (17.40%) [d-d]	0.00788
6	3.629	341.6	HOMO-9 $\rightarrow$ LUMO+3 (29.22%) HOMO $\rightarrow$ LUMO+3 (20.53%) [d-d]	0.00097
2	2.121	584.4	HOMO-9 $\rightarrow$ LUMO (23.27%) HOMO-1 $\rightarrow$ LUMO (16.02%) [d-d]	0.00071

**Table 2**  
Description of the SOC spectrum transitions of  $[\text{Co}(\text{N}_3)_2(\text{OH})_2(\text{Py})(\text{MA})]^-$

State	Energy (eV)	Wavelength (nm)	Major Contributions	Oscillator Strength
38	4.077	304.1	$S_8 (M_s:0)$ 99.90%	0.01226
30	3.665	338.3	$S_6 (M_s:0)$ 99.38%	0.00136
17	2.130	582	$S_2 (M_s:0)$ 99.23%	0.00101
State	Major Contributions			
$S_2$	HOMO-9 $\rightarrow$ LUMO (23.27%) HOMO-1 $\rightarrow$ LUMO (12.97%)			
$S_6$	HOMO-9 $\rightarrow$ LUMO+3 (29.26%) HOMO $\rightarrow$ LUMO+3 (20.44%)			
$S_8$	HOMO $\rightarrow$ LUMO (27.14%) HOMO-9 $\rightarrow$ LUMO (16.92%)			

**Table 3**  
Orbitals involved in the transitions of  $[\text{Co}(\text{N}_3)_2(\text{OH})_2(\text{Py})(\text{MA})]^-$





The peaks at 304, 338 and 582 nm in the SOC spectrum are mainly the peaks at 304, 341 and 584 nm in the UV-Vis spectrum, since the same transitions contribute in a similar percentage to these peaks. These peaks appear more intense; however, the increase is not too significant. Finally, there are no additional peaks observed in the SOC spectrum.

#### 4.1.3 $\text{Co}^{3+}$ with diphenylcarbazide

Diphenylcarbazide is an organic molecule that presents high electronic delocalization due to its two aromatic rings. In addition, it presents carbonyl and amine functional groups in its structure. Moreover, it is well known for forming metallic complexes with metals such as Chromium. Due to the high availability of this reagent in the laboratory, it was chosen as a ligand for a cobalt complex.

The complex  $[\text{Co}(\text{DPC})_2]^-$  was simulated and two optimized structures were obtained considering the singlet multiplicity as the ground state. In the structures, cobalt has an oxidation state of +3 and each diphenylcarbazide has a charge of -2. In both complexes, the ligands are bonded to the metal by the nitrogen and the oxygen. The first structure has a square plane geometry and it is more stable in energy than the second structure by 2.82 kJ/mol. The second structure has a square plane geometry and the ligands are arranged around the metal forming a cave-like structure. With the optimized structures, the corresponding UV-Vis spectra of each was calculated, as well as the UV-Vis considering the Spin-Orbit Coupling contributions. The optimized structures as well as their corresponding spectra are shown in Figures (13-16). Also, the transitions of the spectra (between 300 and 850 nm) will be described in detail and the orbitals involved in these transitions will be shown as well (Tables 4-9).

### 4.1.3.1 Configuration 1

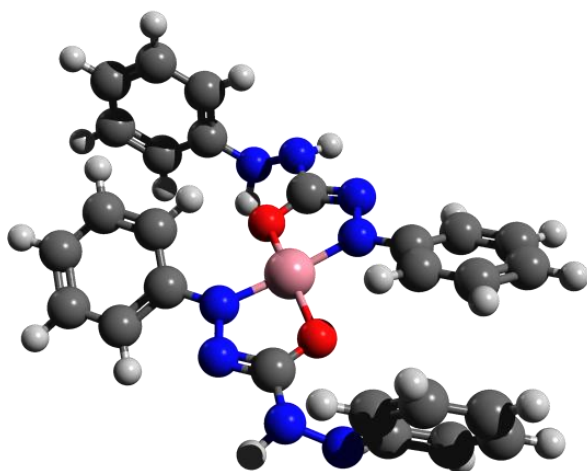


**Figure 13**  
Optimized structure of  $[\text{Co}(\text{DPC})_2]$ , configuration 1

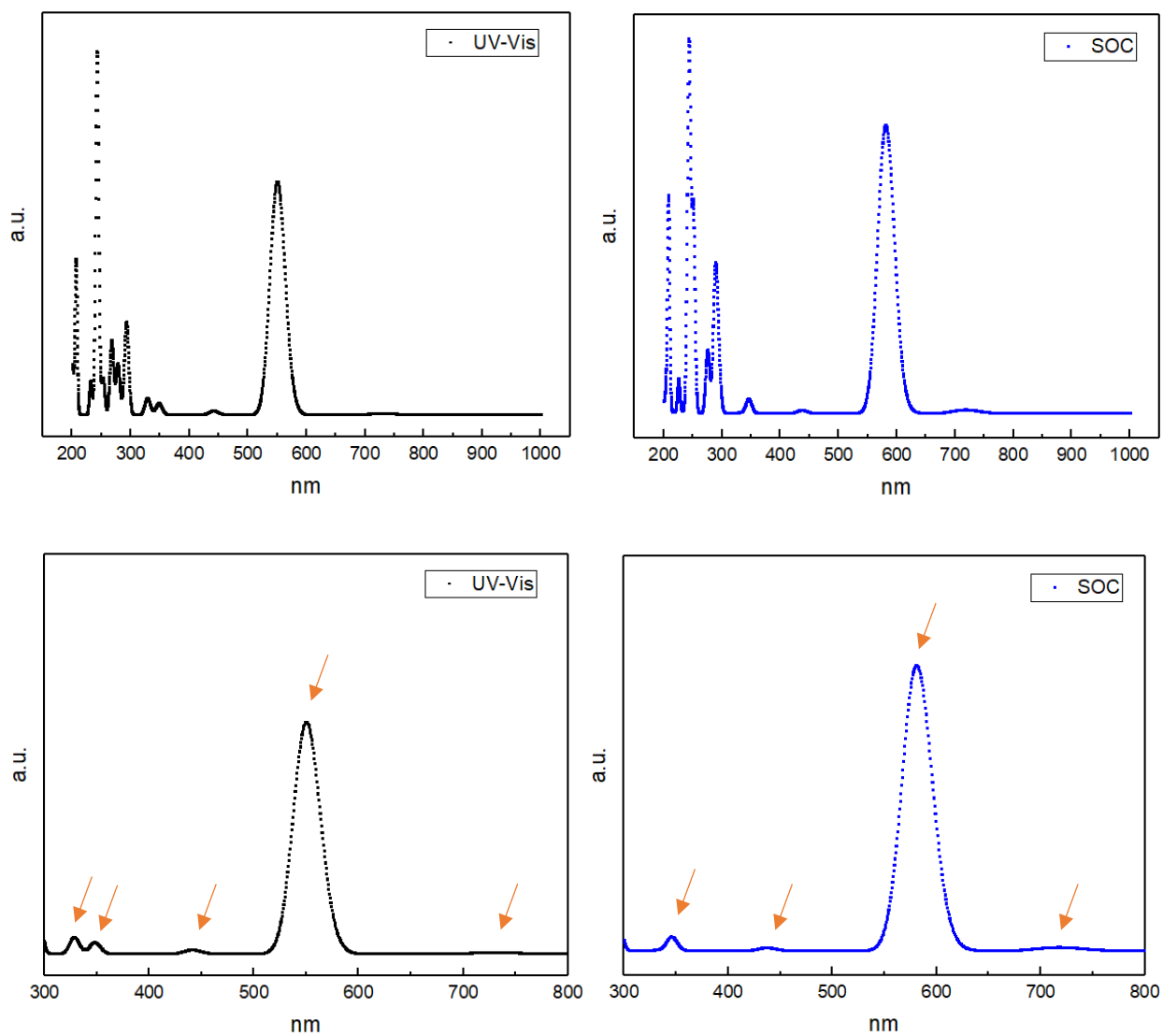


**Figure 14**  
UV-Vis and SOC spectra of  $[\text{Co}(\text{DPC})_2]$ , configuration 1



Four peaks are observed in the UV-Vis spectra (Figure 2) at 328, 347, 439 and 550 nm, respectively. However, the peak at 550 nm is the most intense, so, it suggests that in this case  $\text{Co}^{3+}$  ( $d^6$  species) favors high spin (only 1 transition expected).

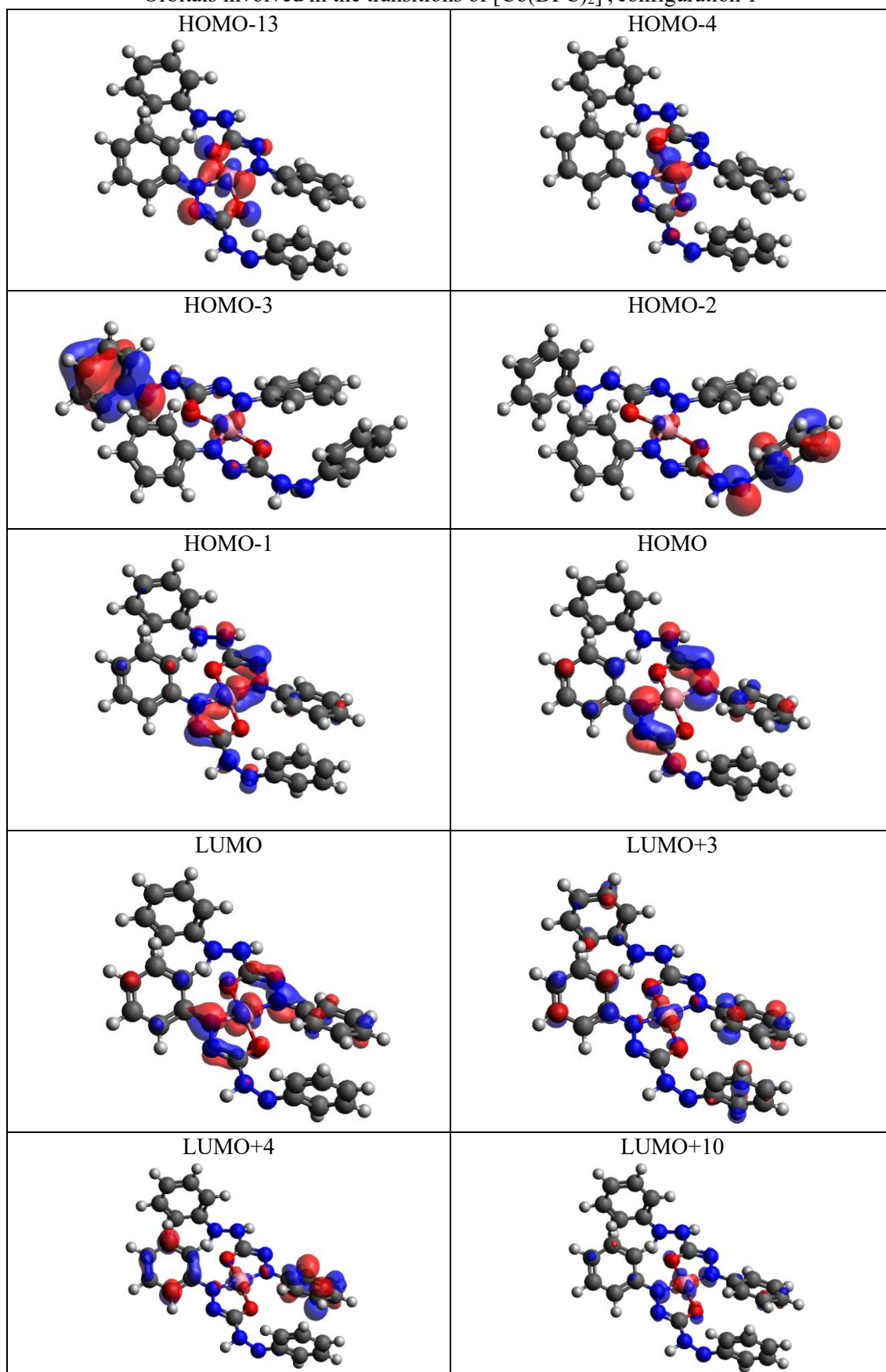
**Table 4**  
Description of the UV-Vis spectrum transitions of  $[\text{Co}(\text{DPC})_2]$ , configuration 1

State	Energy (eV)	Wavelength (nm)	Major Contributions	Oscillator Strength
12	3.776	328.3	HOMO-2 $\rightarrow$ LUMO (68.80%) HOMO-3 $\rightarrow$ LUMO (24.82%) [Ligand to metal]	0.03360
9	3.562	348.0	HOMO-1 $\rightarrow$ LUMO+3 (23.90%) HOMO-1 $\rightarrow$ LUMO+10 (14.74 %) HOMO-1 $\rightarrow$ LUMO+4 (14.64%) [Metal to ligands or d-d]	0.02356
6	2.811	441.0	HOMO-13 $\rightarrow$ LUMO (37.51%) HOMO-4 $\rightarrow$ LUMO+3 (13.42%) [d-d]	0.00839
4	2.254	549.9	HOMO $\rightarrow$ LUMO (89.62%) [Ligand to metal]	0.48157
3	1.700	729.3	HOMO-13 $\rightarrow$ LUMO (38.42%) HOMO-4 $\rightarrow$ LUMO+3 (10.94%) [d-d]	0.00298

**Table 5**  
Description of the SOC spectra transitions of  $[\text{Co}(\text{DPC})_2]$ , configuration 1

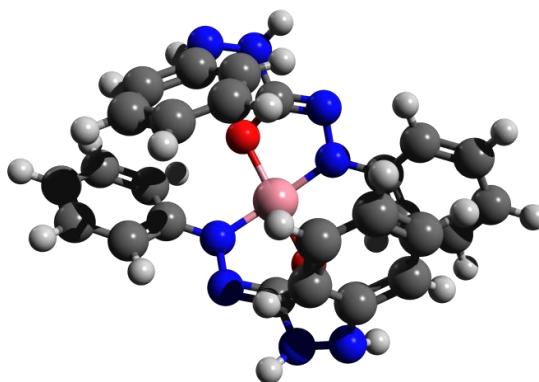
State	Energy (eV)	Wavelength (nm)	Major Contributions	Oscillator Strength
39	3.587	345.6	$S_9 (M_s:0)$ 99.77%	0.02548
33	2.843	436.1	$S_6 (M_s:0)$ 88.45%	0.00506
28	2.135	580.7	$S_4 (M_s:0)$ 99.84%	0.53339
24	1.727	717.6	$S_3 (M_s:0)$ 98.54%	0.00660
State	Major Contributions			
$S_3$	HOMO-13 $\rightarrow$ LUMO (38.98%)			
$S_4$	HOMO $\rightarrow$ LUMO			
$S_6$	HOMO-13 $\rightarrow$ LUMO (38.50 %) HOMO-4 $\rightarrow$ LUMO+3 (12.29%)			
$S_9$	HOMO-1 $\rightarrow$ LUMO+3 (28.70%) HOMO-1 $\rightarrow$ LUMO+4 (18.86 %) HOMO-1 $\rightarrow$ LUMO+10 (14.95%)			

**Table 6**  
Orbitals involved in the transitions of  $[\text{Co}(\text{DPC})_2]^-$ , configuration 1

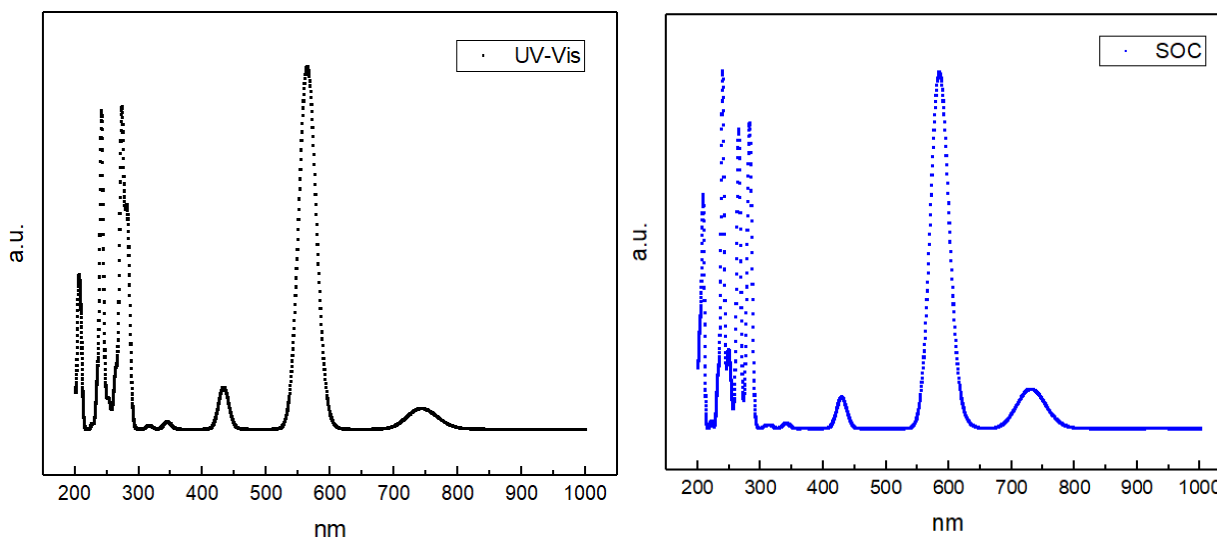


The peaks at 345, 436, 580 and 717 nm in the SOC spectrum are mainly the peaks at 348, 441, 549 and 729 nm in the UV-Vis spectrum, since the same transitions contribute to these peaks, but in a higher percentage. On the other hand, the peak at 328 nm in the UV-Vis spectra probably suffered a shift to lower wavelengths or decreased a lot its intensity and that is the reason why it doesn't appear in the SOC spectrum. Finally, the broad peak that appears at 717 nm in the SOC spectrum is mainly a singlet-singlet transition. However, due to the fact that this peak appears in the SOC spectrum with higher intensity than in the UV-Vis spectrum, and that the percentage of the transition is not 100%, the increase in the intensity is due to SOC effects.

#### 4.1.3.2 Configuration 2



**Figure 15**  
Optimized structure of  $[\text{Co}(\text{DPC})_2]$ , configuration 2



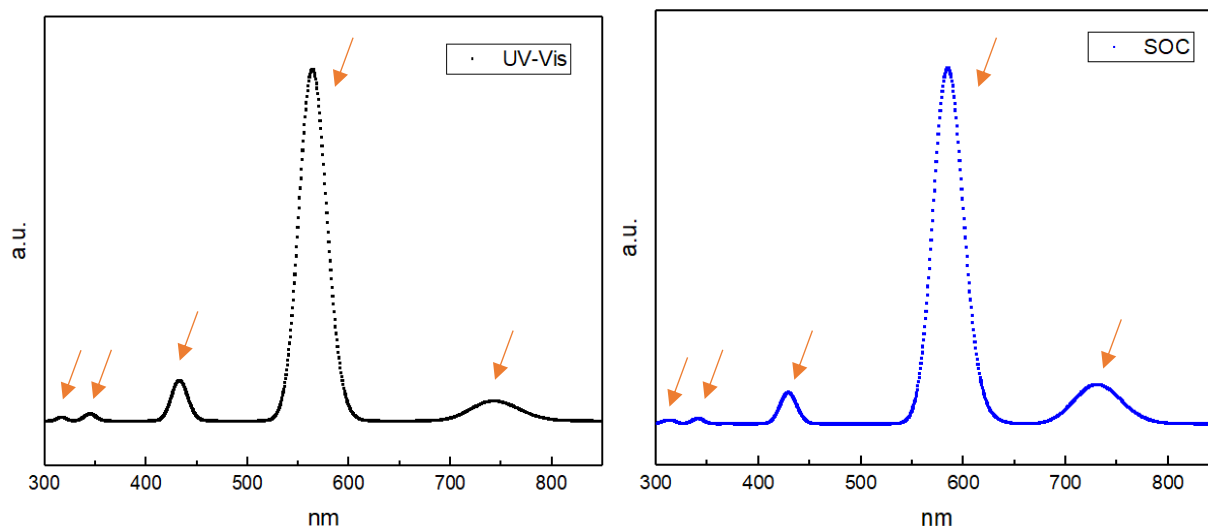


**Figure 16**  
UV-Vis and SOC spectra of  $[\text{Co}(\text{DPC})_2]^-$ , configuration 2

There are five peaks observed in the UV-Vis spectra (Figure 4) at 316, 346, 432, 563 and 740 nm. The presence of 4 peaks indicates that in this case  $\text{Co}^{3+}$  ( $d^6$  species) favors low spin (4 transitions expected).

**Table 7**  
Description of the UV-Vis spectrum transitions of  $[\text{Co}(\text{DPC})_2]^-$ , configuration 2

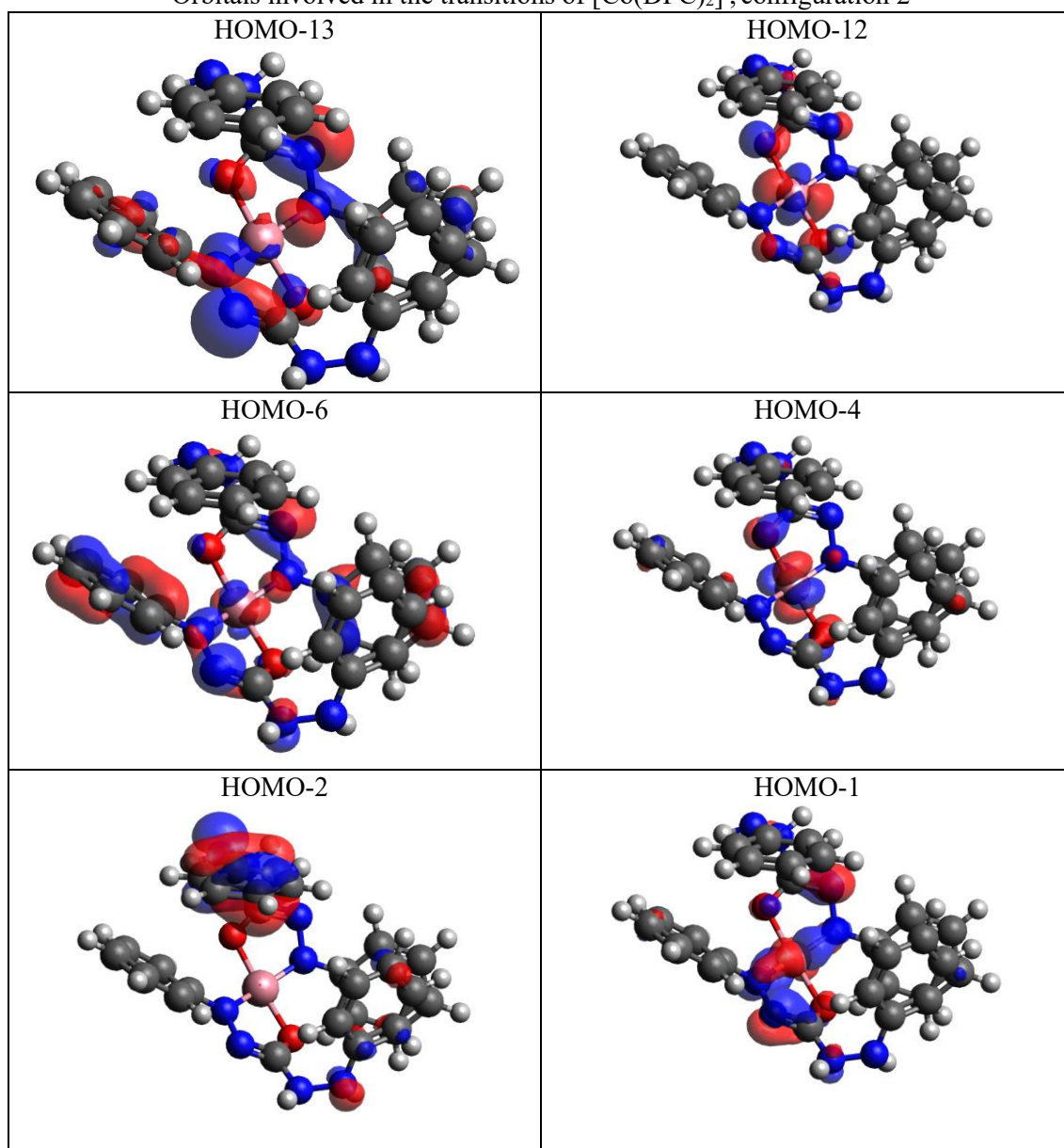
State	Energy (eV)	Wavelength (nm)	Major Contributions	Oscillator Strength
11	3.920	316.2	HOMO-1 $\rightarrow$ LUMO (33.01%) HOMO-13 $\rightarrow$ LUMO (20.74%) [d-d]	0.00400
8	3.594	344.9	HOMO-1 $\rightarrow$ LUMO (30.11%) HOMO-6 $\rightarrow$ LUMO (15.70%) HOMO $\rightarrow$ LUMO+5 (15.32%) [d-d]	0.00376
6	2.867	432.4	HOMO-12 $\rightarrow$ LUMO (33.49%) HOMO-4 $\rightarrow$ LUMO+8 (15.41%) [d-d]	0.04179
4	2.200	563.5	HOMO $\rightarrow$ LUMO (80.15%) [Ligand to metal]	0.36144
3	1.669	742.7	HOMO-12 $\rightarrow$ LUMO (42.11%) [d-d]	0.02056

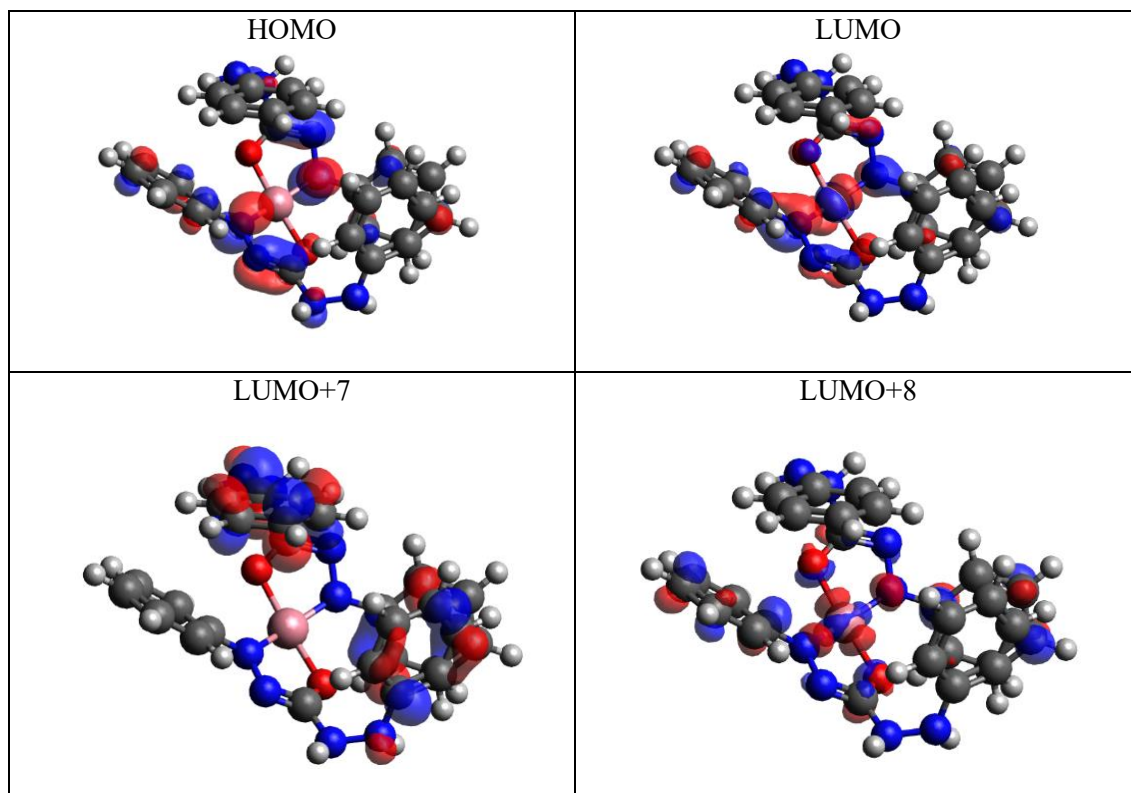
**Table 8**  
Description of the UV-Vis spectrum transitions of  $[\text{Co}(\text{DPC})_2]^-$ , configuration 2

State	Energy (eV)	Wavelength (nm)	Major Contributions	Oscillator Strength
50	3.929	315.5	$S_{11} (M_s:0)$ 48.62% $T_{14} (M_s:0)$ 35.25%	0.00184
41	3.625	341.9	$S_8 (M_s:0)$ 98.23%	0.00481
30	2.890	429.0	$S_6 (M_s:0)$ 89.22%	0.03300
28	2.122	584.2	$S_4 (M_s:0)$ 98.89%	0.39650

24	1.698	729.9	$S_3 (M_s:0)$ 98.62%	0.04420
State	Major Contributions			
$S_3$	HOMO-12 $\rightarrow$ LUMO (40.79%) HOMO $\rightarrow$ LUMO (14.37%)			
$S_4$	HOMO $\rightarrow$ LUMO (76.86%)			
$S_6$	HOMO-12 $\rightarrow$ LUMO (33.94%) HOMO-4 $\rightarrow$ LUMO+8 (15.41%)			
$S_8$	HOMO-1 $\rightarrow$ LUMO (34.27%) HOMO-6 $\rightarrow$ LUMO (23.33%)			
$S_{11}$	HOMO-1 $\rightarrow$ LUMO (32.42%) HOMO-13 $\rightarrow$ LUMO (21.25%)			
$T_{14}$	HOMO-2 $\rightarrow$ LUMO+7 (23.74%) HOMO-2 $\rightarrow$ LUMO (14.66%) [Ligand to ligand or ligand to metal]			

**Table 9**  
Orbitals involved in the transitions of  $[\text{Co}(\text{DPC})_2]^-$ , configuration 2





The peaks at 341, 429, 584 and 729 nm in the SOC spectrum are mainly the peaks at 344, 432, 563 and 742 nm in the UV-Vis spectrum, since the same transitions contribute in a similar percentage to these peaks. The peak at 729 in the SOC spectrum, that appears more intense than in the UV-Vis spectrum, shows a significant contribution from a triplet state, in addition to the same transitions that contribute to the peak at 742 in the UV-Vis spectrum. Therefore, this increase in intensity is due to SOC effects. An important observation is that the SOC effect is different in the two configurations, so, the complex configuration is also an important factor to take into account for the SOC effects.

## 4.2 Synthesis of a cobalt complex with diphenylcarbazine

Since the complex of cobalt with diphenylcarbazine was the one that showed the most useful SOC effect for photoactivation purposes, it was synthesized in laboratory. It is important to mention that first the  $\text{Co}^{2+}$  complex with diphenylcarbazine was synthesized with the purposes of oxidize it later.

### 4.2.1 Characterization results

#### 4.2.1.1 Diphenylcarbazine

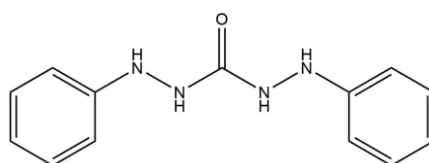


**Figure 17**  
Structure of diphenylcarbazine

The measured melting point is 171.9-173 °C.

The FT-IR spectrum of diphenylcarbazide, as well as the corresponding peak assignment is shown in Figure 18 and Table 10, respectively. In addition, the UV-Vis spectrum is shown in Figure 19.

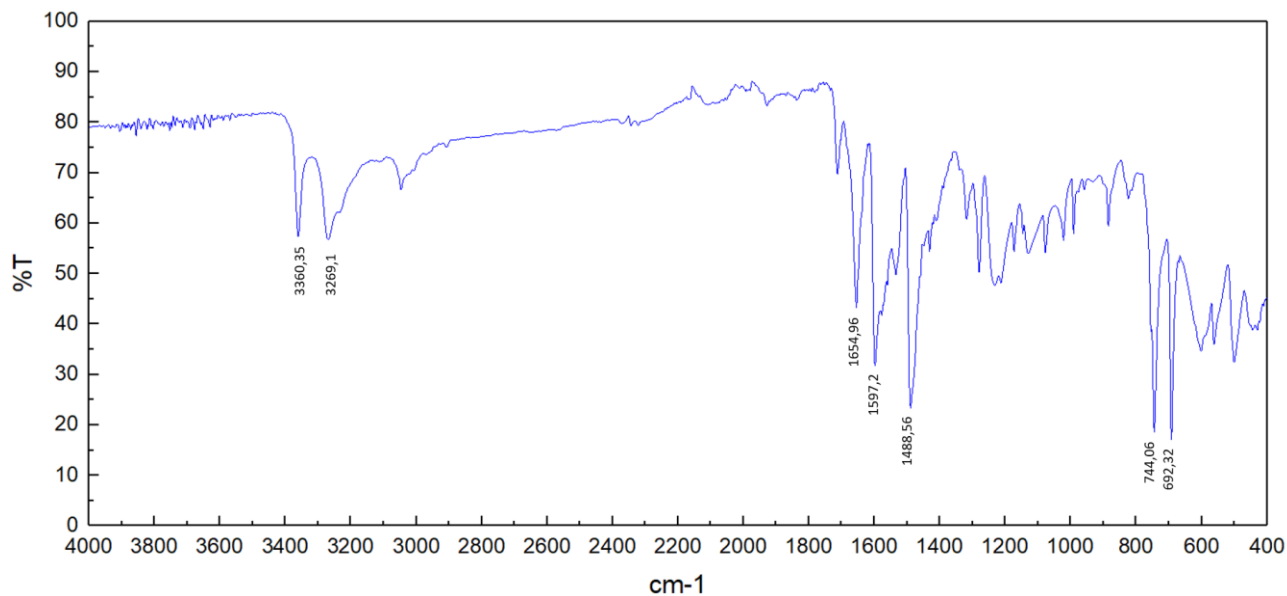


**Figure 18**  
FT-IR spectrum of diphenylcarbazide

**Table 10**  
Peak assignation of the FT-IR spectrum of diphenylcarbazide

Frequency (cm <sup>-1</sup> )	Intensity	Peak assignments
3360.35	57.32	N-H stretch
3269.1	56.73	N-H stretch
1654.96	43.19	C=O stretch
1597.2	31.78	N-H bend
1488.56	23.56	C-N stretch
744.06	18.83	C-H out of plane bending vibrations for monosubstituted benzene
692.32	18.16	

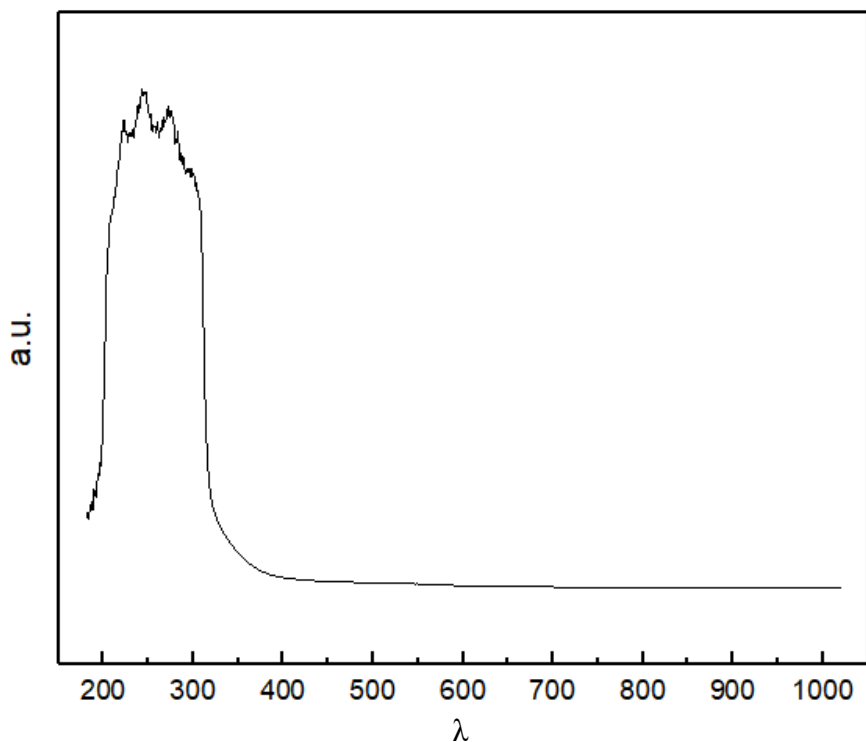


**Figure 19**  
UV-Vis spectrum of diphenylcarbazine

Since diphenylcarbazine is an organic molecule, no transitions in the visible region are expected. Therefore, the group of peaks observed around 200-300 might be due to  $\pi \rightarrow \pi^*$  transitions (11).

Finally, the data obtained in the paramagnetic balance is shown in Table 11.

**Table 11**  
Paramagnetic balance data of diphenylcarbazine

Measurement of tube without sample ( $R_0$ )	-0.35
Weight of tube without sample	0.834 g
Height of sample in tube (L)	1.9 cm
Weight of tube with sample	0.894 g
Measurement of tube with sample (R)	-53
Weight of the sample (M)	0.060 g

The negative result of the paramagnetic balance ( $R_0$ ) indicates that the sample is diamagnetic, so, it doesn't have any free electrons.



#### 4.2.1.2 Cobalt chloride hexahydrate

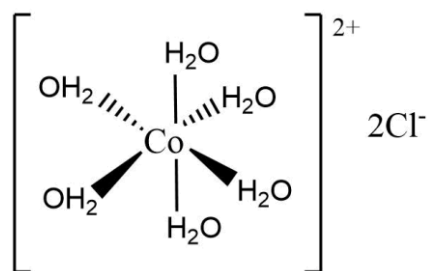


**Figure 20**  
Structure of cobalt chloride hexahydrate

The theoretical melting point is 735 °C, but the available equipment does not reach that temperature, so, the measurement was not possible.

The FT-IR spectrum of cobalt chloride hexahydrate, as well as the corresponding peak assignment is shown in Figure 21 and Table 12 respectively. In addition, the UV-Vis spectrum is shown in Figure 22.

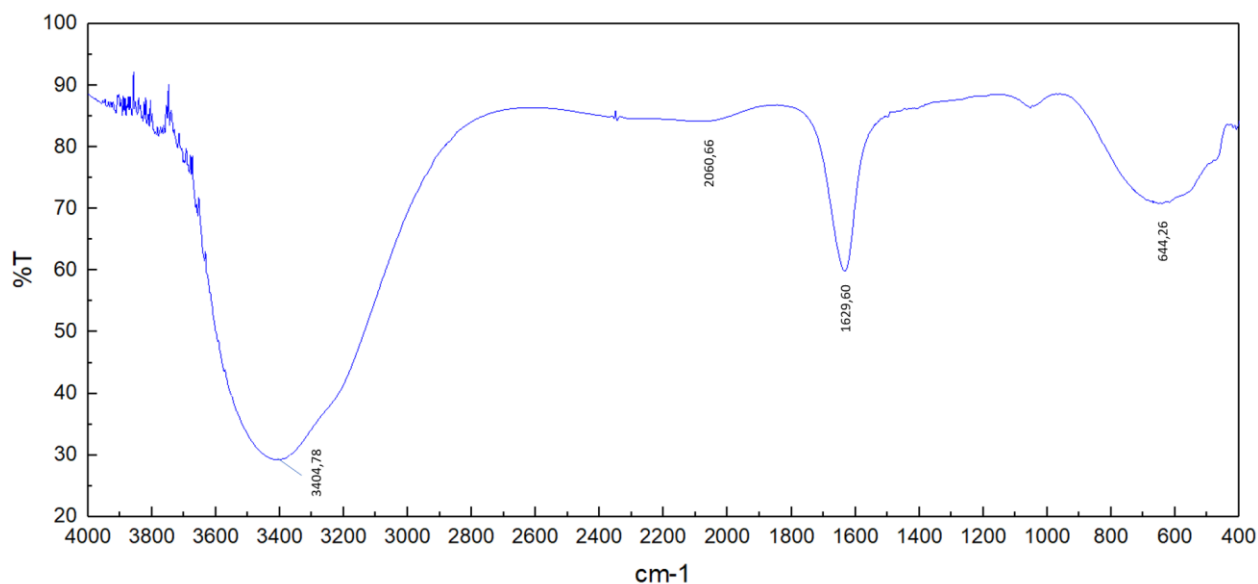


**Figure 21**  
FT-IR spectrum of cobalt chloride hexahydrate

**Table 12**  
Peak assignment of the FT-IR spectrum of cobalt chloride hexahydrate

Frequency (cm <sup>-1</sup> )	Intensity	Vibration
3404.78	29.25	O-H stretching
2060.66	84.31	Coupling of scissors-bending (34)
1629.60	60.02	H-O-H scissors-bending (34)

644.26	70.89	$\rho_r(\text{H}_2\text{O})$ and possible Co-O interaction
--------	-------	--

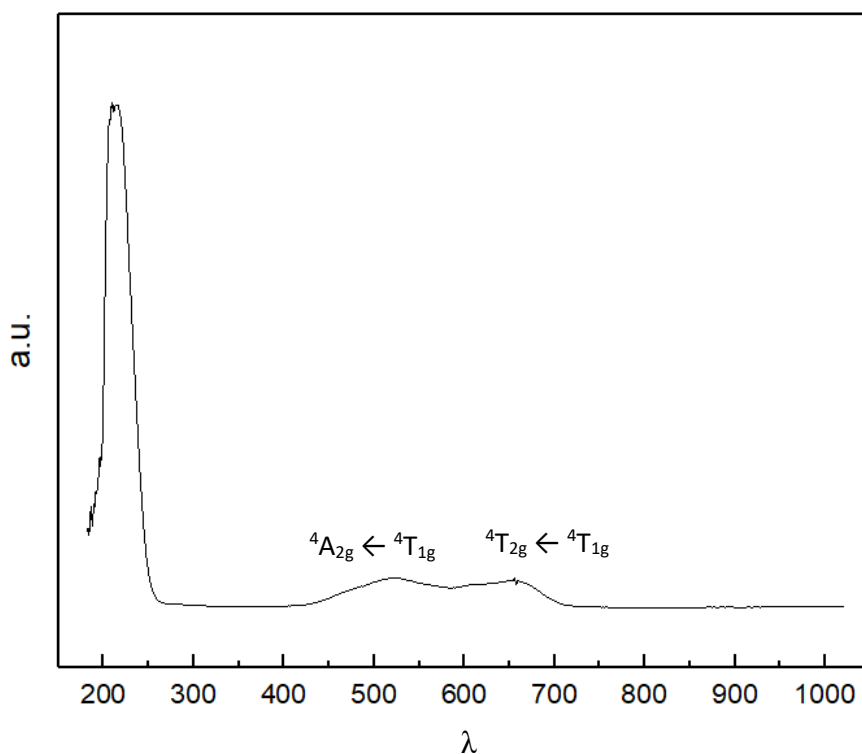


**Figure 22**

UV-Vis spectrum of cobalt chloride hexahydrate

In this case, the metal is a  $d^7$  species. As two d-d transitions are observed at around 525 and 650 nm, the system is suggested to be high spin. The group of peaks observed around 200 nm might be due to charge transfer.

Finally, the calculation of  $\mu_{\text{eff}}$  is shown using the data obtained in the paramagnetic balance (Table 13) with equations 3, 4, 5 and 6.

$$x_g^{\text{measured}} = \frac{C * L(R - R_0)}{10^9 M} \quad \text{(Equation 3)}$$

$$x_M^{\text{measured}} = x_g^{\text{measured}} * MM \quad \text{(Equation 4)}$$

$$x_M^{\text{corrected}} = x_M^{\text{measured}} - x_M^{\text{diamagnetic}} \quad \text{(Equation 5)}$$

$$\mu_{\text{eff}}^{\text{experimental}} = 2.828 \sqrt{x_M^{\text{corrected}}(298 \text{ K})} \quad \text{(Equation 6)}$$

**Table 13**

Paramagnetic balance data of cobalt chloride hexahydrate

Measurement of tube without sample ( $R_0$ )	-32
Weight of tube without sample	0.8275 g
Height of sample in tube (L)	2 cm

Weight of tube with sample	0.9526 g
Measurement of tube with sample (R)	3640
Weight of the sample (M)	0.1251 g

Obtention of the molar magnetic susceptibility:

$$\chi_g^{measured} = \frac{(0.9824) * (2cm) * (3640 - (-32))}{10^9(0.1251 g)} = 5.767 * 10^{-5} cm/g$$

$$\chi_M^{measured} = 5.767 * 10^{-5} \frac{cm}{g} * \left(237.9 \frac{g}{mol}\right) = 0.0137 cm/mol$$

Diamagnetic correction:

$$Co^{2+} = -12 * 10^{-6} emu/mol$$

$$H_2O = -13 * 10^{-6} emu/mol$$

$$Cl = -23.4 * 10^{-6} emu/mol$$

$$\begin{aligned} \chi_M^{diamagnetic} &= (-12 + (-13 * 6) + (-23.4 * 2)) * 10^{-6} \frac{emu}{mol} \\ &= -1.36 * 10^{-4} emu/mol \end{aligned}$$

$$\chi_M^{corrected} = 0.0137 + 1.36 * 10^{-4} \frac{emu}{mol} = 0.0138 emu/mol$$

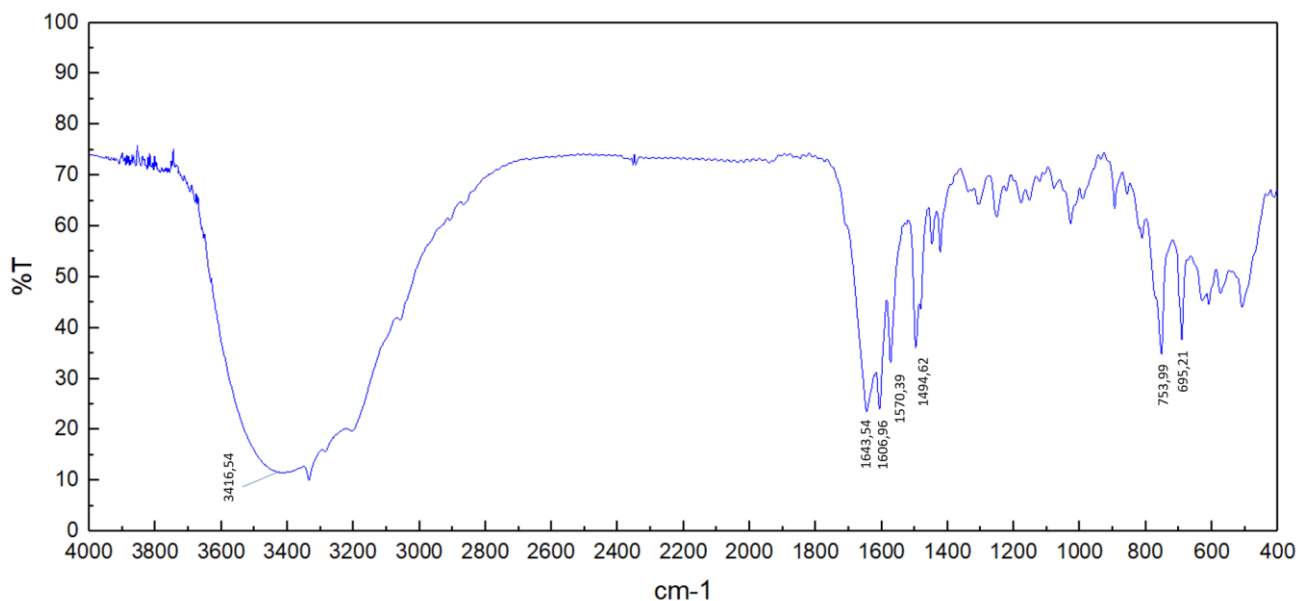
Calculation of  $\mu_{eff}^{experimental}$ :

$$\mu_{eff}^{experimental} = 2.828 \sqrt{0.0138 \frac{emu}{mol} (298 K)} = 5.73 BM$$

The results indicate that the species has unpaired electrons. The experimental magnetic moment expected for  $Co^{2+}$  species is between 4.1 and 5.2 BM, so, the result is a slightly higher than expected, probably due to SOC effects

#### 4.2.1.3 Cobalt complex

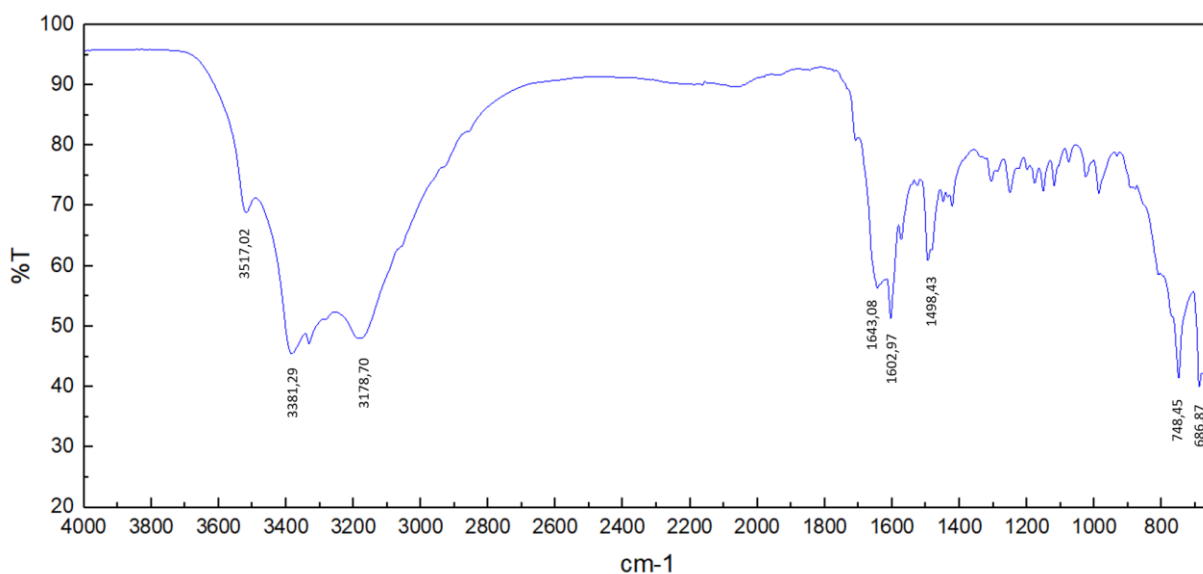
The measured melting point is 210.4-211 °C. The FT-IR spectrum of cobalt with diphenylcarbazine, as well as the corresponding peak assignment is shown in Figure 23 and Table 14, respectively. Due to the presence of moisture, the sample was dried, and the FT-IR was recorded and shown in Figure 24 and the peak assignment is shown in Table 15. In addition, the UV-Vis spectrum is shown in Figure 25.



**Figure 23**  
FT-IR spectrum of cobalt with diphenylcarbazine

**Table 14**  
Peak assignation of the FT-IR spectrum of cobalt with diphenylcarbazine

Frequency (cm <sup>-1</sup> )	Intensity	Vibration
3416.54	11.5	O-H stretch
1643.54	24.06	C=O stretch
1606.96	24.12	C=C stretch (aromatic)
1570.39	35.4	
1494.62	37.8	
753.99	35.56	C-H out of plane bending vibrations for monosubstituted benzene
695.21	42.38	

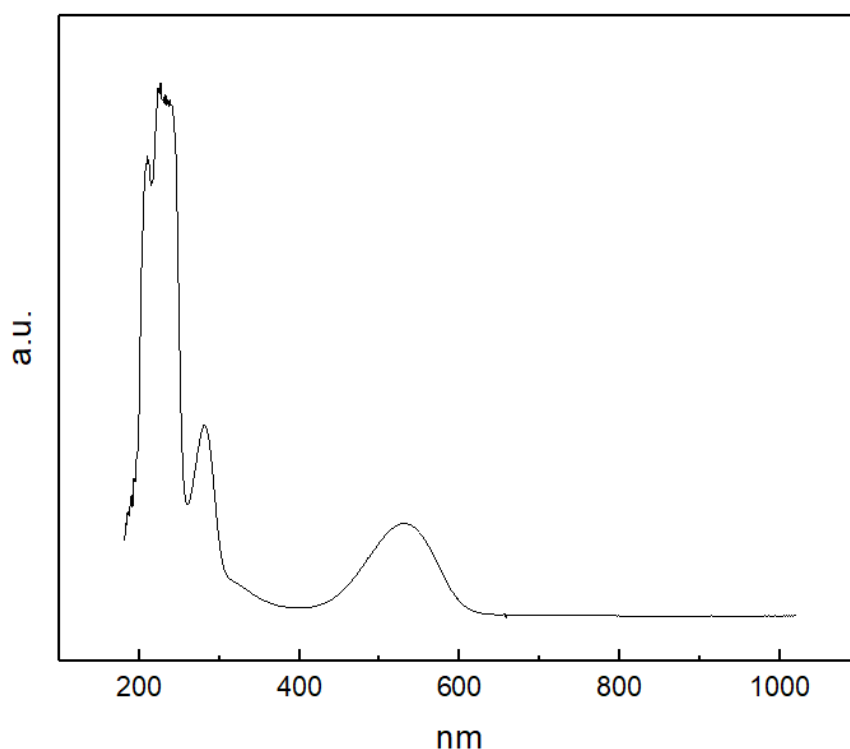


**Figure 24**  
FT-IR spectrum of dried cobalt with diphenylcarbazine

**Table 15**

Peak assignation of the FT-IR spectrum of dried cobalt with diphenylcarbazide

Frequency (cm <sup>-1</sup> )	Intensity	Vibration
3517.02	68.84	N-H stretch
3381.29	45.49	
3178.70	48.01	
1643.08	56.39	C=C stretch (aromatic)
1602.97	52.08	
1498.43	63.13	
748.45	41.68	C-H out of plane bending vibrations for monosubstituted benzene
686.87	40.59	

**Figure 25**

UV-Vis spectrum of cobalt with diphenylcarbazide

One d-d transition is observed around 550 nm. The group of peaks observed around 200-300 nm might be due to charge transfer or  $\pi \rightarrow \pi^*$  transitions.

Finally, the calculation of  $\mu_{\text{eff}}$  is shown using the data obtained in the paramagnetic balance (Table 16) with equations 3, 4, 5 and 6.

**Table 16**  
Paramagnetic balance data of cobalt with diphenylcarbazide

Measurement of tube without sample (R <sub>0</sub> )	-33
Weight of tube without sample	0.8254g
Height of sample in tube (L)	2 cm
Weight of tube with sample	0.8916g
Measurement of tube with sample (R)	834
Weight of the sample (M)	0.0662 g

Obtention of the molar magnetic susceptibility:

$$x_g^{measured} = \frac{(0.9824) * (2cm) * (834 - (-33))}{10^9(0.0662 g)} = 2.57 * 10^{-5} cm/g$$

$$x_M^{measured} = 2.57 * 10^{-5} \frac{cm}{g} * \left(543.49 \frac{g}{mol}\right) = 0.0139 cm/mol$$

Diamagnetic correction:

$$Co^{2+} = -12 * 10^{-6} emu/mol$$

Due to the fact that diphenylcarbazide (C<sub>13</sub>H<sub>14</sub>N<sub>4</sub>O) has not a Pascal's constant for diamagnetic corrections, this constant was calculated with the table for atoms in covalent species (45).

$$C(ring) = -6.24 * 10^{-6} emu/mol$$

$$H = -2.93 * 10^{-6} emu/mol$$

$$N = -5.57 * 10^{-6} emu/mol$$

$$O = -4.6 * 10^{-6} emu/mol$$

$$x_M^{diamagnetic} = [-12 + 13(-6.24) + 14(-2.93) + 4(-5.57) + (-4.6)] * 10^{-6} \frac{emu}{mol}$$

$$= -1.61 * 10^{-4} emu/mol$$

$$x_M^{corrected} = 0.0139 + 1.61 * 10^{-4} \frac{emu}{mol} = 0.01406 emu/mol$$

Calculation of  $\mu_{eff}^{experimental}$ :

$$\mu_{eff}^{experimental} = 2.828 \sqrt{0.01406 \frac{emu}{mol} (298 K)} = 5.78 BM$$

The result indicates that the complex has unpaired electrons. In addition, the calibration curve and the sample's measurement are shown in Figure 26 and the data obtained in an atomic absorption study is shown in Table 17.

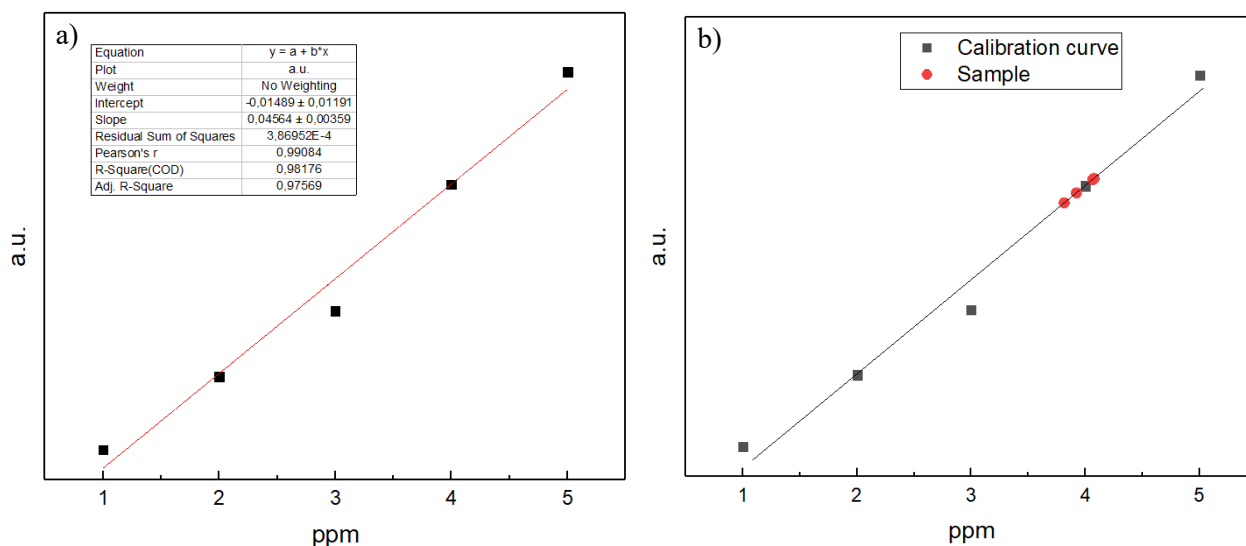


**Figure 26**  
Atomic absorption measurement of the complex. a) Cobalt calibration curve and b) sample's measurement

**Table 17**  
Atomic absorption data of cobalt with diphenylcarbazide

Cobalt standard concentration	10 ppm
Mass of complex	0.1053 g
Dilution of complex	Dissolved in 100 mL, then, 0.75 mL of it dissolved in 25 mL
Average of concentration of cobalt in the sample	$3.9685 \pm 0.12$ ppm

Next, the calculation of the percentage of cobalt present in the sample is shown.

$$\frac{3.9685 \text{ mg Co}}{1 \text{ L sol}} * \frac{25}{0.75} = \frac{132.28 \text{ mg Co}}{1 \text{ L}} * 0.1 \text{ L} = 13.228 \text{ mg Co}$$

$$\frac{0.013228 \text{ g Co}}{0.1053 \text{ g complex}} = 12.53\% \text{ Co}$$

The measurement indicates that 12.53% of the sample's mass corresponds to cobalt.

Also, the results on the conductivity study of the complex of copper with diphenylcarbazide is shown in Table 18.

**Table 18**  
Conductivity data of cobalt with diphenylcarbazide

Sample	Concentration (M)	Conductivity ( $\mu\Omega/\text{cm}$ )
Ethanol	-	0.508
$\text{CoCl}_2 \cdot 6\text{H}_2\text{O}$	$1.412 \times 10^{-3}$	59.84
Complex	$1.000 \times 10^{-3}$	52.49

Finally, the spectrum of the complex obtained by UV-Vis spectroscopy for solid samples is shown in Figure 27. It is important to mention that the resulting spectrum was obtained

in reflectance vs wavelength, and the plot of absorbance vs wavelength was obtained using the Kubelka-Munk's transformation on the data.

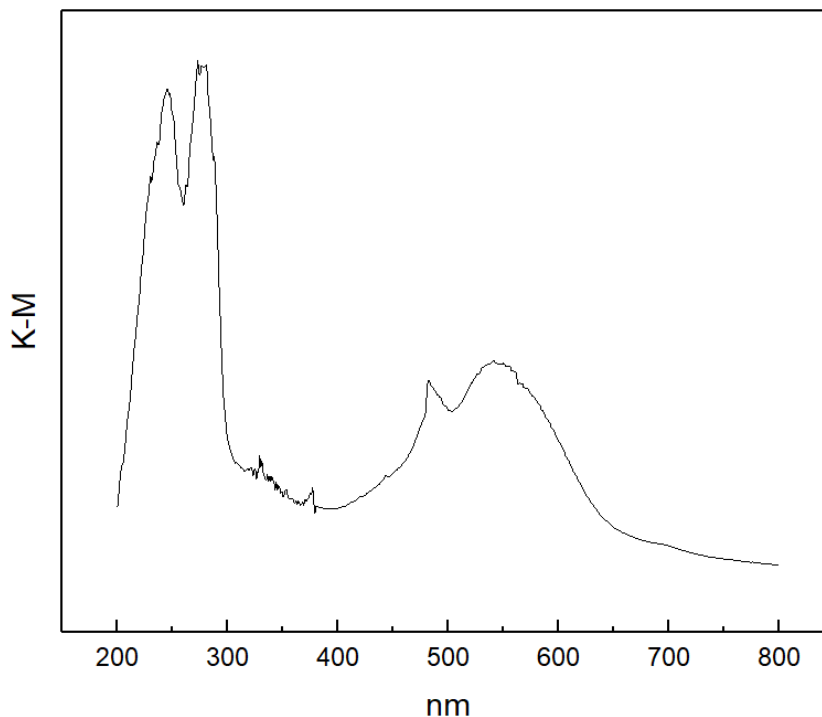


**Figure 27**  
Solid UV-Vis spectrum of the cobalt complex

#### 4.2.2 Elucidation of the complex

The result obtained from the atomic absorption study showed that 12.53% of the sample's mass corresponds to cobalt. If a metal-ligand ratio of 1:2 is supposed, the theoretical mass fraction of each element in the complex would be: Co 10.92%, N 20.77%, O 5.93%, C 57.89% and H 4.48%. Therefore, the percentage of cobalt in the sample indicates that the metal-ligand ratio present in the complex is 1:2. With the previous information, the proposed complex is shown in Figure 28. In this complex, each diphenylcarbazide is complexed to the metal through the oxygen and the nitrogen.



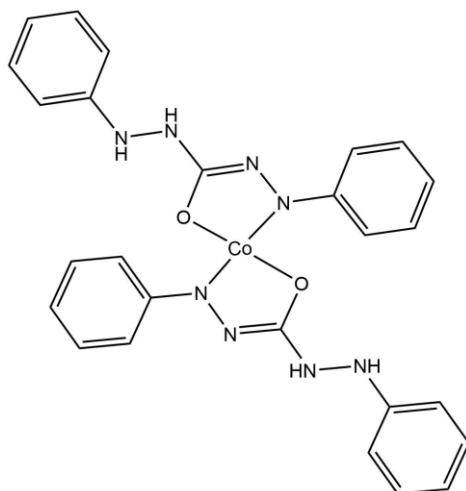


**Figure 28**  
Proposed structure of the cobalt with diphenylcarbazide complex

Given the fact that the initial salt used for the synthesis had cobalt in oxidation state 2+, the complex was first expected to have  $\text{Co}^{2+}$ . In these terms, two simulated structures of the complex were obtained and their FT-IR and UV-Vis spectra were simulated to compare with the experimental ones. The structures and spectra comparison are shown in Figures (29-31), respectively.

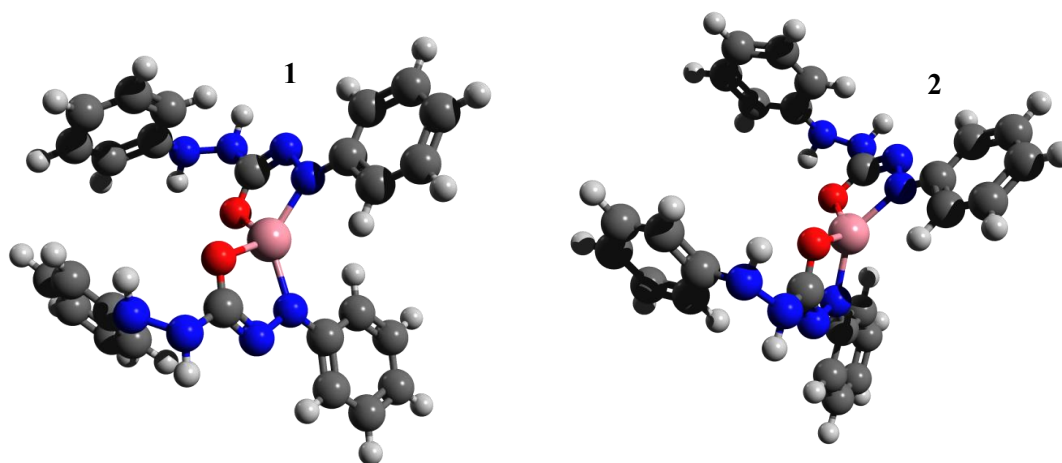


**Figure 29**  
Different cobalt with diphenylcarbazide complexes

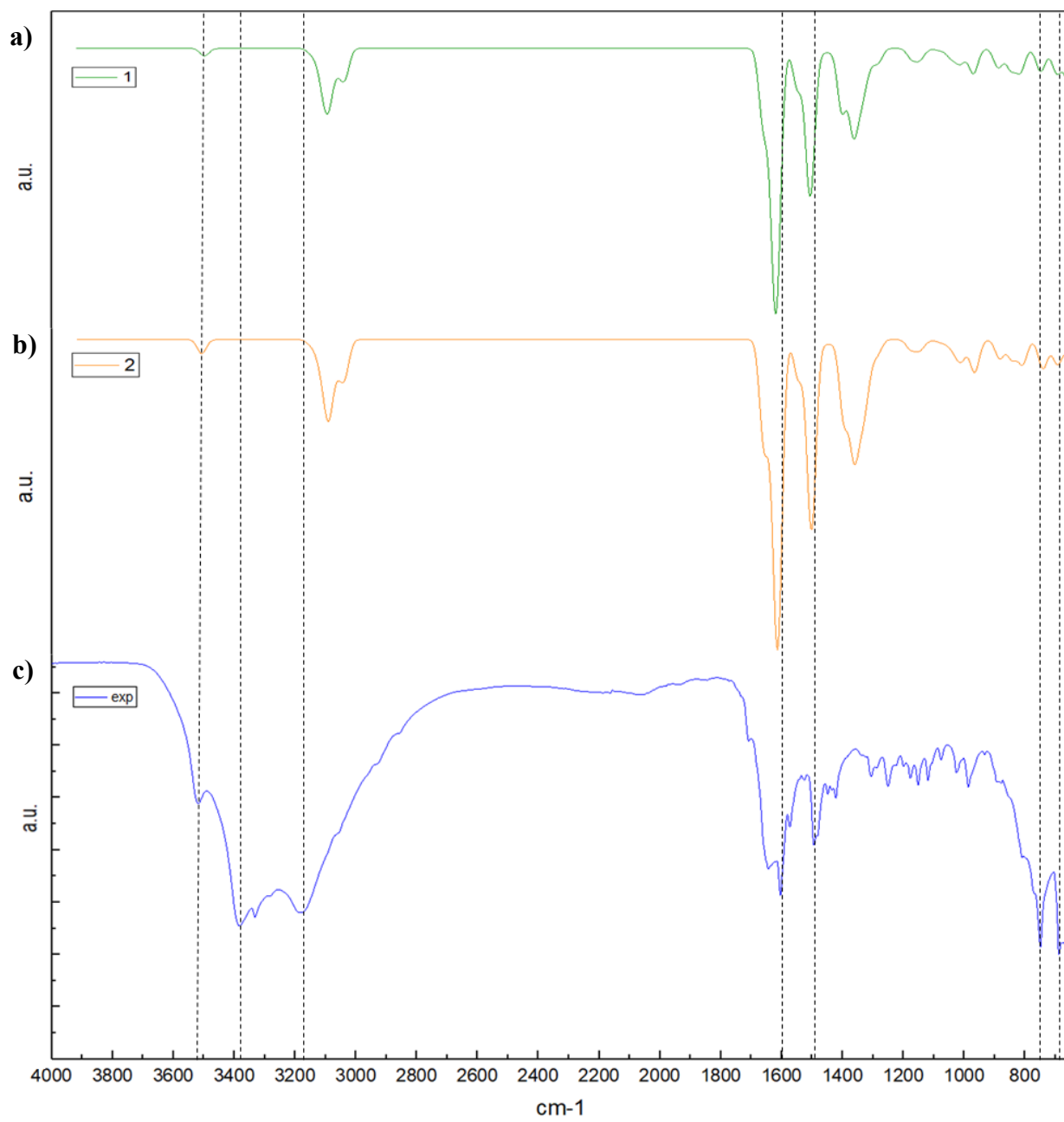


**Figure 30**  
FT-IR spectra of the cobalt with diphenylcarbazide complexes: (a) and (b) simulated and (c) experimental

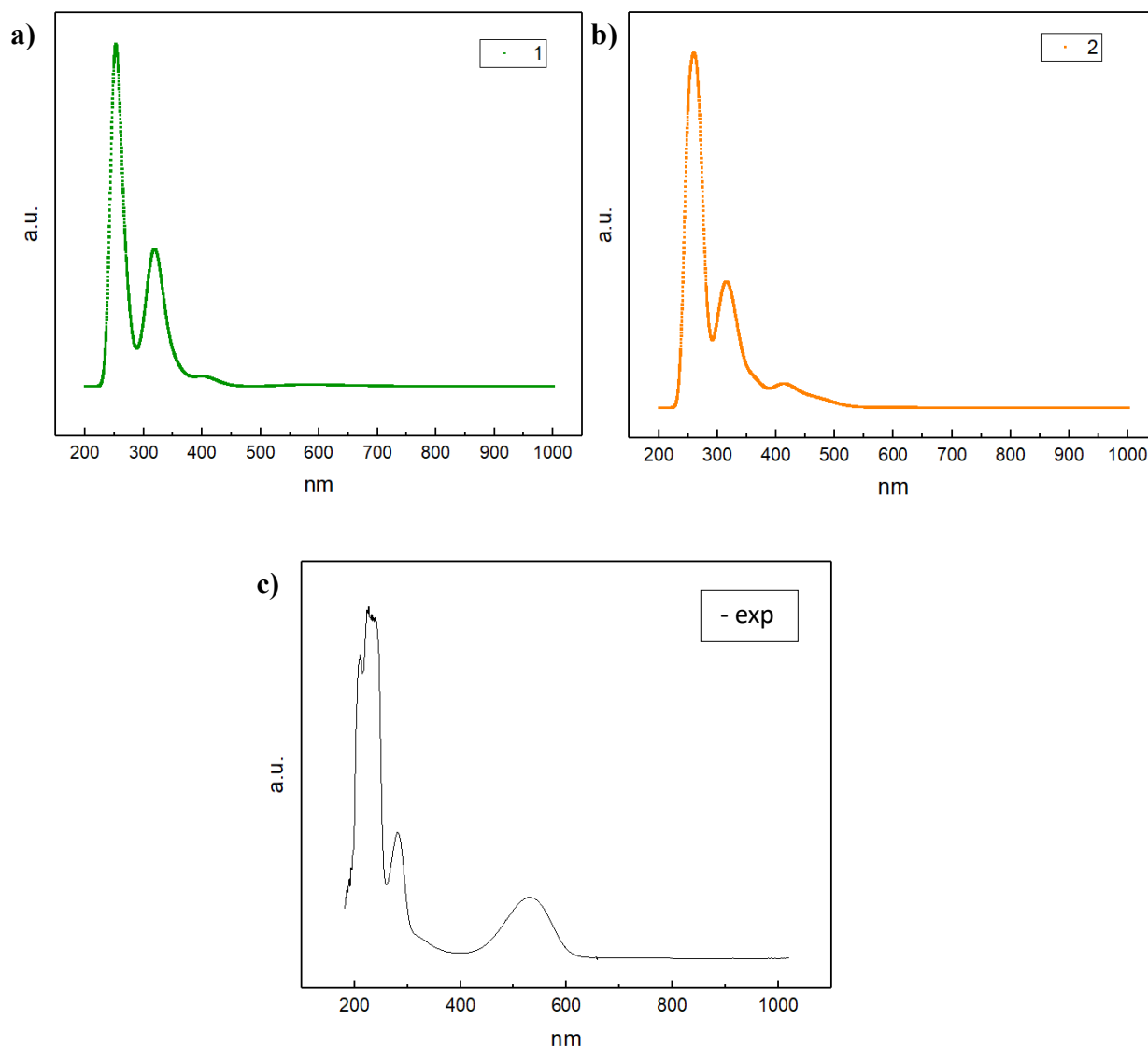


**Figure 31**

UV-Vis spectra of the cobalt with diphenylcarbazide complexes: (a) and (b) simulated and (c) experimental

On one hand, the FT-IR spectra comparison in Figure 30 shows that in all of the structures the peaks at  $1600\text{-}1400\text{ cm}^{-1}$  corresponds well to the experimental FT-IR, as well as the peaks between  $700\text{-}800\text{ cm}^{-1}$  and the peak at  $3500\text{ cm}^{-1}$ . However, it is important to mention that the peaks between  $3200$  and  $3400\text{ cm}^{-1}$  are not well represented by the simulation, and that some peaks appear in the simulation and are not present in the experimental spectrum, such as the peaks at  $3300\text{ cm}^{-1}$  and the peak at  $1400\text{ cm}^{-1}$ . Therefore, it is possible that the structure is not correctly represented by the simulation. On the other hand, none of the UV-Vis spectra shown in Figure 31 corresponds well to the experimental spectra, given the fact that the peak observed experimentally around  $550\text{ nm}$  is not present in neither of the structures. These results indicate that there is probably a mixture with another cobalt complex in the sample.

Consequently, one of the  $\text{Co}^{3+}$  complex with diphenylcarbazide presented previously was used to compare with the experimental results. As it is possible to see in Figure 32, the simulated UV-Vis spectrum of the complex shows a peak at around  $600\text{ nm}$ .

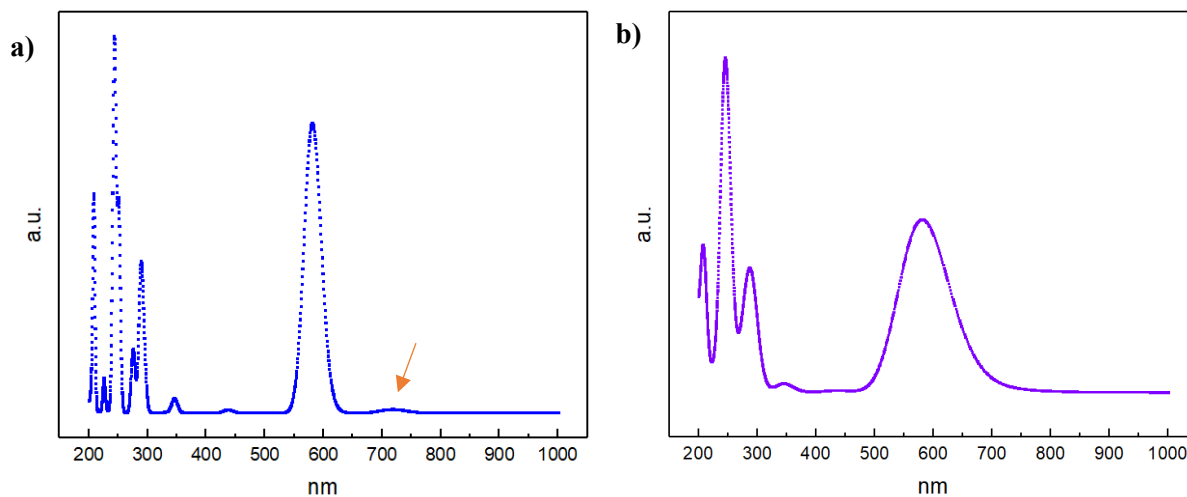
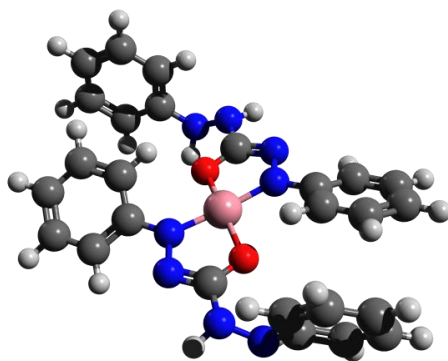


**Figure 32**

$\text{Co}^{3+}$  complex with diphenylcarbazide and the corresponding UV-Vis simulated spectrum with a) peak width 1000 and b) peak width 3000

Since the simulated spectrum shown in Figure 32 is not completely similar to the experimental one, a UV-Vis spectrum was created using a linear combination of the UV-Vis spectra of complex 1 (Figure 31.a) and of the complex with  $\text{Co}^{3+}$  (Figure 32.a). The resulting UV-Vis spectrum is shown in Figure 33 and it corresponds accurately to the experimental UV-Vis spectrum. Therefore, it is possible that the complex obtained has a mixture of both  $\text{Co}^{2+}$  and  $\text{Co}^{3+}$  complexes. This could be possible if the complexation of  $\text{Co}^{2+}$  with diphenylcarbazide modified its redox potential, making  $\text{Co}^{2+}$  more willing to be oxidated to  $\text{Co}^{3+}$  by the exposure to air.

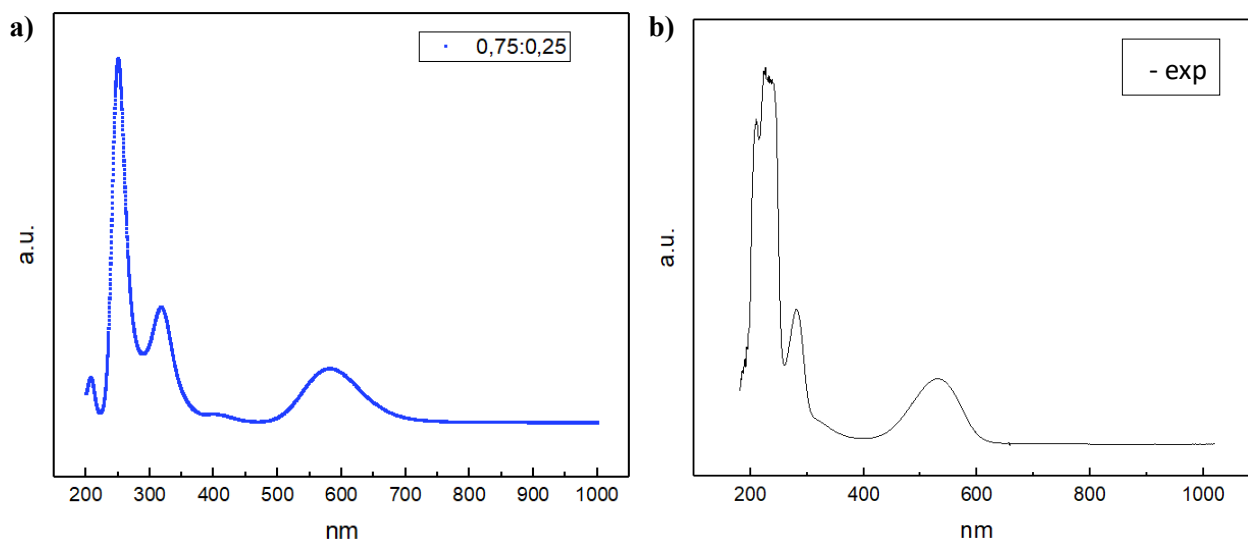


**Figure 33**

(a) UV-Vis simulated spectrum with 75% of Co<sup>2+</sup> complex and 25% of Co<sup>3+</sup> complex and (b) experimental spectrum

The presence of Co<sup>3+</sup> is confirmed by the value of the effective magnetic moment obtained from the complex. Considering the Spin-Orbit Coupling contributions, 4 values of effective magnetic moment are expected for the following species: (Co<sup>2+</sup> HS: 4.79 BM), (Co<sup>2+</sup> LS: 3.31 BM), (Co<sup>3+</sup> HS: 5.65 BM) and (Co<sup>3+</sup> LS: 0 BM). Moreover, in the literature, 11 tetracoordinate Co<sup>2+</sup> complexes of the type L<sub>2</sub>CoX<sub>2</sub> showing an effective magnetic moment between 4.39 and 4.76 BM, while a Co<sup>3+</sup> complex formed with polyanionic chelating agents showing an effective magnetic moment of 5.1 BM were reported (35,36). Therefore, given the fact that the experimental magnetic moment of the complex obtained was 5.78 BM, this value couldn't have been obtained if only Co<sup>2+</sup> was present in the sample.

It is also important to mention that in the proposed structure shown in Figure 28, diphenylcarbazide is complexed by the oxygen and the nitrogen to the metal, so, it would have a charge of 2-. For the two possible oxidation states of cobalt, a charged complex will be obtained, which is confirmed by the results of the conductivity study.

Finally, it is noteworthy that the Co<sup>3+</sup> complex with diphenylcarbazide has a peak in the UV-Vis spectrum that increases its intensity due to SOC effects (Figure 32.a). As shown in the solid UV-Vis spectrum of the complex (Figure 34), a small peak at around 700 nm is observed. Therefore, the peak that appears due to SOC effects expected computationally is observed experimentally, confirming the presence of the Co<sup>3+</sup> complex.

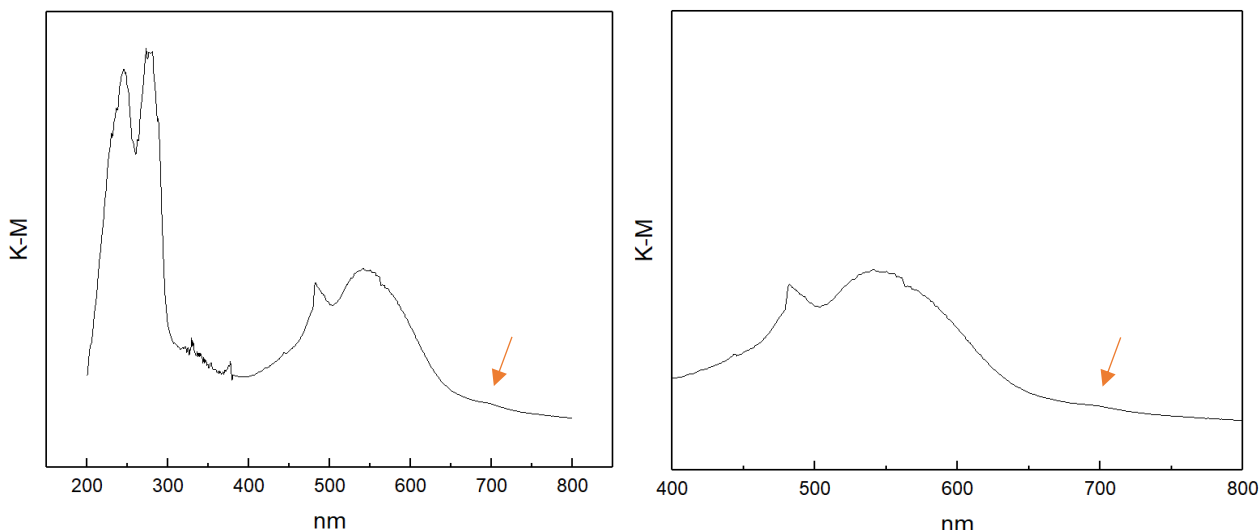


**Figure 34**  
Solid UV-Vis spectrum of the cobalt complex

### 4.3 Strategies to enhance Spin-Orbit Coupling effect in the metallic complexes with diphenylcarbazide

#### 4.3.1 Study of metallic-diphenylcarbazide complexes

Due to the fact that SOC effect increases with the atomic number of the metal, it will be useful to study complexes of the same ligands with different metals, in order to determine how SOC effect changes. Therefore, complexes of diphenylcarbazide with  $\text{Cu}^+$  (lower atomic number) and  $\text{Pt}^{4+}$  (higher atomic number) are studied. It is important to mention that these oxidation numbers were chosen due to the fact that their respective electronic configurations allow singlet-to-triplet transitions. Also, this study will be useful to understand the ligand contribution to the SOC effect and to prove if in this case the heavy-atom effect is fulfilled.

##### 4.3.1.1 $\text{Cu}^+$ complex with diphenylcarbazide

###### 4.3.1.1.1 Configuration 1

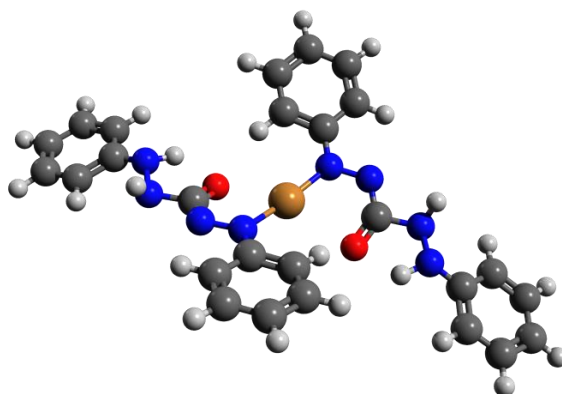


**Figure 35**  
Optimized structure of  $[\text{Cu}(\text{DPC})_2]^+$ , configuration 1

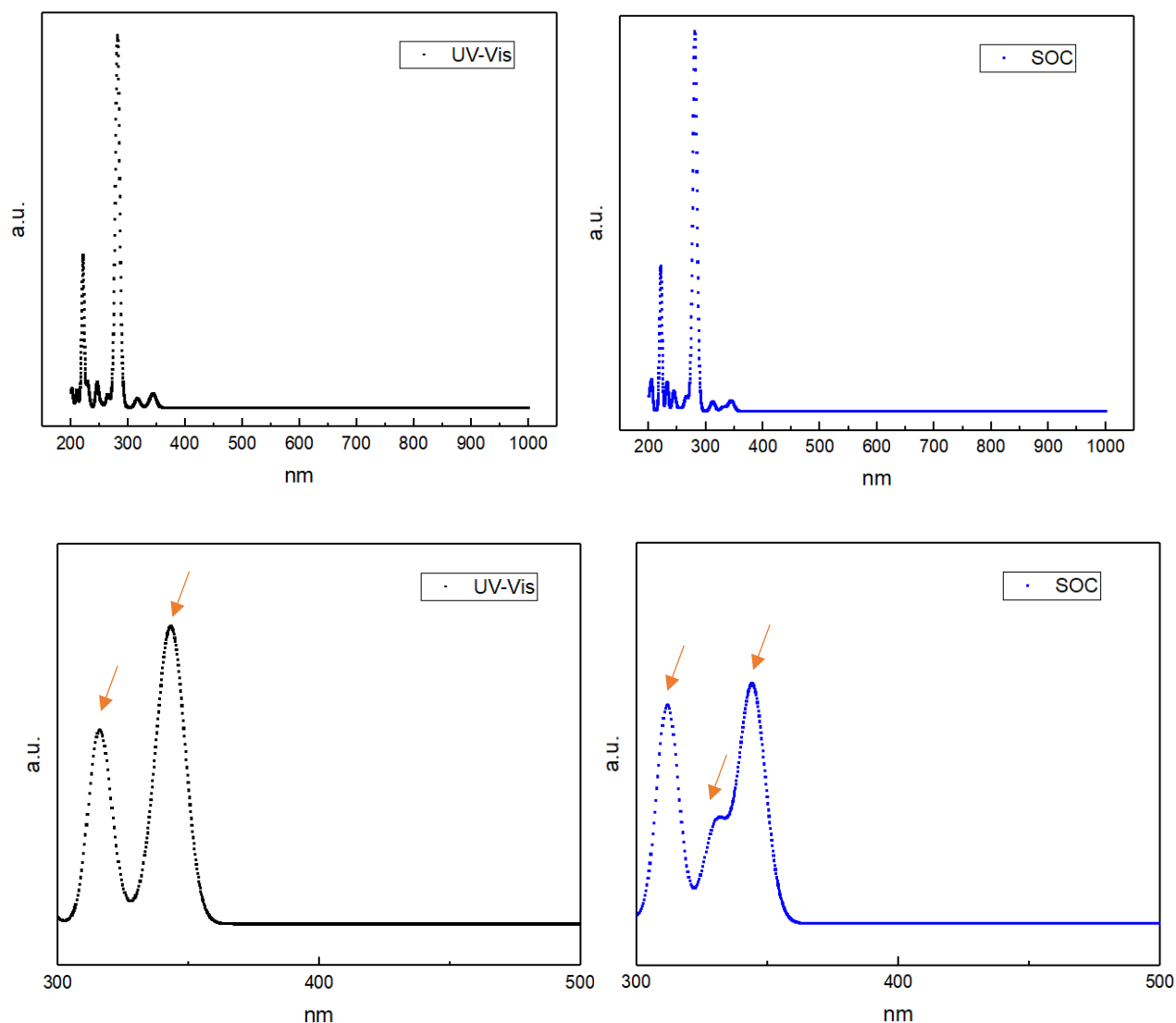


**Figure 36**  
UV-Vis and SOC spectra of  $[\text{Cu}(\text{DPC})_2]^{3-}$ , configuration 1

There are two peaks observed in the UV-Vis spectra (Figure 35) at 339 and 344 nm. However, copper is a  $d^{10}$  species, so, no d-d transitions are expected. Therefore, the transitions observed might be due to Charge Transfer (46).

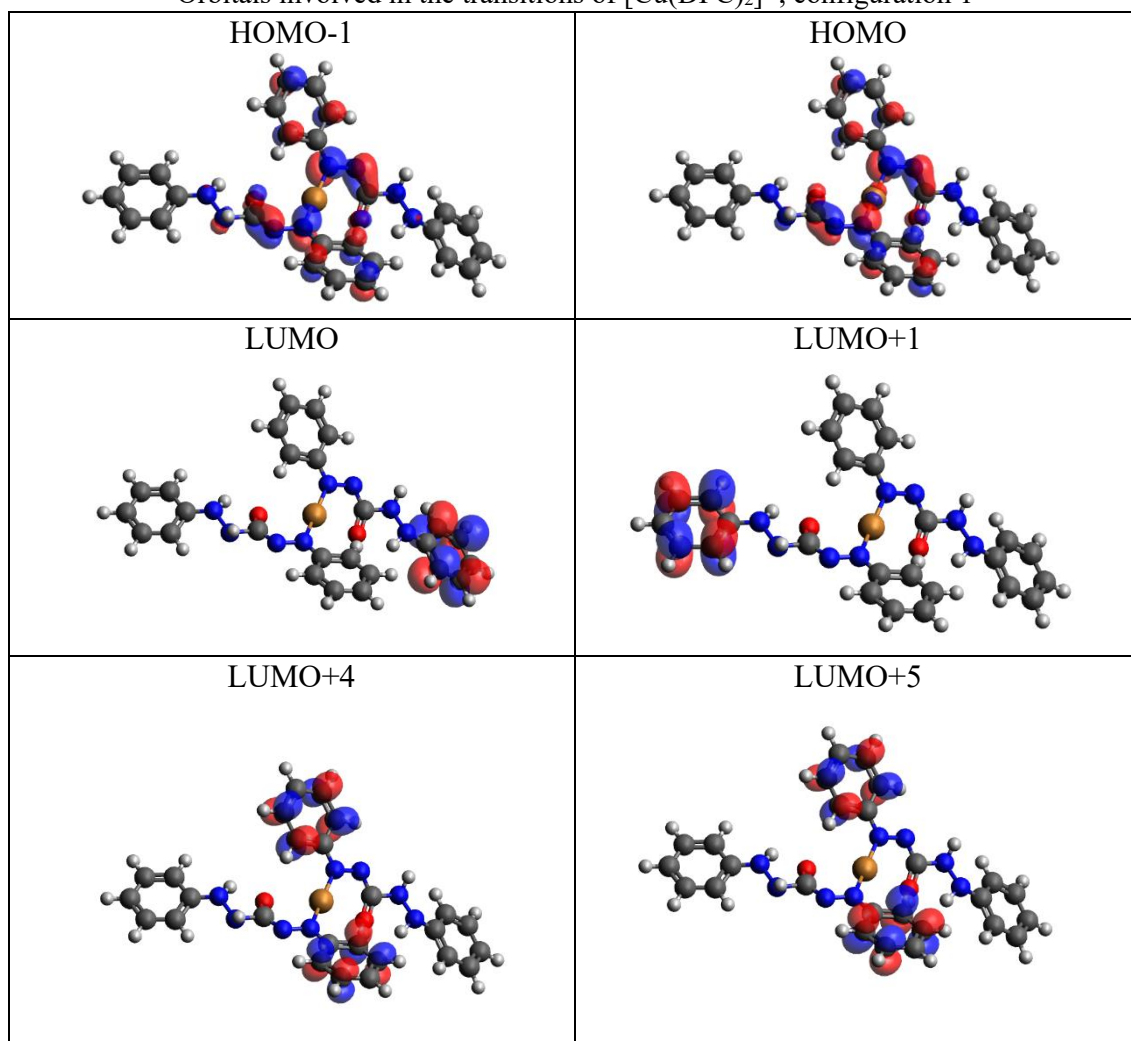
**Table 19**  
Description of the UV-Vis spectrum transitions of  $[\text{Cu}(\text{DPC})_2]^{3-}$ , configuration 1

State	Energy (eV)	Wavelength (nm)	Major Contributions	Oscillator Strength
5	3.652	339.5	HOMO $\rightarrow$ LUMO (48.05%) HOMO-1 $\rightarrow$ LUMO (18.41%) [Metal to ligand]	0.01636
1	3.602	344.2	HOMO $\rightarrow$ LUMO+4 (66.92%) HOMO-1 $\rightarrow$ LUMO+5 (25.76%) [Metal to ligand]	0.05129

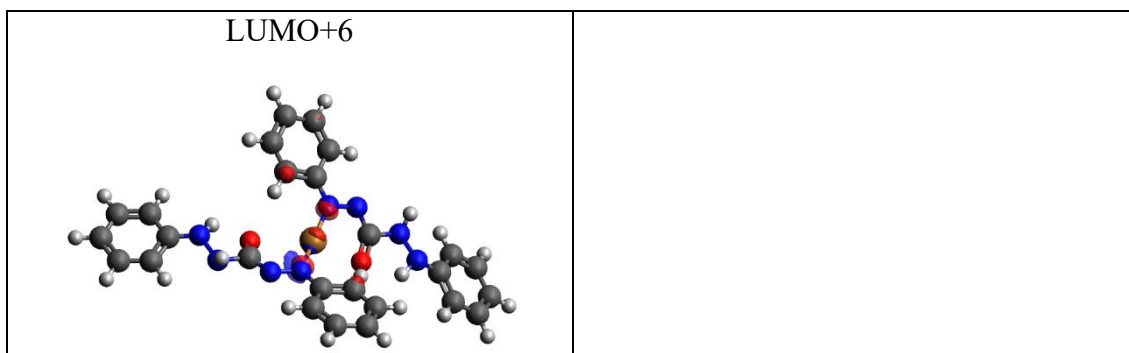
**Table 20**  
Description of the SOC spectra transitions of  $[\text{Cu}(\text{DPC})_2]^{3-}$ , configuration 1

State	Energy (eV)	Wavelength (nm)	Major Contributions	Oscillator Strength
48	3.746	331.0	$S_5 (M_s:0)$ 99.98%	0.01869
41	3.620	342.4	$T_9 (M_s:-1)$ 41.83% $T_9 (M_s:1)$ 41.83% $S_2 (M_s:0)$ 12.79%	0.00014
37	3.604	344.0	$S_1 (M_s:0)$ 99.91%	0.05121
State	Major Contributions			
$S_1$	HOMO $\rightarrow$ LUMO+4 (67.04%) HOMO-1 $\rightarrow$ LUMO+5 (26.06%)			
$S_2$	HOMO $\rightarrow$ LUMO+5 (57.89%) HOMO-1 $\rightarrow$ LUMO+4 (35.37%) [Metal to ligand]			
$S_5$	HOMO $\rightarrow$ LUMO (40.04%) HOMO $\rightarrow$ LUMO+1 (19.68%)			
$T_9$	HOMO $\rightarrow$ LUMO+6 (81.99%) [Ligand to metal or d-d]			

**Table 21**  
Orbitals involved in the transitions of  $[\text{Cu}(\text{DPC})_2]^{3-}$ , configuration 1

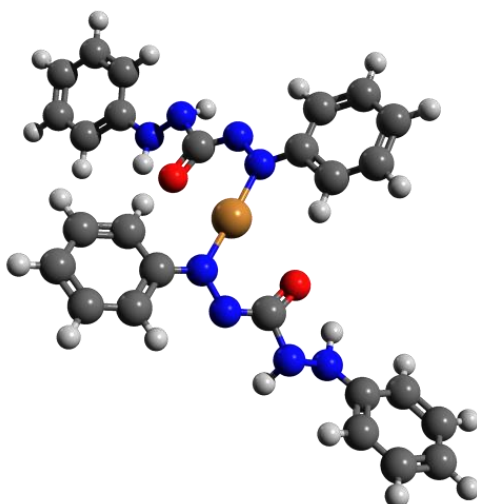




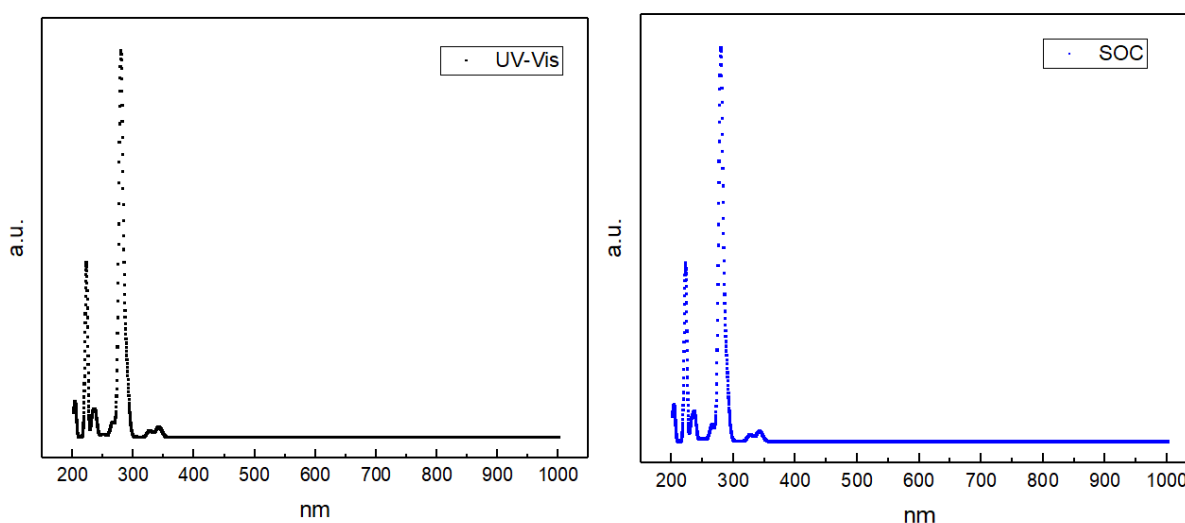


The peak at 344 nm in the SOC spectrum is mainly the peak at 344 nm in the UV-Vis spectrum, due to the fact that the same transitions contribute in a similar percentage to these peaks. On the other hand, the peaks at 331 and 342 nm in the SOC spectrum are different to the peak at 339 nm in the UV-Vis spectrum, so, they seem to be result of SOC effect, principally the peak at 342 nm, that has an important triplet contribution.

#### 4.3.1.1.2 Configuration 2



**Figure 37**  
Optimized structure of  $[\text{Cu}(\text{DPC})_2]^{3-}$ , configuration 2



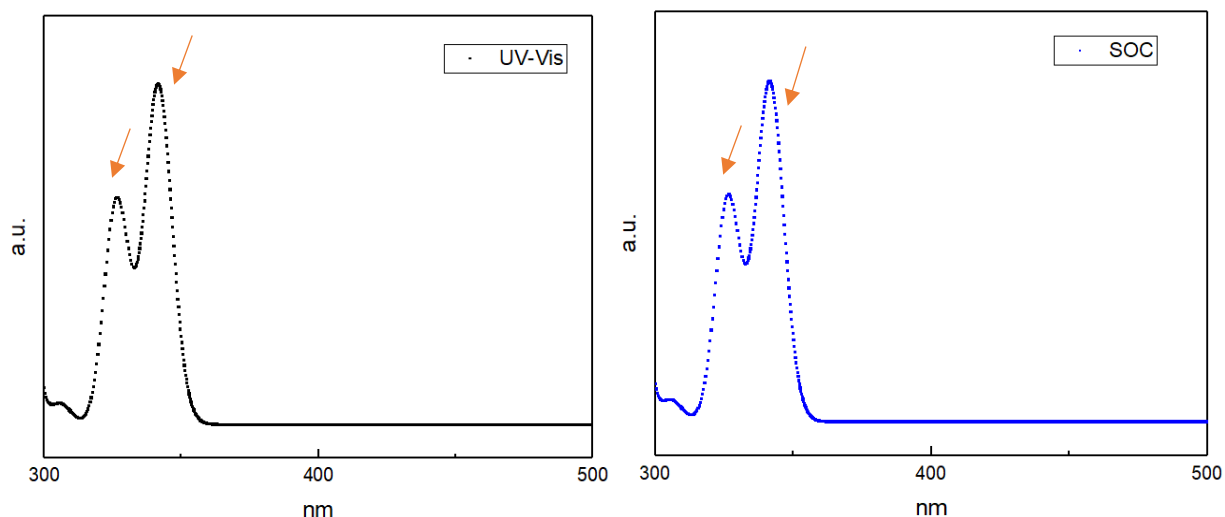


**Figure 38**  
UV-Vis and SOC spectra of  $[\text{Cu}(\text{DPC})_2]^{3-}$ , configuration 2

There are two peaks observed in the UV-Vis spectra (Figure 38) at 325 and 341 nm. As expected for Cu(I), no d-d transitions are observed, so, the transitions observed might be due to Charge Transfer.

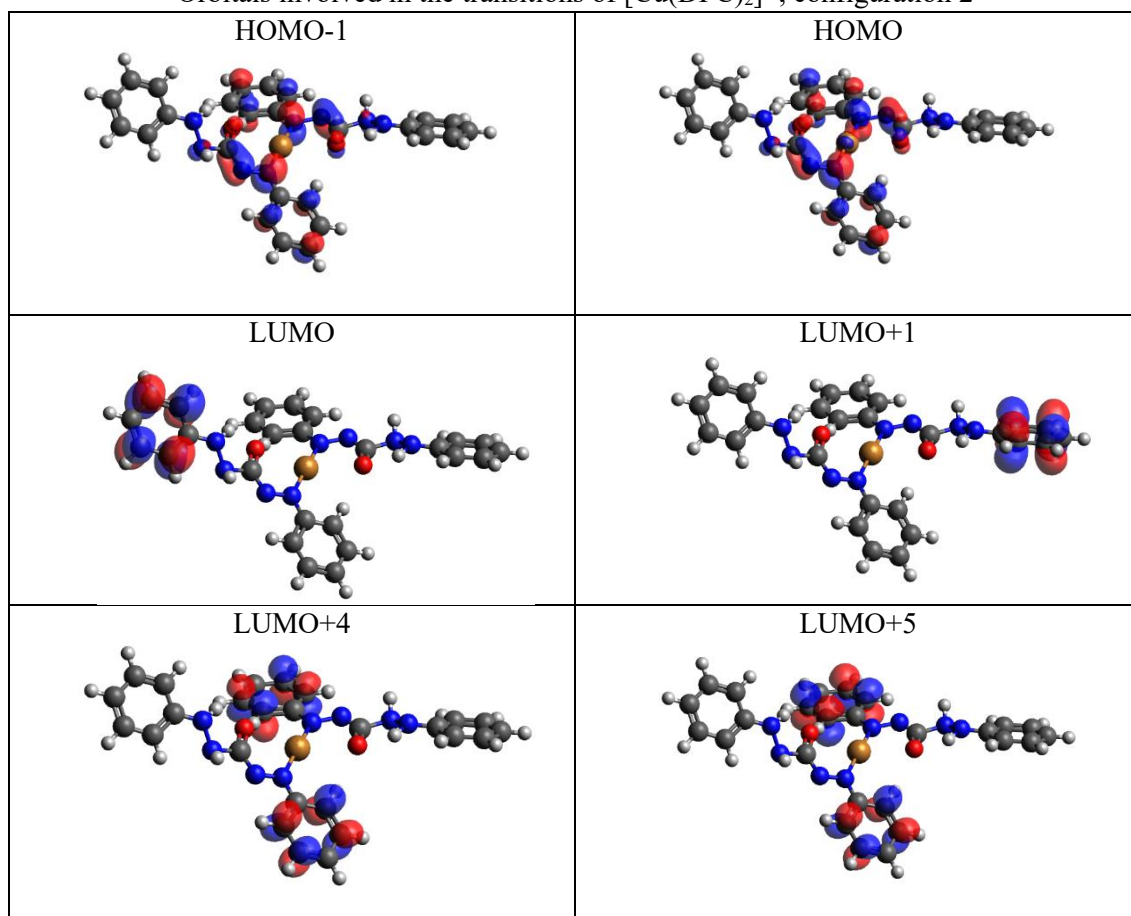
**Table 22**  
Description of the UV-Vis spectrum transitions of  $[\text{Cu}(\text{DPC})_2]^{3-}$ , configuration 2

State	Energy (eV)	Wavelength (nm)	Major Contributions	Oscillator Strength
5	3.807	325.6	HOMO $\rightarrow$ LUMO (29.13%) HOMO $\rightarrow$ LUMO+1 (27.42%) [Metal to ligand]	0.02123
1	3.631	341.4	HOMO $\rightarrow$ LUMO+4 (64.28%) HOMO-1 $\rightarrow$ LUMO+5 (25.61%) [Metal to ligand or ligand to ligand]	0.04569

**Table 23**  
Description of the SOC spectra transitions of  $[\text{Cu}(\text{DPC})_2]^{3-}$ , configuration 2

State	Energy (eV)	Wavelength (nm)	Major Contributions	Oscillator Strength
46	3.808	325.6	$S_5 (M_s:0)$ 99.90%	0.02141
43	3.631	341.4	$S_1 (M_s:0)$ 80.10%	0.04566
State	Major Contributions			
$S_1$	HOMO $\rightarrow$ LUMO+4 (64.29%) HOMO-1 $\rightarrow$ LUMO+5 (25.63%)			
$S_5$	HOMO $\rightarrow$ LUMO (29.32%) HOMO $\rightarrow$ LUMO+1 (27.24%)			

**Table 24**  
Orbitals involved in the transitions of  $[\text{Cu}(\text{DPC})_2]^{3-}$ , configuration 2



The peaks at 325 and 341 nm in the SOC spectrum are mainly the peaks at 325 and 341 nm in the UV-Vis spectrum, due to the fact that the same transitions contribute in a similar percentage to these peaks. Therefore, as no additional peaks are observed, nor an increase in intensity, no SOC effect is observed in this case.

#### 4.3.1.2 $\text{Pt}^{4+}$ complex with diphenylcarbazide

The complex  $[\text{Pt}(\text{DPC})_2]$  was simulated and one optimized structure was obtained (Figure 9) considering the singlet multiplicity as the ground state. The complex has a square-plane structure and the metal is complexed to the ligands by the nitrogen and the oxygen. However, the results indicated that the complex is more stable in triplet state rather than in singlet state. Therefore, it was not possible to study the singlet-triplet transitions.

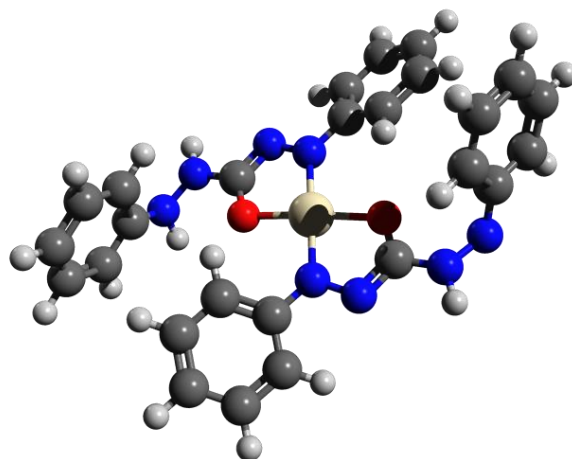


**Figure 39**  
Optimized structure of  $[\text{Pt}(\text{DPC})_2]$

#### 4.3.2 Study the complex with aromatic ring substitutions

It was proposed previously that attaching chemical substituents to a system in different positions lead to substantially different optoelectronic properties, such as shifts in the UV-Vis absorption spectra (37). Therefore, it is expected that SOC effects are also affected by aromatic ring substitutions. Then, the configuration 1 of the optimized complex  $[\text{Co}(\text{DPC})_2]^-$  was used to determine if of the ring substitutions with different functional groups can enhance SOC effect. The functional groups studied are strongly activating (hydroxyl and amine groups), strongly deactivating (cyanide and nitro groups) and not activating nor deactivating (methyl group).

In all of the cases, the complex was simulated and one optimized structure was obtained, considering the singlet multiplicity as the ground state. The resulting complex in all cases shows a square plane geometry. With the optimized structure, the corresponding UV-Vis spectrum was calculated, as well as the SOC spectrum. These spectra as well as the optimized structure for each substitution are shown in Figure 40-44. Also, the peaks that show singlet-to-triplet transitions are indicated in each case. The complete description of the transitions associated with the bands in the spectra (between 300 and 850 nm) and the orbitals involved in these transitions are showed in Annexes I.

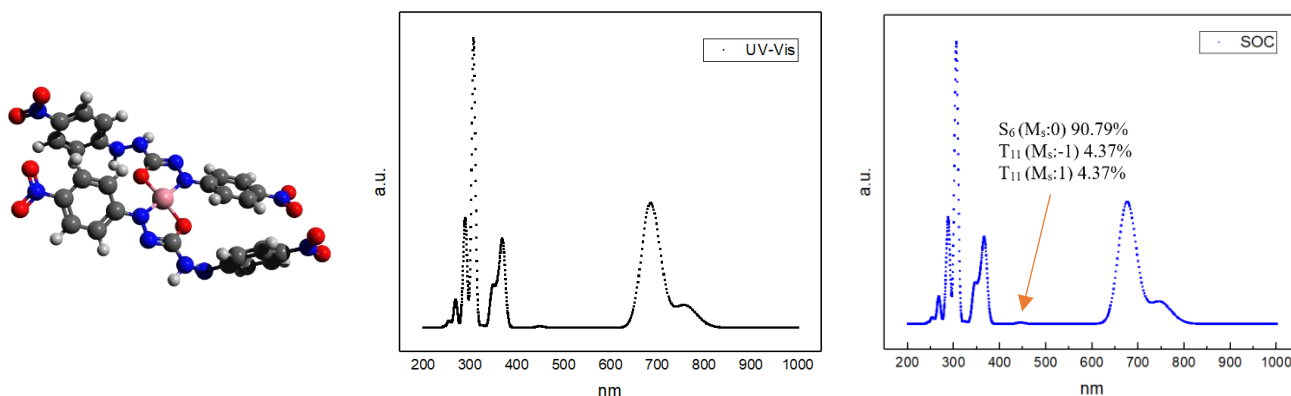


**Figure 40**  
UV-Vis and SOC spectra of  $[\text{Co}(\text{DPC})_2]^-$  with 4 nitro groups

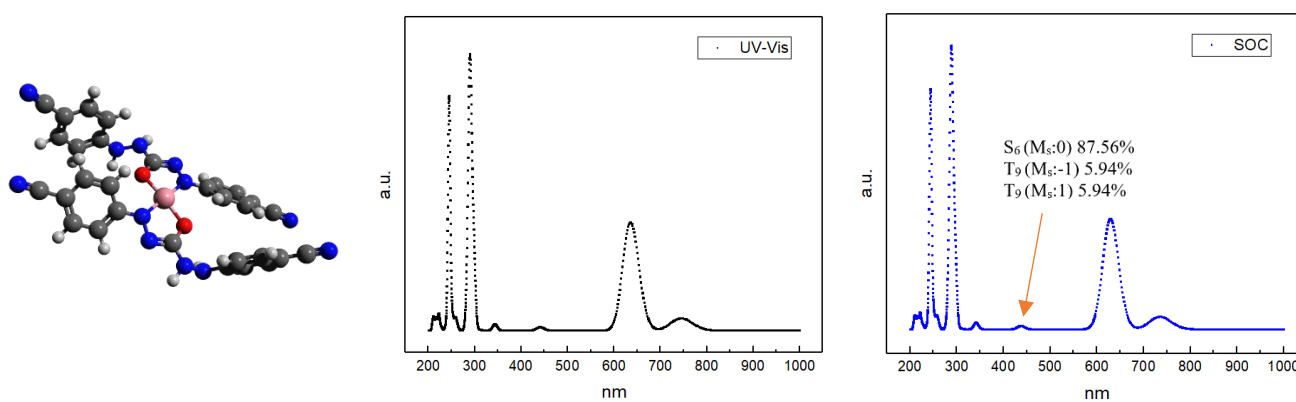


**Figure 41**  
UV-Vis and SOC spectra of  $[\text{Co}(\text{DPC})_2]^-$  with 4 cyanide groups

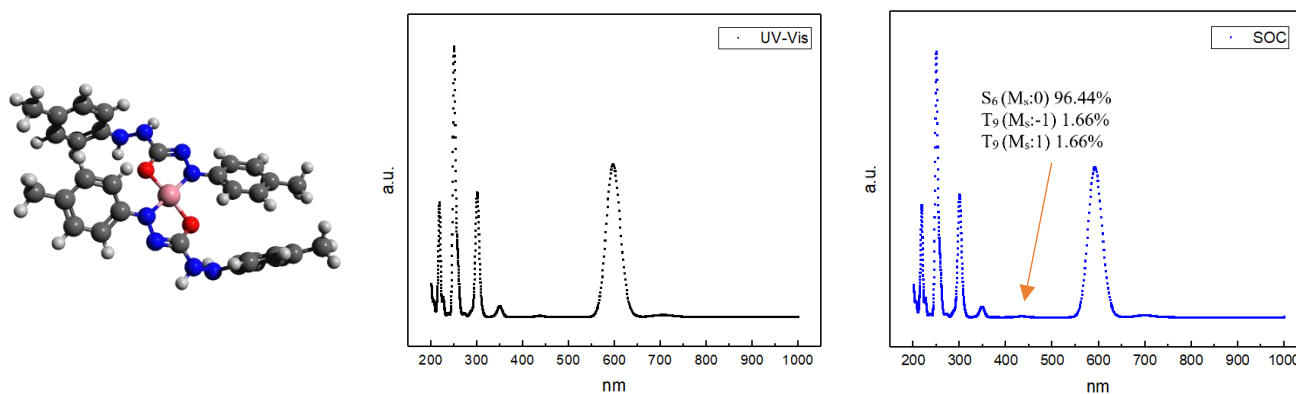


**Figure 42**  
UV-Vis and SOC spectra of  $[\text{Co}(\text{DPC})_2]^-$  with 4 methyl groups

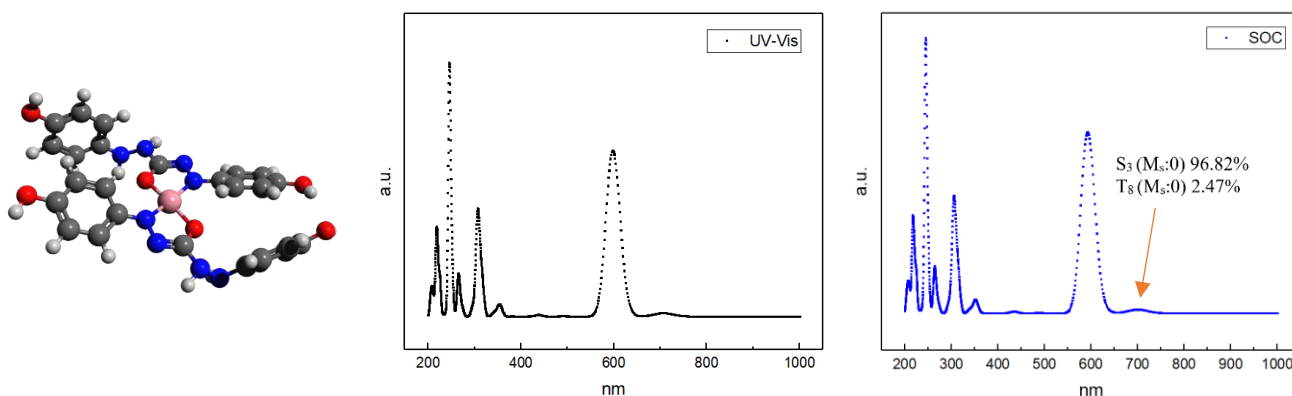


**Figure 43**  
UV-Vis and SOC spectra of  $[\text{Co}(\text{DPC})_2]^-$  with 4 hydroxyl groups

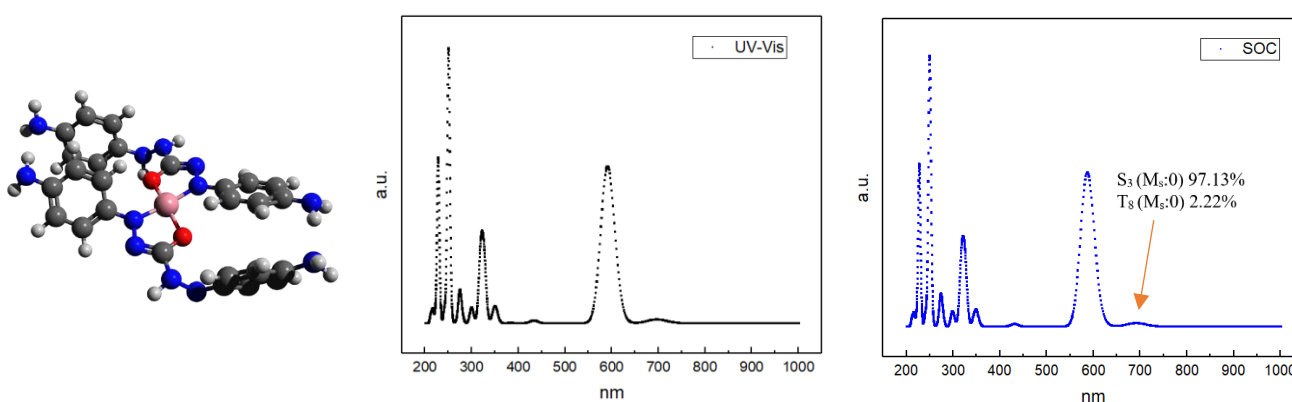


**Figure 44**  
UV-Vis and SOC spectra of  $[\text{Co}(\text{DPC})_2]^-$  with 4 amine groups

#### 4.3.3 Study the complex in different solvents

Solvent-solute interaction can tune the wavelength of absorption and emission spectra, and also, it can have a large impact on the rates or mechanisms of nonradiative transitions, such as intersystem crossing (21). This phenomenon depends strongly on the magnitude and the orientation of the solute's static dipole moments in the ground and excited states (21). Therefore, the solvent-solute interaction can stabilize a state over the other, for instance, solvent reorganization can stabilize the charge distribution in the excited state, destabilizing the ground state (21). The favorable or non-favorable interaction in polar solvents can cause bathochromic or hypsochromic shifts respectively (21). If solvent can interact with the excited states, it is expected that it can modify the SOC effects. Consequently, study the  $[\text{Co}(\text{DPC})_2]^-$  complex in different polar and non-polar solvents is useful to understand how solvents affect SOC effect. In this case, three solvents were studied: water, methanol and hexane, which are very polar, less polar and non-polar respectively.

In all of the cases the complex was simulated using implicit solvent models, and one optimized structure was obtained considering the singlet multiplicity as the ground state. The resulting complex in all cases shows a square plane geometry. With the optimized structure, the corresponding UV-Vis spectra was calculated, as well as the SOC spectrum.

These spectra as well as the optimized structure for each substitution are shown in Figure 44-46. Also, the peaks that show singlet-to-triplet transitions are signaled in each case, and each of these contributions are described in Table 25. The complete description of the transitions associated with the bands in the spectra (between 300 and 850 nm) and the orbitals involved in these transitions are shown in Annexes II.

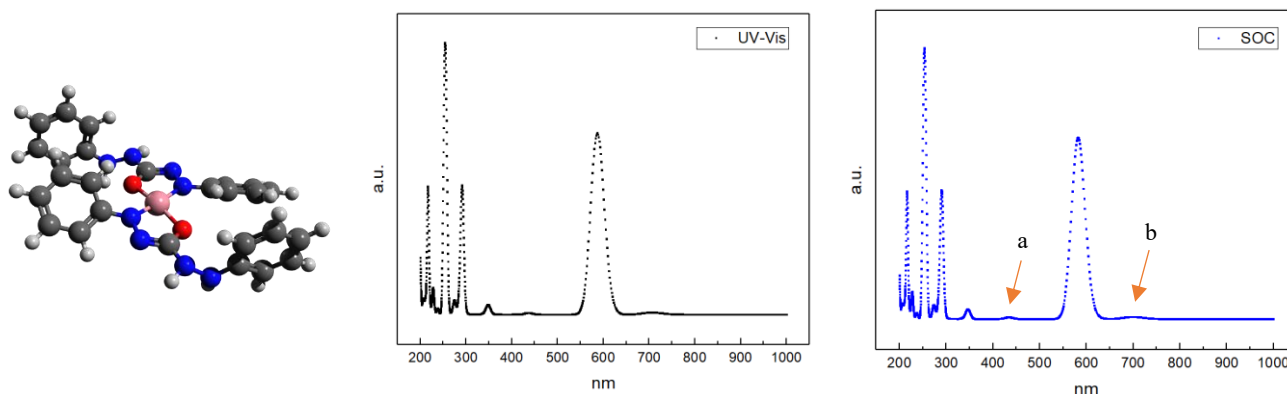


**Figure 45**  
UV-Vis and SOC spectra of  $[\text{Co}(\text{DPC})_2]^-$  in water

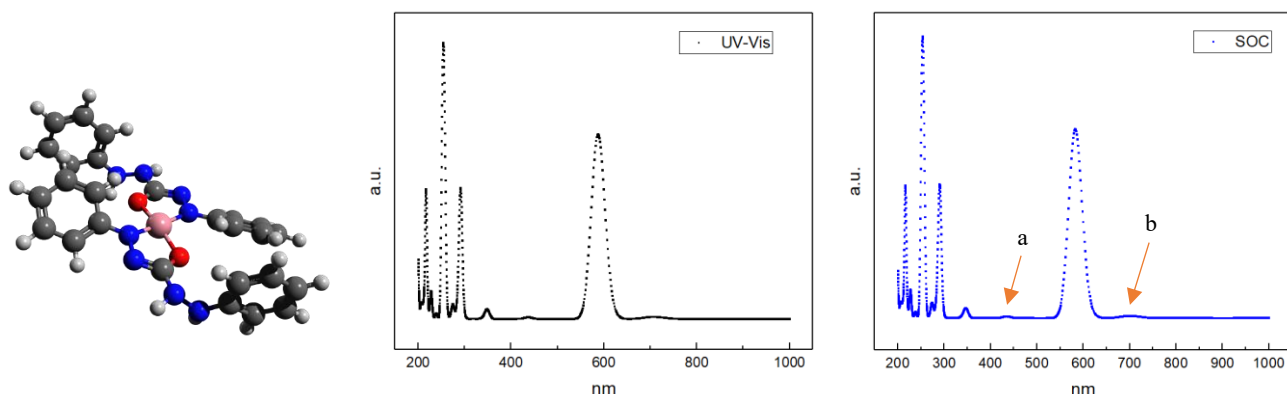


**Figure 46**  
UV-Vis and SOC spectra of  $[\text{Co}(\text{DPC})_2]^-$  in methanol

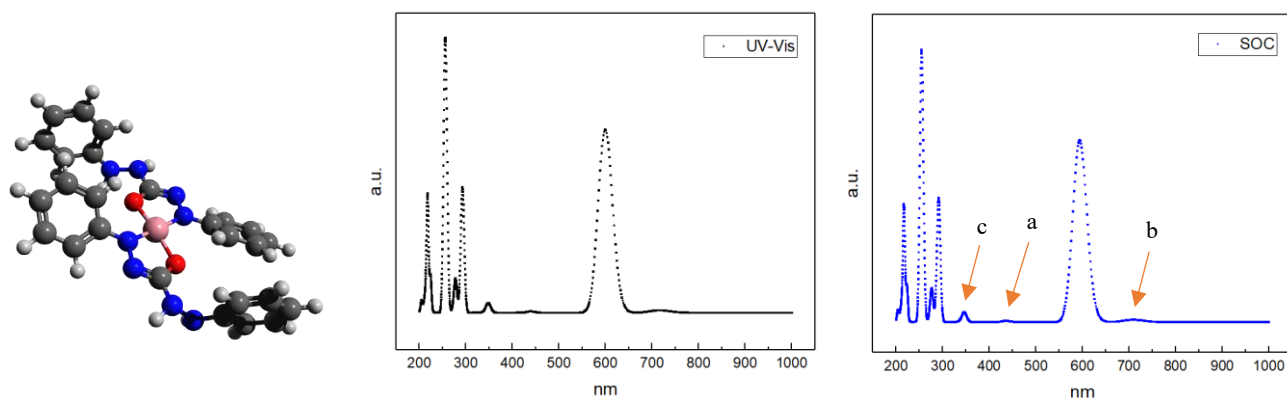


**Figure 47**  
UV-Vis and SOC spectra of  $[\text{Co}(\text{DPC})_2]^-$  in hexane

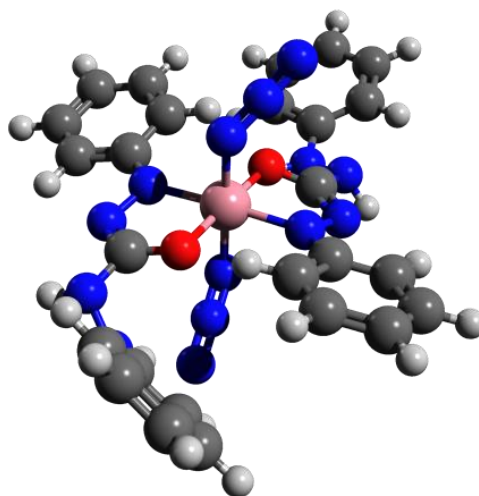
**Table 25**

Description of the peaks that show singlet-to-triplet contributions with different solvents

Solvent	Peak	Wavelength (nm)	Major Contributions
Water	a	433.2	S <sub>6</sub> (M <sub>s</sub> :0) 93.72% T <sub>9</sub> (M <sub>s</sub> :-1) 2.99% T <sub>9</sub> (M <sub>s</sub> :1) 2.99%
	b	699.8	S <sub>3</sub> (M <sub>s</sub> :0) 97.50% T <sub>8</sub> (M <sub>s</sub> :0) 1.86%
Methanol	a	433.3	S <sub>6</sub> (M <sub>s</sub> :0) 93.44% T <sub>9</sub> (M <sub>s</sub> :-1) 3.12% T <sub>9</sub> (M <sub>s</sub> :1) 3.12%
	b	700.2	S <sub>3</sub> (M <sub>s</sub> :0) 97.53% T <sub>8</sub> (M <sub>s</sub> :0) 1.83%
Hexane	c	345.8	S <sub>9</sub> (M <sub>s</sub> :0) 97.43% T <sub>12</sub> (M <sub>s</sub> :-1) 1.21% T <sub>12</sub> (M <sub>s</sub> :1) 1.21%
	a	434.9	S <sub>6</sub> (M <sub>s</sub> :0) 86.16% T <sub>9</sub> (M <sub>s</sub> :-1) 6.59% T <sub>9</sub> (M <sub>s</sub> :1) 6.59%
	b	708.4	S <sub>3</sub> (M <sub>s</sub> :0) 97.98% T <sub>8</sub> (M <sub>s</sub> :0) 1.41%

#### 4.4 Addition of leaving ligands to the Co<sup>3+</sup> complex with diphenylcarbazide

Given the fact that it appears that the complex has a SOC effect that increases its absorbance around 700 nm, it is important to know what would happen if azide ligands are added to the complex, in order to determine if the light absorption of the complex in this range will also favor the release of azide cytotoxic species. Therefore, the complex [Co(DPC)<sub>2</sub>(N<sub>3</sub>)<sub>2</sub>]<sup>3-</sup> was simulated and one optimized structure was obtained (Figure 56), considering the singlet multiplicity as the ground state. The resulting complex shows a octahedral geometry. With the optimized structure, the corresponding UV-Vis spectra was calculated, as well as the SOC spectrum (Figure 57). Also, the transitions associated with the bands in the spectra (between 300 and 850 nm) and the orbitals involved in these transitions will be shown in Tables 26-28.

**Figure 48**Optimized structure of [Co(DPC)<sub>2</sub>(N<sub>3</sub>)<sub>2</sub>]<sup>3-</sup>



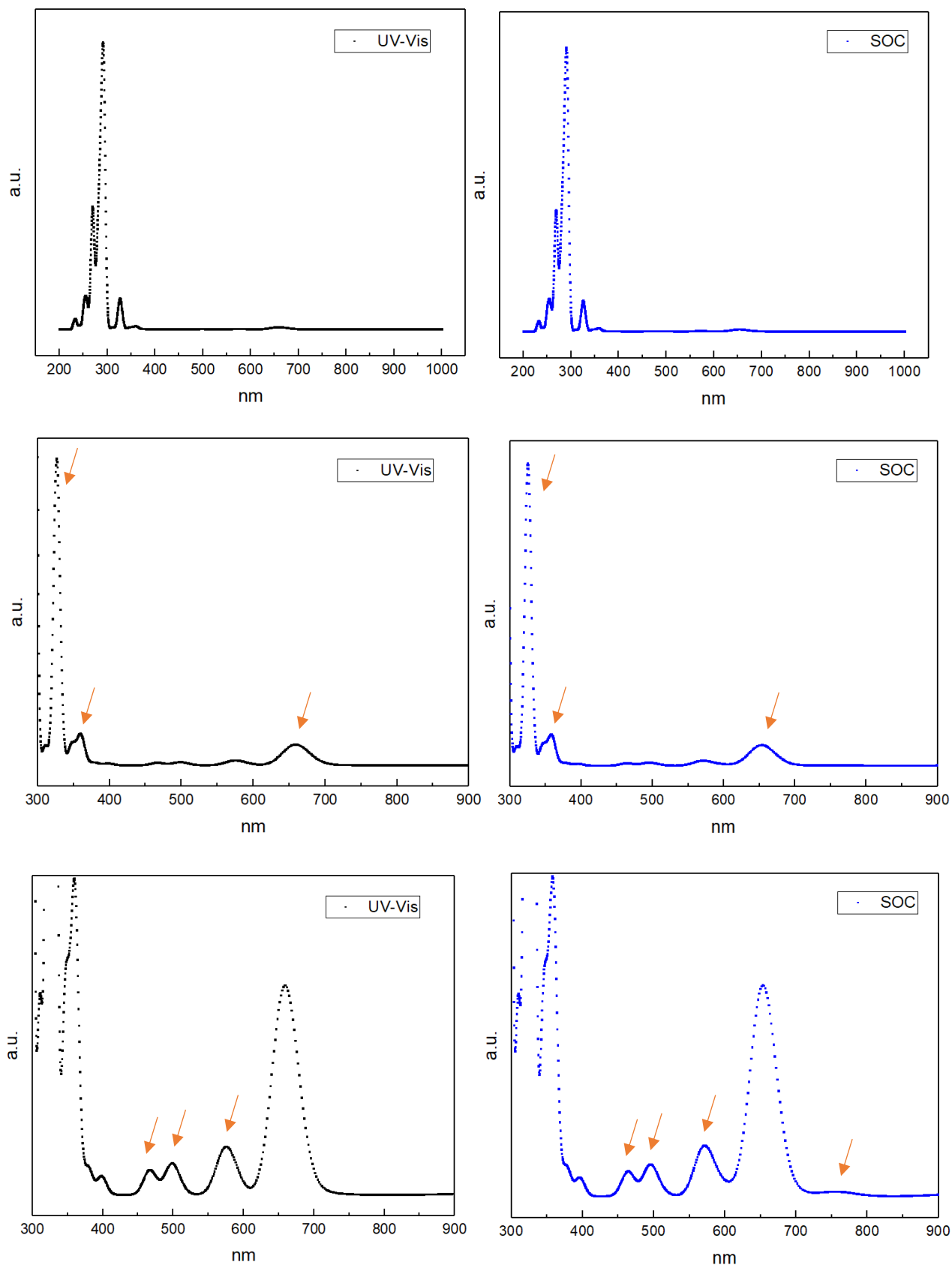


**Figure 49**  
UV-Vis and SOC spectra of  $[\text{Co}(\text{DPC})_2(\text{N}_3)_2]^{3-}$

There are three big peaks observed in the UV-Vis spectra (Figure 57) at 327, 357 and 658 nm. Also, other small peaks are observed.

**Table 26**  
Description of the UV-Vis spectrum transitions of  $[\text{Co}(\text{DPC})_2(\text{N}_3)_2]^{3-}$

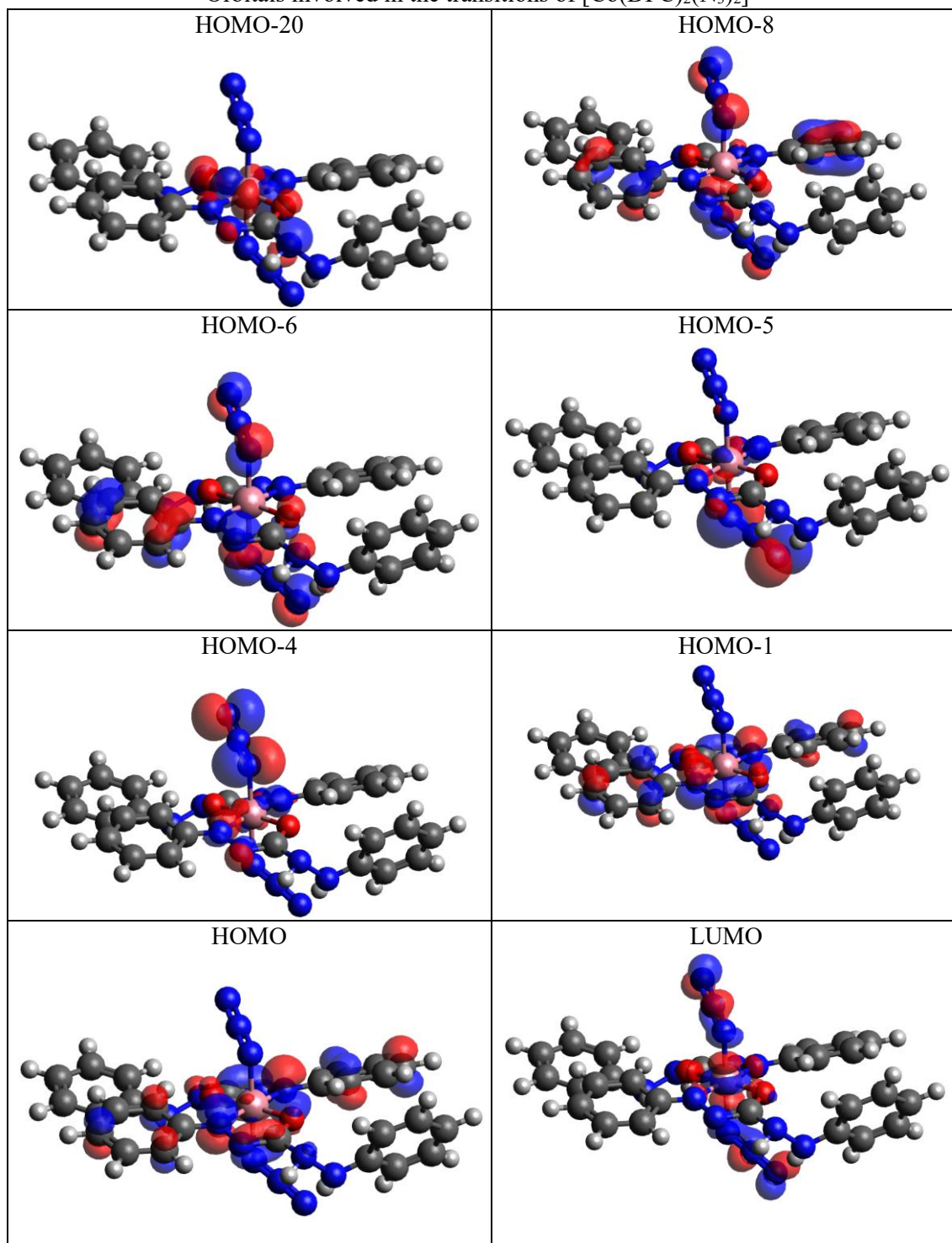
State	Energy (eV)	Wavelength (nm)	Major Contributions	Oscillator Strength
12	3.797	326.5	HOMO → LUMO+7 (25.55%) HOMO → LUMO+6 (17.56%) [Metal to ligand [aromatic rings]]	0.1226
10	3.445	359.9	HOMO-4 → LUMO (42.33%) HOMO-5 → LUMO (12.99%) [Ligand (azide) to metal]	0.0130
7	2.657	466.7	HOMO-1 → LUMO+1 (48.40%) HOMO-20 → LUMO+1 (28.21%) [d-d]	0.0010
6	2.487	498.4	HOMO → LUMO (23.30%) HOMO-5 → LUMO (16.61%) [d-d]	0.0013
5	2.157	574.8	HOMO-1 → LUMO+1 (41.65%) HOMO-20 → LUMO+1 (16.04%) [d-d]	0.0020
3	1.882	658.6	HOMO-1 → LUMO (92.04%) [Ligand (DPC) to metal]	0.0090

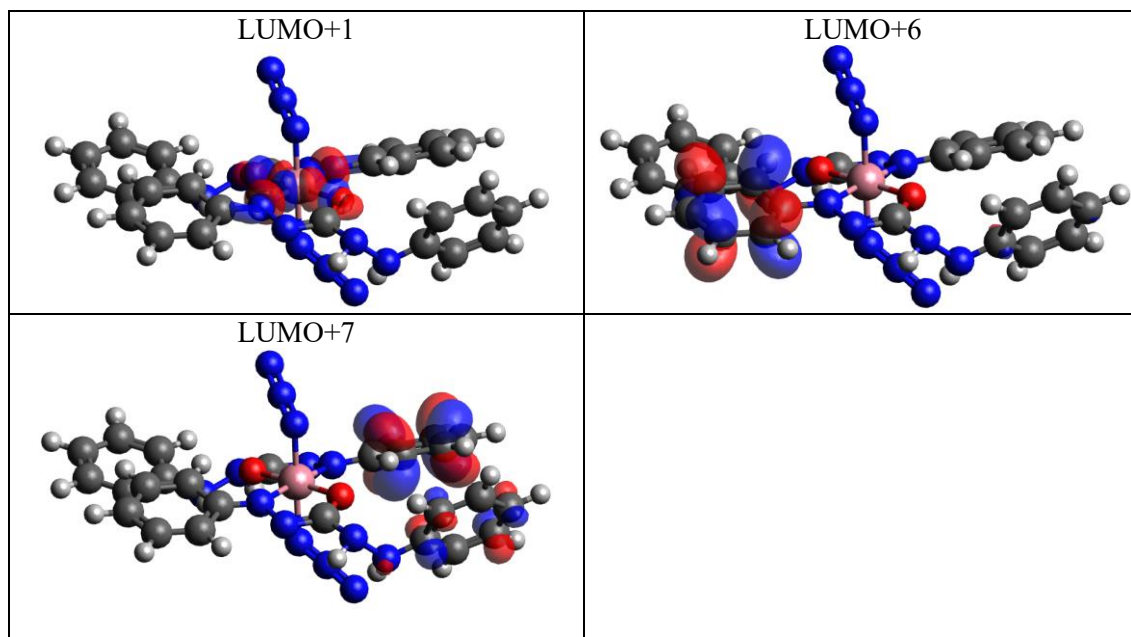
**Table 27**  
Description of the UV-Vis spectrum transitions of  $[\text{Co}(\text{DPC})_2(\text{N}_3)_2]^{3-}$

State	Energy (eV)	Wavelength (nm)	Major Contributions	Oscillator Strength
72	3.813	325.1	S <sub>12</sub> (M <sub>s</sub> :0) 100%	0.1215
58	3.463	358.0	S <sub>10</sub> (M <sub>s</sub> :0) 67.12% T <sub>16</sub> (M <sub>s</sub> :0) 24.66% T <sub>16</sub> (M <sub>s</sub> :1) 4.07% T <sub>16</sub> (M <sub>s</sub> :-1) 4.07%	0.0083
34	2.672	463.9	S <sub>7</sub> (M <sub>s</sub> :0) 98.22%	0.0010
33	2.504	495.0	S <sub>6</sub> (M <sub>s</sub> :0) 99.50%	0.0013
26	2.174	570.3	S <sub>5</sub> (M <sub>s</sub> :0) 98.38%	0.0020
21	1.898	653.0	S <sub>3</sub> (M <sub>s</sub> :0) 99.97%	0.0090
16	1.639	756.2	T <sub>5</sub> (M <sub>s</sub> :0) 84.45% T <sub>5</sub> (M <sub>s</sub> :-1) 7.46% T <sub>5</sub> (M <sub>s</sub> :1) 7.46%	0.0001
<b>State</b>	<b>Major Contributions</b>			
S <sub>3</sub>	HOMO-1 → LUMO (92.04%)			
S <sub>5</sub>	HOMO-1 → LUMO+1 (41.65%) HOMO-20 → LUMO+1 (16.04%)			
S <sub>6</sub>	HOMO → LUMO (23.30%) HOMO-5 → LUMO (16.61%)			
S <sub>7</sub>	HOMO-1 → LUMO+1 (48.40%) HOMO-20 → LUMO+1 (28.21%)			
S <sub>10</sub>	HOMO-4 → LUMO (42.34%)			

	HOMO-5 → LUMO (12.99%)
S <sub>12</sub>	HOMO → LUMO+7 (25.55%) HOMO → LUMO+6 (17.56%)
T <sub>5</sub>	HOMO-1 → LUMO (28.26%) HOMO-20 → LUMO+1 (19.42%)
T <sub>16</sub>	HOMO-6 → LUMO (31.12%) HOMO-8 → LUMO (30.05%)

**Table 28**  
Orbitals involved in the transitions of [Co(DPC)<sub>2</sub>(N<sub>3</sub>)<sub>2</sub>]<sup>3-</sup>





The peaks at 325, 358 and 653 nm in the SOC spectrum are mainly the peaks at 327, 357 and 658 nm in the UV-Vis spectrum, due to the fact that the same transitions contribute in a similar percentage to these peaks. No significant differences are observed between both spectra, which mean that there are no important SOC effects in this case. However, there are some singlet-to-triplet contributions to the peaks and it is also important to mention that a very small peak appears in the SOC spectrum at around 756 nm.

## 4.5 Discussion

### 4.5.1 Obtention of a $\text{Co}^{3+}$ complex with SOC effects

The three studied complexes with  $\text{Co}^{3+}$  show totally different UV-Vis spectra. For the case of the complex with  $\text{CN}^-$ , no transitions in the UV-Vis are observed. In the case of the complex with the same ligands as a known platinum complex, no evident SOC effect is observed but a significant decrease on the singlet-to-singlet transition of one of the peaks. Besides this, the spectrum and the transitions responsible for these peaks are the same. Finally, for the complex of  $\text{Co}^{3+}$  with diphenylcarbazide, in the 2 configurations it is observed a significant decrease on the singlet-to-singlet transition of one of the peaks when SOC effect is considered. Furthermore, the most important SOC effect is the increase in the intensity of a peak around 700 nm, which also shows a small decrease in the singlet-to-singlet transition as well. In conclusion:

- i. Although  $\text{Co}^{3+}$  is expected to show a SOC effect, this effect is also highly ligand dependent
- ii. Two complexes with the same ligands but different metal do not necessarily have the same SOC effect, this effect is also highly metal dependent, as demonstrated with the  $[\text{Co}(\text{N}_3)_2(\text{OH})_2(\text{Py})(\text{MA})]^-$  complex.
- iii. The SOC effect depends on both the metal and the ligands and the synergy between them.

The  $\text{Co}^{3+}$  complex with diphenylcarbazide showed the most promising SOC effect for photoactivation purposes: an increase in the intensity of an absorption peak in the specific wavelength of activation (620-850 nm). Finally, it is noteworthy that even though the experimentally obtained sample has a mixture  $\text{Co}^{2+}$  and  $\text{Co}^{3+}$  species, the  $\text{Co}^{3+}$  complex with diphenylcarbazide is present in the obtained sample and the peak at around 700 nm is observed experimentally as well. Therefore, this complex can be synthesized, and the peak that appears due to SOC effects, expected computationally, is observed experimentally as well. Consequently, relying on computational calculations to predict if a complex has SOC effect is an efficient strategy.

#### 4.5.2 Strategies to enhance SOC effects in the $\text{Co}^{3+}$ complex with diphenylcarbazide

##### 4.5.2.1 Use of different metals

The analysis of  $\text{Cu}^+$ ,  $\text{Co}^{3+}$  and  $\text{Pt}^{4+}$  complexed to two diphenylcarbazide had different results. In the case of  $\text{Pt}^{4+}$ , the most stable structure gave a triplet electronic configuration, so, it wasn't possible to determine the singlet-to-triplet transitions. In the case of  $\text{Co}^{3+}$ , as analyzed before, the SOC effect observed was an increase in the intensity of a peak at 700 nm, the appearance of a singlet-to-triplet contribution in a peak and a small decrease in the singlet-to-singlet transitions. In the case of  $\text{Cu}^+$ , a new peak that has mainly singlet-to-triplet contributions is observed in one of the configurations, and, a small decrease in the singlet-to-singlet transitions was observed. Analyzing the orbitals involved in the transitions, it was possible to determine that in the  $\text{Co}^{3+}$  complex, the triplet contribution that appears is a ligand-to-ligand or ligand-to-metal transition, whereas in the  $\text{Cu}^+$  complex, the triplet contribution is a ligand-to-metal or d-d transition. Both occur in peaks that are around 315-345 nm in their respective UV-Vis spectrum. In conclusion, for the case of the same ligand with different metals:

- i. In the  $\text{Cu}^+$  and  $\text{Co}^{3+}$  complexes, a singlet-to-triplet contribution appears in peaks that are around the same wavelength ( $\sim 300$  nm), which seems to be ligand-to-metal transitions. Probably, the ligand favors the appearance of singlet-to-triplets transitions in the same range. It is noteworthy that the singlet-to-triplet transitions are not always d-d transitions.
- ii. SOC effects are observed at different wavelengths; for  $\text{Co}^{3+}$ : 300-700 nm and for  $\text{Cu}^+$ :  $\sim 300$  nm. Therefore, it seems that the SOC effects in the  $\text{Cu}^+$  complex appear due to the ligand while in the  $\text{Co}^{3+}$  complex they appear due to the ligand and the metal.
- iii. SOC effect is metal dependent.

The  $\text{Co}^{3+}$  complex with diphenylcarbazide shows SOC effects at higher frequencies ( $\sim 700$  nm), so, it is more useful for photoactivation purposes given that it absorbs in the desired wavelength.

##### 4.5.2.2 Use of different aromatic ring substitutions

The analysis of the  $\text{Co}^{3+}$  complex with diphenylcarbazide with different ring substitutions showed different UV-Vis spectra for each case. In all of the cases, the 4 peaks of the original complex were maintained ( $\sim 340$ ,  $\sim 440$ ,  $\sim 550$  and  $\sim 717$  nm). Also, in some cases

a peak at ~300 nm appeared. These peaks are result of transitions between other orbitals different to the original complex, and different between each substituent used, except for the peak at ~550 nm, that is always result of a HOMO→LUMO transition. The peaks showed a shift in the UV-Vis spectra, and in some cases, an important increase in the intensity was observed. For example, for the substituents: nitro, cyanide, amine and hydroxyl, the peak at ~730 nm showed wavelengths of 758, 734, 690 and 700 nm, and intensities of 0.1, 0.06, 0.013 and 0.011 respectively, compared to the intensity of this peak in the original complex of 717 nm and 0.006. Also, it is important to mention that in the case of the nitro substituents, two peaks appeared at 357 and 368 nm instead of the single peak observed in the original complex at 340 nm with an important increase in intensity (0.15 and 0.39 vs. 0.03). These peaks are the result of ligand-to-ligand transitions concentrated on the nitro groups. Finally, in all of the cases, the SOC effect observed was a small decrease in the singlet-to-singlet transitions and the appearance of a small singlet-to-triplet contribution in different peaks for deactivating and activating substituents. For instance, this singlet-to-triplet transition appeared in the peak at ~400 nm in the complex with nitro (T<sub>11</sub>), cyanide and methyl (T<sub>9</sub>) and in the peak at ~700 nm in the complex with hydroxyl and amine (T<sub>8</sub>) with different contribution percentage: 8.74%, 11.88%, 3.32%, 2.47% and 2.22% respectively. No new peaks nor increase of intensity was observed in any case. In conclusion, taking into account that the substituents hydroxyl and amine are the most activating and cyanide and nitro are the most deactivating:

- i. The aromatic ring substitutions show significant changes in the UV-Vis spectrum with respect to the UV-Vis spectrum of the original complex, showing shifts and increase of intensity of the peaks.
- ii. SOC effects increase slightly with the addition of aromatic ring substituents. It is probable that the effect is more significant if the aromatic ring is directly coordinated to the metal.
- iii. The effect caused by the addition of the substituents happens only when they are in the aromatic ring, not when they are directly complexed to the metal, as it was possible to see in the complex [Co(CN)<sub>6</sub>]<sup>3-</sup>.
- iv. The total percentage of singlet-to-triplet transitions increases as the substituent is more deactivating (11.88% for nitro and 2.22% for amine) as shown in Figure 58.

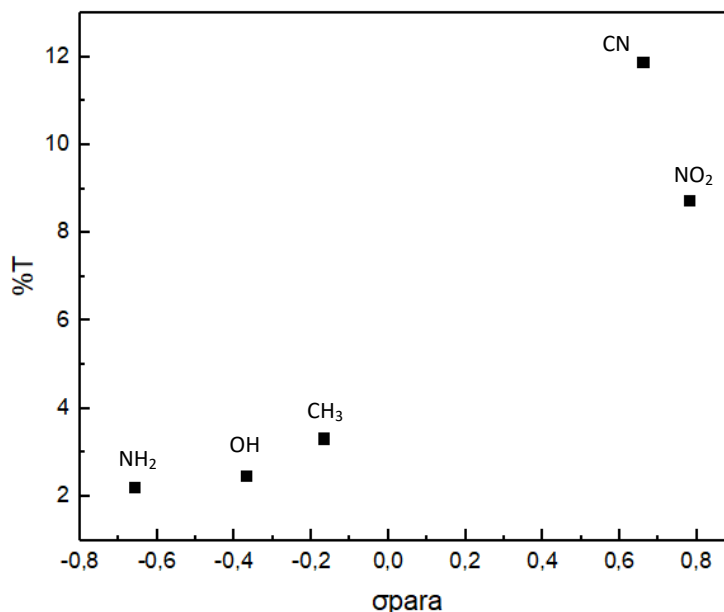


**Figure 50**

Plot of the Hammett Sigma Constants of the aromatic substituents vs. the triplet contribution

- v. The singlet-to-triplet transitions appear at different peaks depending on the nature of the substituent: around  $\sim 700$  nm for activating and around  $\sim 400$  nm for deactivating substituents.
- vi. The singlet-to-triplet transitions in the peaks around  $\sim 700$  nm have a spin multiplicity ( $M_s$ ) of 0, whereas the transitions in the peaks around  $\sim 400$  nm have  $M_s=1,-1$  as shown in Annexes (Annexes I). Moreover, the singlet-to-triplet transitions with  $M_s=1,-1$  have higher contribution percentage to the peak than the transitions with  $M_s=0$ .
- vii. The different SOC effect observed with the substituents can be explained by analyzing the orbitals involved in the singlet-to-triplet transitions (Annexes I). In all of the cases, the HOMO is localized in the metal and in the atoms to which it is complexed. On the contrary, the LUMO changes depending on the substituent: in deactivating substituents the LUMO is more localized in the metal whereas in activating substituents the LUMO is delocalized in the metal and in the aromatic rings (Figure 51). Therefore, the substituents affect the LUMO delocalization.
- viii. For photoactivation purposes it is more useful to favor singlet-to-triplet contributions with  $M_s=0$  using activating substituents (that delocalize the LUMO), given the fact that they appear at peaks around  $\sim 700$  nm, which is in the specific wavelength of activation (620-850 nm).

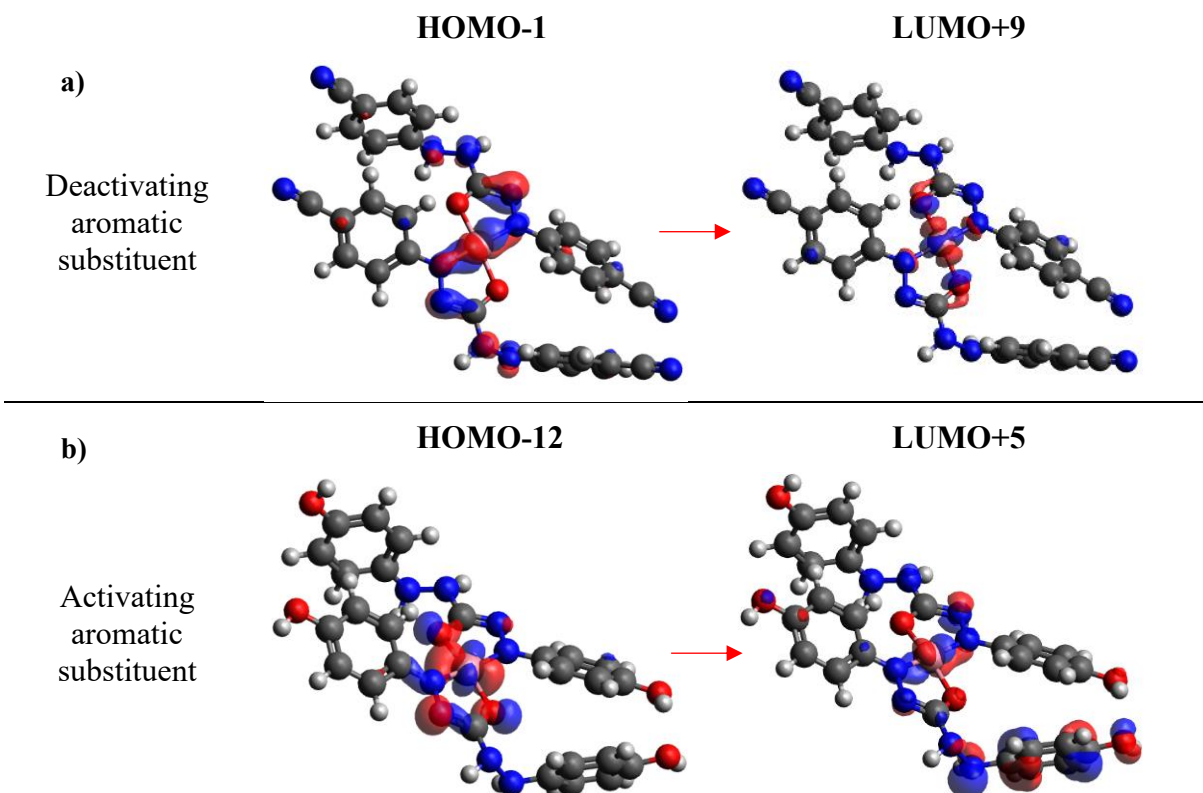


**Figure 51**

Orbitals involved in the singlet-to-triplet transitions of aromatic substituents: a) cyanide and b) hydroxyl.

#### 4.5.2.3 Use of different solvents

The study of the  $\text{Co}^{3+}$  complex with diphenylcarbazide with different solvents showed similar UV-Vis spectra compared to the original complex (studied in ethanol). In all of the cases, 4 of the peaks present in the original spectra are maintained, but the orbitals involved in the transitions responsible for these peaks change depending on the solvent. The change in the orbitals involved in the transitions is more significant for apolar solvents (hexane). Also, the SOC effects observed with the change of solvents are a little shift in the peaks' wavelengths, a decrease in the singlet-to-singlet contribution to the peaks and the appearance of a singlet-to-triplet transition in different peaks depending on the solvent. In water, a singlet-to-triplet transition appears in the peak at  $\sim 700$  nm (1.86%). In methanol, singlet-to-triplet transitions appear in the peak at  $\sim 700$  nm (1.83%) and in the peak at  $\sim 433$  nm (6.24%). In hexane, singlet-to-triplet transitions appear in the peak at  $\sim 700$  nm (1.41%), in the peak at  $\sim 433$  nm (13.18%) and in the peak at  $\sim 345$  nm (2.42%). It is also important to mention that the transitions are mostly d-d, except for the singlet-to-triplet transition for the peak at  $\sim 345$  nm with hexane, which appears to be metal to ligand. In conclusion, for the case of the  $\text{Co}^{3+}$  complex with different solvents:

- i. The change of the solvent modifies the orbitals involved in the transitions responsible for the peaks observed.



- ii. Even though no new peaks nor a change in intensity is observed in the SOC spectra with different solvents, singlet-to-triplet transitions appear in the peaks that are maintained.
- iii. The total percentage of singlet-to-triplet transitions increases with the apolarity of the solvent.
- iv. The singlet-to-triplet transitions appear at different peaks depending on the solvent: for water and methanol these transitions appear in the peaks at around ~700 and 400 nm, whereas for hexane they appear in the peaks at around ~700, 400 and 300 nm.
- v. The singlet-to-triplet transitions appear at different percentage in the peaks depending on the solvent. The singlet-to-triplet transitions in the peaks around ~700 nm have  $M_s=0$ , whereas the transitions in the peaks around ~400 and 300 nm have  $M_s=1,-1$  as shown in Annexes I. The percentage of the transitions with  $M_s=0$  increases with polarity, whereas the percentage of the transitions with  $M_s=1,-1$  increase with apolarity.
- vi. For photoactivation purposes it is more useful to favor singlet-to-triplet contributions with  $M_s=0$  using polar solvents, given the fact that they appear at peaks around ~700 nm, which is in the specific wavelength of activation (620-850 nm).

#### 4.5.3 Addition of a leaving ligand to the $\text{Co}^{3+}$ complex with diphenylcarbazide

The addition of the azide ligands into the complex  $[\text{Co}(\text{DPC})_2(\text{N}_3)_2]^{3-}$  cause significant changes in the UV-Vis spectrum. Three peaks with considerable intensity are observed at different values (326, 359 and 658 nm) and with different orbitals involved. It is important to mention that an important singlet-to-triplet transition appears in the peak at 359 nm (32.8%). Also, a new very small peak appears in the SOC spectrum at around 756 nm that is the result of singlet-to-triplet transitions. Therefore, the complex shows important SOC effects.

Regarding the dissociation of the azide ligand, it is useful to refer to the study of the platinum complex *trans,trans,trans*- $[\text{Pt}(\text{N}_3)_2(\text{OH})_2(\text{Py})(\text{MA})]$ . This prodrug for photoactivation has 3 important peaks in the SOC spectrum: 1 peak is maintained from the UV-Vis spectrum while the other 2 are mainly of singlet-to-triplet transitions (348, 384 and 415 nm respectively). The transitions responsible for these 3 peaks favor the dissociation of the azide ligands. Therefore, SOC effects in this case contribute by making more dissociation channels available for this complex. However, it is important to mention that the absorption peaks for this complex are not in the specific wavelength of activation (620-850 nm). The complete description of the electronic transitions and the orbitals involved in them is shown in Annexes (Annexes III).

On the other hand, the study of the  $[\text{Co}(\text{DPC})_2(\text{N}_3)_2]^{3-}$  complex showed that two of the most intense peaks have transitions involved that favor the azide ligand dissociation (359 and 658 nm). The SOC effect contributes with an important singlet-to-triplet contribution to one of these peaks (359 nm), which also favors the azide dissociation. In addition, a very small new peak appears around 750 nm, which also favors the azide dissociation. Therefore, SOC effects contribute with more dissociation channels for this ligand. It is noteworthy that two peaks that favor the azide dissociation (the peaks at 658 and 750 nm)

are in the correct and desired range for photoactivation. Therefore, this complex could be a potential prodrug for photoactivation.

## Chapter 5: Conclusions

---

1. The  $\text{Co}^{3+}$  complex with diphenylcarbazide  $[\text{Co}(\text{DPC})_2]^-$  shows a SOC effect in the desired range for photoactivation: an increase in the intensity of an absorbance peak at around 700 nm. It is noteworthy that this complex can be synthesized and that the peak at 700 nm is observed experimentally.
2. The SOC effects in  $[\text{Co}(\text{DPC})_2]^-$  change by varying the metal, ligands, aromatic substituents and the solvent. From this study, the following can be stated on the strategies to enhance SOC effect for photoactivation purposes in metallic complexes (in order of importance on SOC effect):
  - i. Metals present specific SOC effects depending on the ligand to which they are complexed
  - ii. The ligands present specific SOC effects depending on the metal to which they are complexed, but they are always present at low wavelengths.
  - iii. The use of activating aromatic ring substituents favor singlet-to-triplet transitions with  $M_s=0$ , which occur in peaks at around ~700 nm.
  - iv. The use of polar solvents favor singlet-to-triplet transitions with  $M_s=0$ , which occur in peaks at around ~700 nm.
3. The addition of azide ligands to the  $[\text{Co}(\text{DPC})_2]^-$  complex with diphenylcarbazide gives a potential prodrug for photoactivation, since one of the absorption peaks that favor the azide dissociation is in the accepted range for photoactivation. Moreover, the presence of singlet-to-triplet transitions that favors the azide dissociation contributes with more dissociation channels. Therefore, the complex  $[\text{Co}(\text{DPC})_2(\text{N}_3)_2]^{3-}$  shows promising photoactivation potential.

Finally, based on this study, a general strategy for the construction of metallic prodrugs for photoactivation is presented:

- 1) Choose a metal that is expected to have SOC effects.
- 2) Choose a ligand that favors absorption of the complex in the desired range and that has SOC effect when complexed to the metal.
- 3) Add a ligand that can dissociate to form cytotoxic radicals.
- 4) If aromatic rings are present, add activating substituents on them to increase SOC effects in the desired wavelength of activation and increase the available dissociation channels.
- 5) Use a polar solvent to favor the singlet-to-triplet transitions in the desired wavelength of activation and increase the available dissociation channels.

## Chapter 6: Bibliography

---

- (1) Pucci, C.; Martinelli, C.; Ciofani, G. Innovative Approaches for Cancer Treatment: Current Perspectives and New Challenges. *Ecancermedicalscience* **2019**, *13*. <https://doi.org/10.3332/ecancer.2019.961>.
- (2) *What Is Cancer?* National Cancer Institute. <https://www.cancer.gov/> (accessed 2023-06-12).
- (3) Shi, H.; Imberti, C.; Sadler, P. J. Diazido platinum(IV) complexes for photoactivated anticancer chemotherapy. *Inorg. Chem. Front.* **2019**, *6* (7). DOI: 10.1039/c9qi00288j
- (4) Foresto, E.; Gilardi, P.; Ibarra, L. E.; Cogno, I. S. Light-activated green drugs: How we can use them in photodynamic therapy and mass-produce them with biotechnological tools. *Phytomed. Plus* **2021**, *1* (3). DOI: 10.1016/j.phyplu.2021.100044
- (5) Gallaga-González, U.; Morales-Avila, E.; Torres-García, E.; Estrada, J. A.; Díaz-Sánchez, L. E.; Izquierdo, G.; Aranda-Lara, L.; Isaac-Olivé, K. Photoactivation of Chemotherapeutic Agents with Cerenkov Radiation for Chemo-Photodynamic Therapy. *ACS Omega* **2022**. DOI: 10.1021/acsomega.2c02153
- (6) Shi, H.; Sadler, P. J. How promising is phototherapy for cancer? *Br. J. Cancer* **2020**, *123* (6), 871–873. DOI: 10.1038/s41416-020-0926-3
- (7) Yang, Z.; Zhang, Z.; Sun, Y.; Lei, Z.; Wang, D.; Ma, H.; Tang, B. Z. Incorporating spin-orbit coupling promoted functional group into an enhanced electron D-A system: A useful designing concept for fabricating efficient photosensitizer and imaging-guided photodynamic therapy. *Biomaterials* **2021**, *275*. DOI: 10.1016/j.biomaterials.2021.120934
- (8) *23.1: Metal Complexes*. Chemistry LibreTexts. <https://chem.libretexts.org/> (accessed 2023-06-12).
- (9) Dickerson, R.; Gray, H.; Haight, G. *Chemical principles*; The Benjamin/Cummings Publishing Company, Inc., **1979**. Chapter 20. Inorganic Complexes
- (10) Nandy, A.; Duan, C.; Taylor, M. G.; Liu, F.; Steeves, A. H.; Kulik, H. J. Computational Discovery of Transition-metal Complexes: From High-throughput Screening to Machine Learning. *Chem. Rev.* **2021**, *121* (16). DOI: 10.1021/acs.chemrev.1c00347
- (11) *Electronic Spectra of Complexes*. Al-Mustansiriyah University. <https://uomustansiriyah.edu.iq/> (accessed 18/06/2023).
- (12) *Chapter 20: d-block metal chemistry: coordination complexes*. University of North Florida. <https://www.unf.edu/> (accessed 18/06/2023).
- (13) Prof. Dr. A. DAYALAN. *15-(SP-1): ELECTRONIC SPECTRA OF METAL COMPLEXES*. PROPERTIES OF CHEMISTRY(PoC). <https://dradchem.wordpress.com/> (accessed 2023-06-12).
- (14) *11.3.1: Selection Rules*. Chemistry LibreTexts. <https://chem.libretexts.org/> (accessed 18/06/2023).
- (15) Dalal, M. *A textbook of inorganic chemistry-Volume I*; Dalal Institute, n.d. Chapter 8. Electronic Spectra of Transition Metal Complexes

- (16) *Forbidden transitions*. Oxford Reference, <https://www.oxfordreference.com/> (accessed 18/06/2023).
- (17) Freitag, L.; González, L. The Role of Triplet States in the Photodissociation of a Platinum Azide Complex by a Density Matrix Renormalization Group Method. *J. Phys. Chem. Lett.* **2021**, *12* (20). DOI: 10.1021/acs.jpcclett.1c00829
- (18) Farrer, N. J.; Salassa, L.; Sadler, P. J. Photoactivated chemotherapy (PACT): the potential of excited-state d-block metals in medicine. *Dalt. Trans.* **2009**, (48). DOI: 10.1039/b917753a
- (19) Imran, M.; Ayub, W.; Butler, I. S.; Zia-ur-Rehman. Photoactivated platinum-based anticancer drugs. *Coord. Chem. Rev.* **2018**, *376*. DOI: 10.1016/j.ccr.2018.08.009
- (20) Marian, C. M. Spin-orbit coupling and intersystem crossing in molecules. *Wiley Interdiscip. Rev.* **2011**, *2* (2). DOI: 10.1002/wcms.83
- (21) Marian, C. M. Understanding and Controlling Intersystem Crossing in Molecules. *Annu. Rev. Phys. Chem.* **2021**, *72* (1). DOI: 10.1146/annurev-physchem-061020-053433
- (22) Ito, A.; Tanaka, K. Applications of Carbon Nanotubes and Graphene in Spin Electronics. En *Carbon Nanotubes and Graphene*; Elsevier, **2014**. DOI: 10.1016/b978-0-08-098232-8.00011-5
- (23) Majumdar, S.; Majumdar, H. S.; Österbacka, R.; McCarthy, E. Organic Spintronics. En *Reference Module in Materials Science and Materials Engineering*; Elsevier, **2016**. DOI: 10.1016/b978-0-12-803581-8.00577-4
- (24) Browne, A. J.; Krajewska, A.; Gibbs, A. S. Quantum materials with strong spin-orbit coupling: challenges and opportunities for materials chemists. *J. Mater. Chem. C* **2021**, *9* (35). DOI: 10.1039/d1tc02070f
- (25) Jo, D.; Go, D.; Lee, H.-W. Gigantic intrinsic orbital Hall effects in weakly spin-orbit coupled metals. *Phys. Rev. B* **2018**, *98* (21). DOI: 10.1103/physrevb.98.214405
- (26) Stephen Remillard. *Spin-Orbit Coupling, PHYS 372*. YouTube, March 26, 2021. <https://www.youtube.com/watch?v=BkqYa9i79eI> (accessed 2023-07-17).
- (27) Cooper, D. L.; Stutchbury, N. C. J.; Richards, W. G. The spin-orbit interaction in the  $\pi^* \rightarrow n$  phosphorescence of formaldehyde. *J. Chem. Phys.* **1982**, *76* (9). DOI: 10.1063/1.443548
- (28) Pedash, Y. F.; Prezhdo, O. V.; Kotelevskiy, S. I.; Prezhdo, V. V. Spin-orbit coupling and luminescence characteristics of conjugated organic molecules. I. Polyacenes. *J. Mol. Struct.* **2002**, *585* (1-3). DOI: 10.1016/s0166-1280(02)00035-0
- (29) Contributors to Wikimedia projects. *Internal conversion (chemistry) - Wikipedia*. Wikipedia, the free encyclopedia, August 2, **2005**. <https://en.wikipedia.org/> (accessed 2023-07-17).
- (30) Zvyagin, A. V.; Manson, N. B. Optical and Spin Properties of Nitrogen-Vacancy Color Centers in Diamond Crystals, Nanodiamonds, and Proximity to Surfaces. En *Ultananocrystalline Diamond*; Elsevier, **2012**. DOI: 10.1016/b978-1-4377-3465-2.00010-4
- (31) Lefebvre-Brion, H.; Field, R. W. Dynamics. En *The Spectra and Dynamics of Diatomic Molecules*; Elsevier, **2004**. DOI: 10.1016/b978-012441455-6/50012-3

- (32) *Intersystem crossing*. Oxford Reference, n.d. <https://www.oxfordreference.com/> (accessed 18/06/2023).
- (33) Cárdenas, P. Theoretical study on the Photoactivated anticancer drugs based on platinum coordination compounds. Chemistry degree, University Yachay Tech, Urcuqui, **2020**.
- (34) Mojet, B. L.; Ebbesen, S. D.; Lefferts, L. Light at the interface: the potential of attenuated total reflection infrared spectroscopy for understanding heterogeneous catalysis in water. *Chem. Soc. Rev.* **2010**, *39* (12). DOI: 10.1039/c0cs00014k
- (35) Nicolini, M.; Pecile, C.; Turco, A. A high spin-low spin conformational equilibrium in the complex dithiocyanatobis(triethylphosphine)cobalt(II). *Coord. Chem. Rev.* **1966**, *1* (1-2). DOI: 10.1016/s0010-8545(00)80166-6
- (36) Collins, T. J.; Richmond, T. G.; Santarsiero, B. D.; Treco, B. G. R. T. Paramagnetic cobalt(III) complexes of polyanionic chelating ligands. *J. Am. Chem. Soc.* **1986**, *108* (8). DOI: 10.1021/ja00268a058
- (37) Liu, X.; Xu, Z.; Cole, J. M. Molecular Design of UV-vis Absorption and Emission Properties in Organic Fluorophores: Toward Larger Bathochromic Shifts, Enhanced Molar Extinction Coefficients, and Greater Stokes Shifts. *J. Phys. Chem. C* **2013**, *117* (32). DOI: 10.1021/jp404170w
- (38) *Hammett Sigma Constants*. <http://www.wiredchemist.com/> (accessed 18/06/2023).
- (39) Qiu, W.; Cai, X.; Chen, Z.; Wei, X.; Li, M.; Gu, Q.; Peng, X.; Xie, W.; Jiao, Y.; Gan, Y.; et al. A “Flexible” Purely Organic Molecule Exhibiting Strong Spin-Orbital Coupling: Toward Nondoped Room-Temperature Phosphorescence OLEDs. *J. Phys. Chem. Lett.* **2022**. DOI: 10.1021/acs.jpcclett.2c01205
- (40) Grimme, S.; Ehrlich, S.; Lars Goerigk. Effect of the Damping Function in Dispersion Corrected Density Functional Theory. *Journal of Computational Chemistry* **2011**, *32* (7). <https://doi.org/10.1002/jcc.21759>.
- (41) Grimme, S.; Antony, J.; Ehrlich, S.; Krieg, H. A Consistent and Accurate *Ab Initio* Parametrization of Density Functional Dispersion Correction (DFT-D) for the 94 Elements H-Pu. *Journal of Chemical Physics* **2010**, *132* (15). <https://doi.org/10.1063/1.3382344>.
- (42) Florian Weigend; Ahlrichs, R. Balanced Basis Sets of Split Valence, Triple Zeta Valence and Quadruple Zeta Valence Quality for H to Rn: Design and Assessment of Accuracy. *Physical Chemistry Chemical Physics* **2005**, *7* (18). <https://doi.org/10.1039/b508541a>.
- (43) Florian Weigend. Accurate Coulomb-Fitting Basis Sets for H to Rn. *Physical Chemistry Chemical Physics* **2006**, *8* (9). <https://doi.org/10.1039/b515623h>.
- (44) Lampman, G. M.; Kriz, G. S.; Pavia, D. L.; Vyvyan, J. A. *Introduction to Spectroscopy*; Brooks/Cole, **2013**.
- (45) Bain, G. A.; Berry, J. F. Diamagnetic Corrections and Pascal's Constants. *J. Chem. Educ.* **2008**, *85* (4), 532. DOI: 10.1021/ed085p532
- (46) Baldenebro-Lopez, J.; Flores-Holguin, N.; Castorena-Gonzalez, J.; Almaral-Sanchez, J.; Glossman-Mitnik, D. Theoretical Study of Copper Complexes: Molecular Structure, Properties, and Its Application to Solar Cells. *Int. J. Photoenergy* **2013**, *2013*. DOI: 10.1155/2013/613064

- (47) Campagna, S.; Puntoriero, F.; Nastasi, F.; Bergamini, G.; Balzani, V. Photochemistry and Photophysics of Coordination Compounds: I & II. *Springer eBooks* **2007**, Vol I. DOI:10.1007/128\_2007\_133.
- (48) Campagna, S.; Puntoriero, F.; Nastasi, F.; Bergamini, G.; Balzani, V. Photochemistry and Photophysics of Coordination Compounds: I & II. *Springer eBooks* **2007**, Vol II. DOI: 10.1007-978-3-540-73349-2.

## ANNEXES

### I. Computational study of $[\text{Co}(\text{DPC})_2]^-$ with different ring substitutions

In all of the cases the complex was simulated and one optimized structure was obtained, considering the singlet multiplicity as the ground state. The resulting complex in all cases shows a square plane geometry. With the optimized structure, the corresponding UV-Vis spectra was calculated, as well as the SOC spectrum. The transitions of the spectra (between 300 and 850 nm) will be described in detail and the orbitals involved in these transitions will be shown as well.

#### I.1 Nitro-DPC

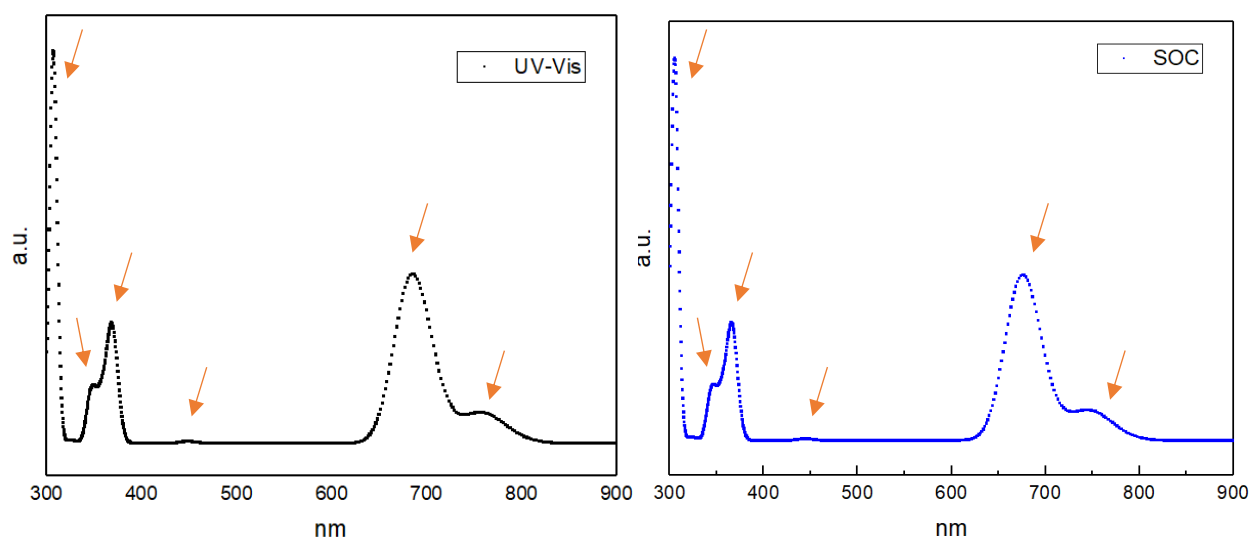


**Figure 1**

UV-Vis and SOC spectra of  $[\text{Co}(\text{DPC})_2]^-$  with 4 nitro groups

There are five peaks observed in the UV-Vis spectra (Figure 1) at 347, 369, 450, 685 and 760 nm.

**Table 1**

Description of the UV-Vis spectrum transitions of  $[\text{Co}(\text{DPC})_2]^-$  with 4 nitro groups

State	Energy (eV)	Wavelength (nm)	Major Contributions	Oscillator Strength
18	4.038	307.1	HOMO-7 $\rightarrow$ LUMO (29.81%) [Ligand to metal] HOMO-3 $\rightarrow$ LUMO+2 (19.10%) [Ligand to ligand]	1.1514
12	3.465	357.8	HOMO $\rightarrow$ LUMO+2 (35.63%) [Ligand to ligand] HOMO-1 $\rightarrow$ LUMO+9 (24.39%) [d-d]	0.1538
9	3.361	368.9	HOMO $\rightarrow$ LUMO+2 (57.56%) [Ligand to ligand] HOMO $\rightarrow$ LUMO+4 (26.27%) [Ligand to metal]	0.3980
6	2.765	448.3	HOMO-4 $\rightarrow$ LUMO+9 (32.27%) HOMO-12 $\rightarrow$ LUMO (26.94%)	0.0071



			[d-d]	
4	1.810	685.0	HOMO → LUMO (74.87%) [Ligand to metal]	0.5936
3	1.635	758.3	HOMO-12 → LUMO (29.94%) HOMO-4 → LUMO+9 (16.15%) [d-d]	0.1058

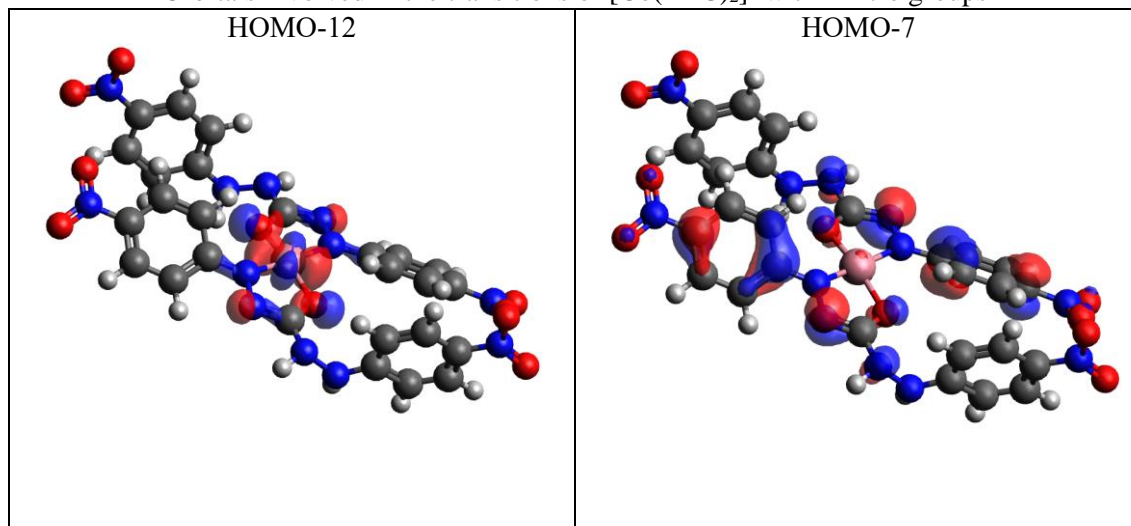
**Table 2**

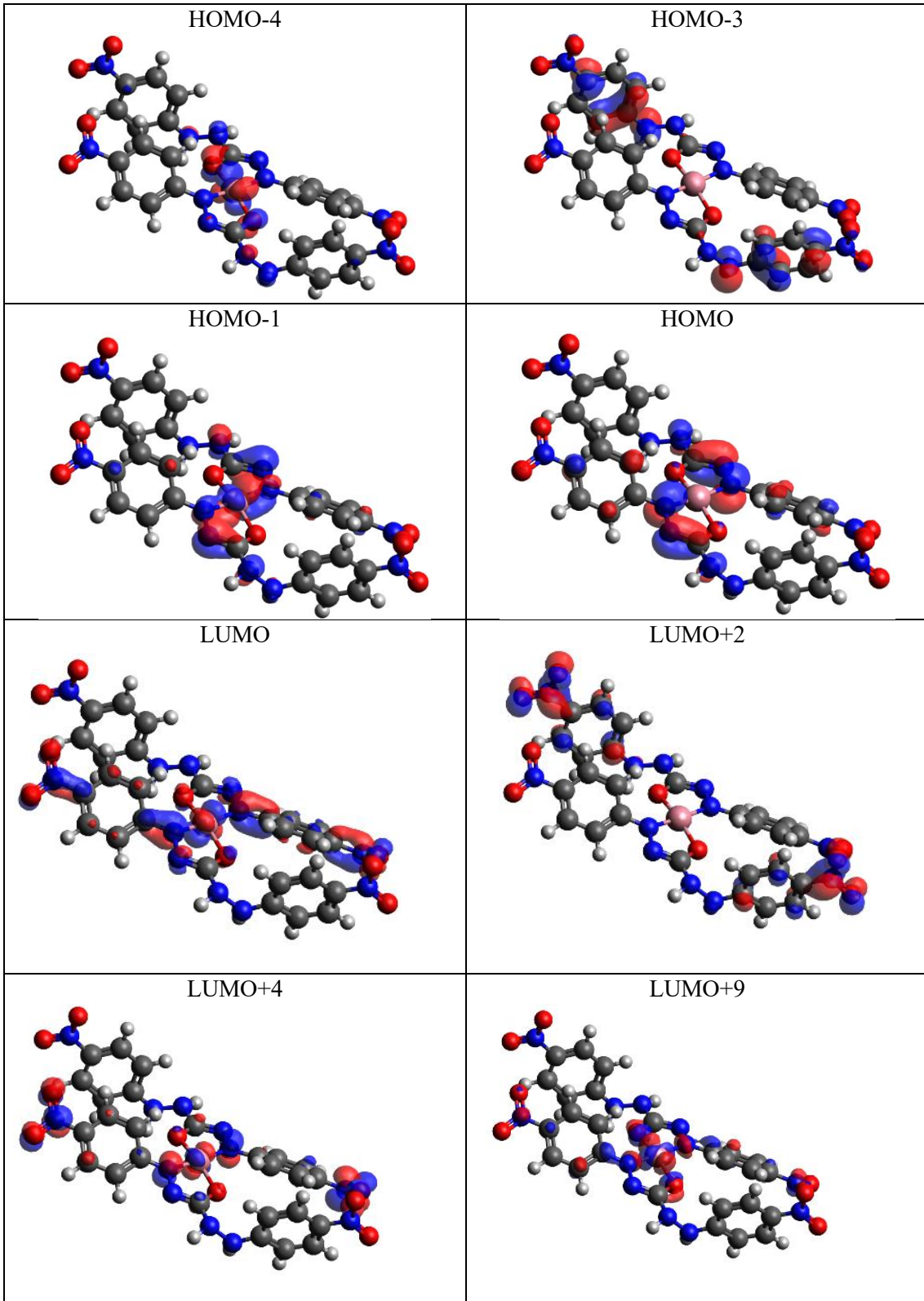
Description of the UV-Vis spectrum transitions of  $[\text{Co}(\text{DPC})_2]^-$  with 4 nitro groups

State	Energy (eV)	Wavelength (nm)	Major Contributions	Oscillator Strength
114	4.063	305.1	S <sub>18</sub> (M <sub>s</sub> :0) 99.64%	1.0525
60	3.490	355.2	S <sub>12</sub> (M <sub>s</sub> :0) 99.79%	0.1431
48	3.386	366.2	S <sub>9</sub> (M <sub>s</sub> :0) 99.78%	0.3641
36	2.787	444.7	S <sub>6</sub> (M <sub>s</sub> :0) 90.79% T <sub>11</sub> (M <sub>s</sub> :-1) 4.37% T <sub>11</sub> (M <sub>s</sub> :1) 4.37%	0.0061
25	1.835	675.5	S <sub>4</sub> (M <sub>s</sub> :0) 99.48%	0.5474
24	1.661	746.3	S <sub>3</sub> (M <sub>s</sub> :0) 98.93%	0.0987
State	Major Contributions			
S <sub>3</sub>	HOMO-12 → LUMO (29.94%) HOMO-4 → LUMO+9 (16.15%)			
S <sub>4</sub>	HOMO → LUMO (74.87%)			
S <sub>6</sub>	HOMO-4 → LUMO+9 (32.27%) HOMO-12 → LUMO (26.94%)			
S <sub>9</sub>	HOMO → LUMO+2 (57.56%) HOMO → LUMO+4 (26.27%)			
S <sub>12</sub>	HOMO → LUMO+2 (35.63%) HOMO-1 → LUMO+9 (24.39%)			
S <sub>18</sub>	HOMO-7 → LUMO (29.81%) HOMO-3 → LUMO+2 (19.10%)			
T <sub>11</sub>	HOMO-1 → LUMO+9 (58.27%) [d-d]			

**Table 31**

Orbitals involved in the transitions of  $[\text{Co}(\text{DPC})_2]^-$  with 4 nitro groups





## I.2 Cyanide-DPC

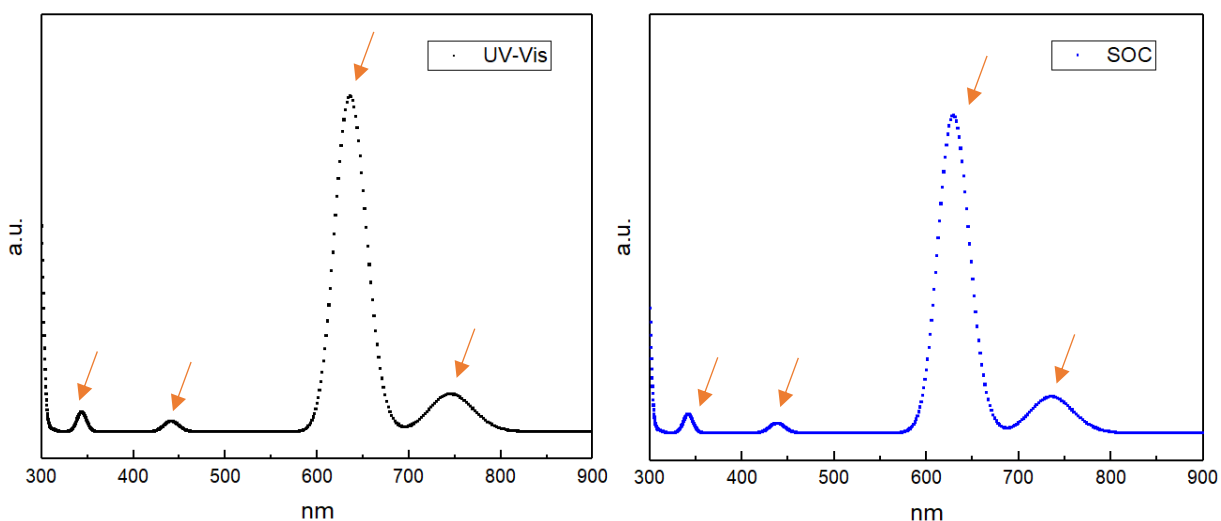


**Figure 2**

UV-Vis and SOC spectra of  $[\text{Co}(\text{DPC})_2]^-$  with 4 cyanide groups

There are four peaks observed in the UV-Vis spectra (Figure 2) at 342, 445, 636 and 747 nm.

**Table 4**

Description of the UV-Vis spectrum transitions of  $[\text{Co}(\text{DPC})_2]^-$  with 4 cyanide groups

State	Energy (eV)	Wavelength (nm)	Major Contributions	Oscillator Strength
9	3.610	343.4	HOMO-1 $\rightarrow$ LUMO+9 (47.47%) HOMO-1 $\rightarrow$ LUMO+10 (11.03%) [d-d]	0.0323
6	2.813	440.7	HOMO-12 $\rightarrow$ LUMO (30.23%) HOMO-4 $\rightarrow$ LUMO+9 (28.69%) [d-d]	0.0177
4	1.951	635.3	HOMO $\rightarrow$ LUMO (80.49%) [Ligand to metal or d-d]	0.5579
3	1.665	744.5	HOMO-12 $\rightarrow$ LUMO (37.77%) HOMO-4 $\rightarrow$ LUMO+9 (14.72%) [d-d]	0.0631

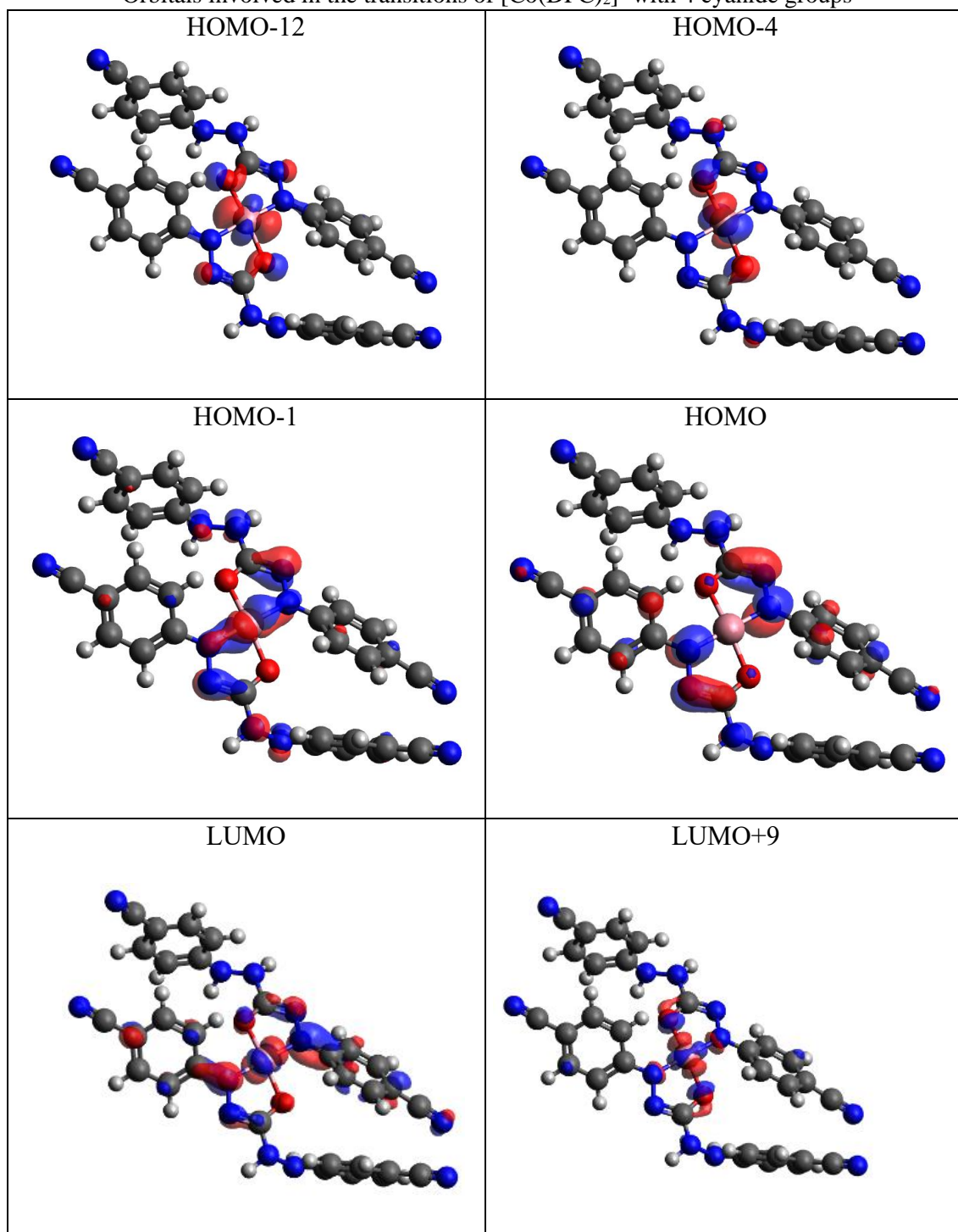
**Table 5**

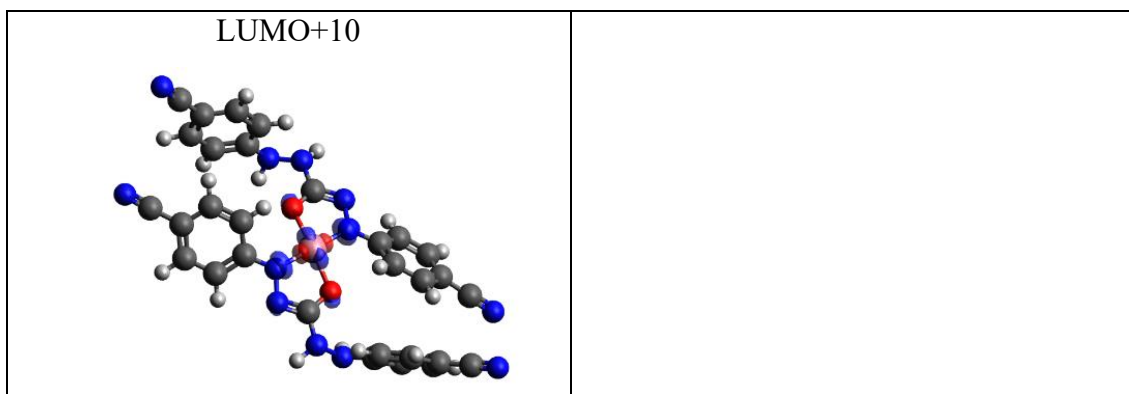
Description of the UV-Vis spectrum transitions of  $[\text{Co}(\text{DPC})_2]^-$  with 4 cyanide groups

State	Energy (eV)	Wavelength (nm)	Major Contributions	Oscillator Strength
51	3.632	341.3	$S_9 (M_s:0)$ 99.87%	0.0305
30	2.830	438.0	$S_6 (M_s:0)$ 87.56% $T_9 (M_s:-1)$ 5.94% $T_9 (M_s:1)$ 5.94%	0.0152
25	1.971	628.8	$S_4 (M_s:0)$ 97.31%	0.5205
24	1.687	734.7	$S_3 (M_s:0)$ 98.75%	0.0603
<b>State</b>	<b>Major Contributions</b>			
$S_3$	HOMO-12 $\rightarrow$ LUMO (37.77%) HOMO-4 $\rightarrow$ LUMO+9 (14.72%)			

S <sub>4</sub>	HOMO → LUMO (80.49%)
S <sub>6</sub>	HOMO-12 → LUMO (30.23%) HOMO-4 → LUMO+9 (28.69%)
S <sub>9</sub>	HOMO-1 → LUMO+9 (47.47%) HOMO-1 → LUMO+10 (11.03%)
T <sub>9</sub>	HOMO-1 → LUMO+9 (45.03%) HOMO-1 → LUMO+10 (11.23%) [d-d]

**Table 6**  
Orbitals involved in the transitions of [Co(DPC)<sub>2</sub>]<sup>-</sup> with 4 cyanide groups





### I.3 Methyl-DPC

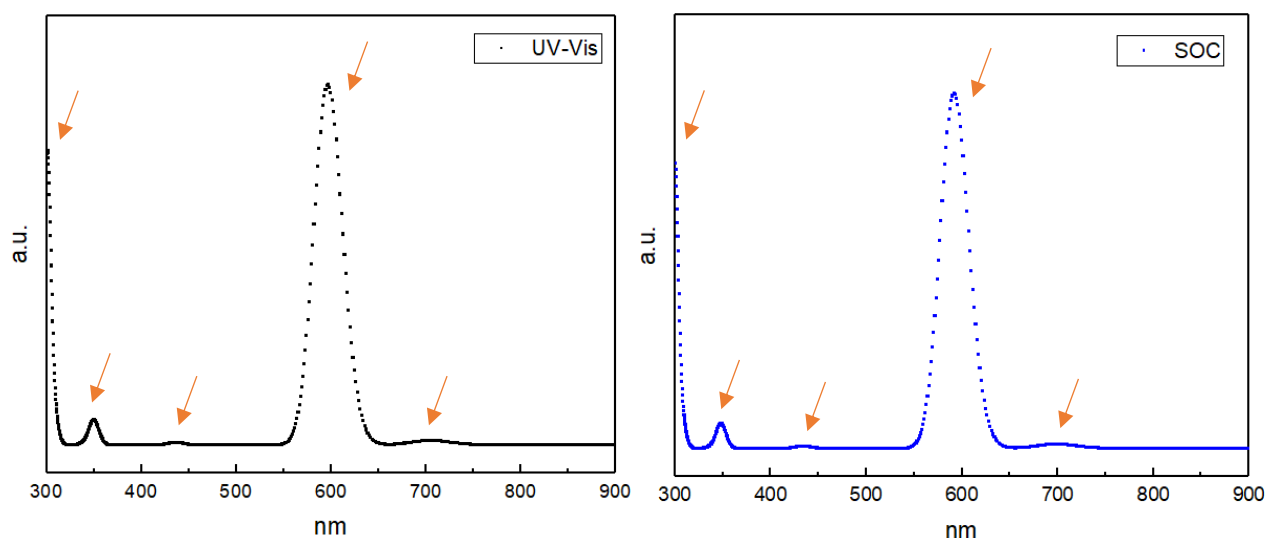


**Figure 3**

UV-Vis and SOC spectra of  $[\text{Co}(\text{DPC})_2]^-$  with 4 methyl groups

There are five peaks observed in the UV-Vis spectra (Figure 3) at 350, 436, 595 and 704 nm.

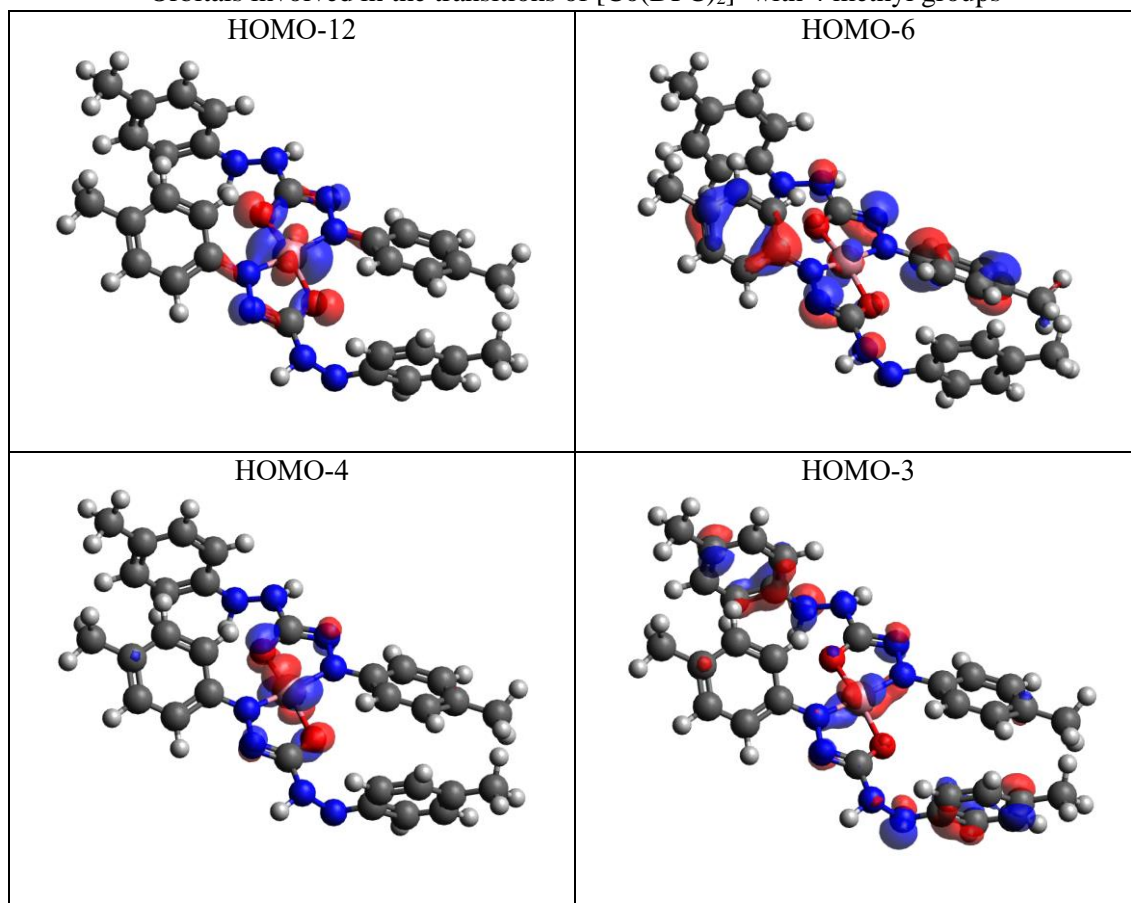
**Table 7**

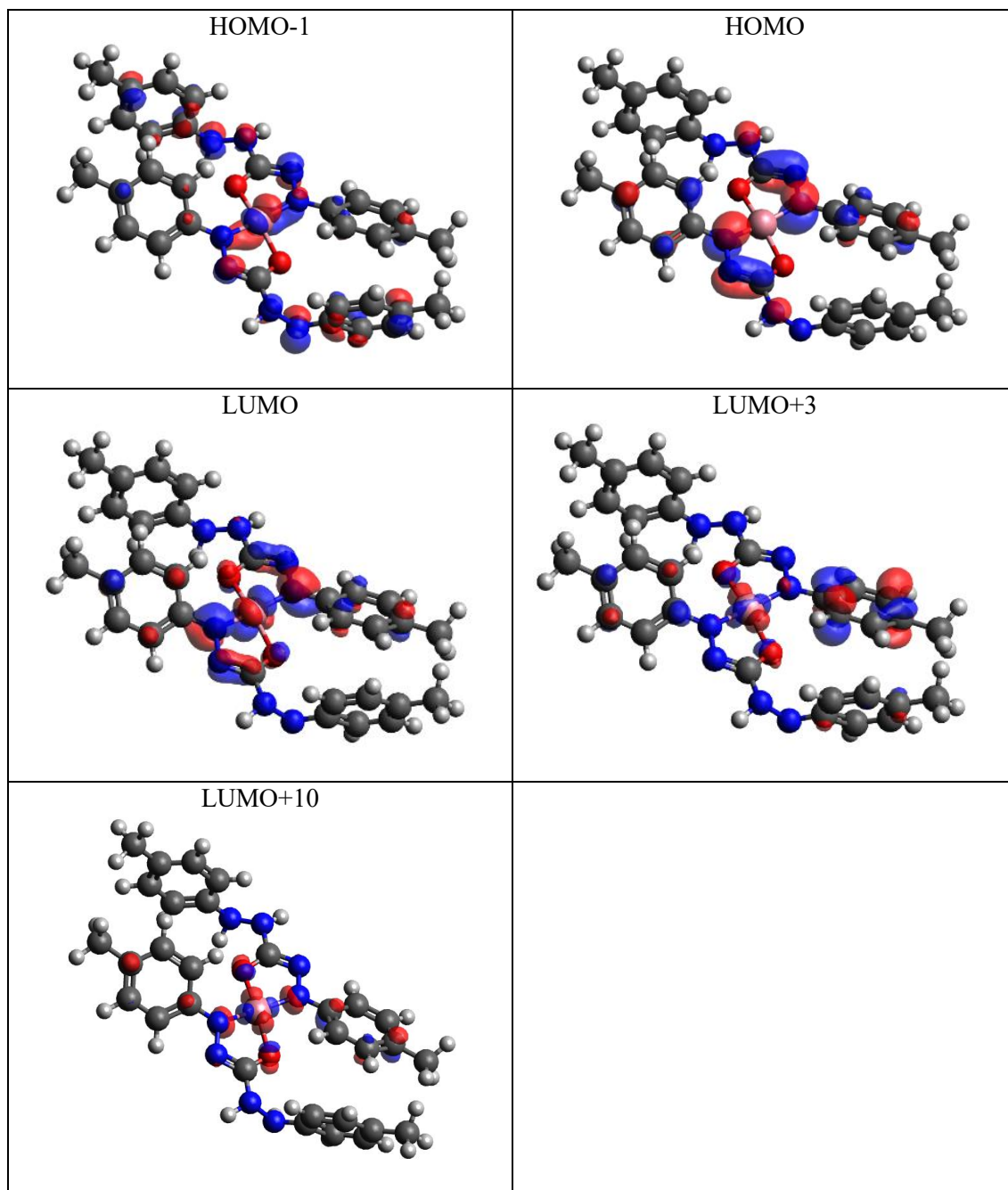
Description of the UV-Vis spectrum transitions of  $[\text{Co}(\text{DPC})_2]^-$  with 4 methyl groups

State	Energy (eV)	Wavelength (nm)	Major Contributions	Oscillator Strength
14	4.127	300.4	HOMO-6 $\rightarrow$ LUMO (82.59%) [d-d or ligand to metal]	0.4676
9	3.548	349.5	HOMO-1 $\rightarrow$ LUMO+3 (20.51%) HOMO-3 $\rightarrow$ LUMO+3 (12.58%) [d-d]	0.0407
6	2.842	436.3	HOMO-12 $\rightarrow$ LUMO (40.42%) HOMO-4 $\rightarrow$ LUMO+3 (14.62%) [d-d]	0.0042
4	2.080	596.2	HOMO $\rightarrow$ LUMO (89.23%) [Ligand to metal or d-d]	0.5814
3	1.760	704.6	HOMO-12 $\rightarrow$ LUMO (41.83%) HOMO-4 $\rightarrow$ LUMO+3 (11.28%) [d-d]	0.0073

**Table 8**Description of the UV-Vis spectrum transitions of  $[\text{Co}(\text{DPC})_2]^-$  with 4 methyl groups

State	Energy (eV)	Wavelength (nm)	Major Contributions	Oscillator Strength
77	4.144	299.1	$S_{14} (M_s:0)$ 99.96%	0.4545
45	3.565	347.7	$S_9 (M_s:0)$ 99.78%	0.0397
33	2.862	433.2	$S_6 (M_s:0)$ 96.44% $T_9 (M_s:-1)$ 1.66% $T_9 (M_s:1)$ 1.66%	0.0039
28	2.096	591.3	$S_4 (M_s:0)$ 99.79%	0.5666
24	1.775	698.4	$S_3 (M_s:0)$ 97.56%	0.0070
State	Major Contributions			
$S_3$	HOMO-12 $\rightarrow$ LUMO (41.83%) HOMO-4 $\rightarrow$ LUMO+3 (11.28%)			
$S_4$	HOMO $\rightarrow$ LUMO (89.23%)			
$S_6$	HOMO-12 $\rightarrow$ LUMO (40.42%) HOMO-4 $\rightarrow$ LUMO+3 (14.62%)			
$S_{14}$	HOMO-6 $\rightarrow$ LUMO (82.59%)			
$S_9$	HOMO-1 $\rightarrow$ LUMO+3 (20.51%) HOMO-3 $\rightarrow$ LUMO+3 (12.58%)			
$T_9$	HOMO-1 $\rightarrow$ LUMO+3 (19.14%) HOMO-1 $\rightarrow$ LUMO+10 (12.29%) [d-d]			

**Table 9**Orbitals involved in the transitions of  $[\text{Co}(\text{DPC})_2]^-$  with 4 methyl groups



The peaks at 299, 347, 433, 591 and 698 nm in the SOC spectrum are mainly the peaks at 300, 350, 436, 595 and 704 nm in the UV-Vis spectrum, due to the fact that the same transitions contribute in a similar percentage to these peaks. No significant differences are observed between both spectra, which mean that there are not important SOC effects in this case.

## I.4 Hydroxyl-DPC

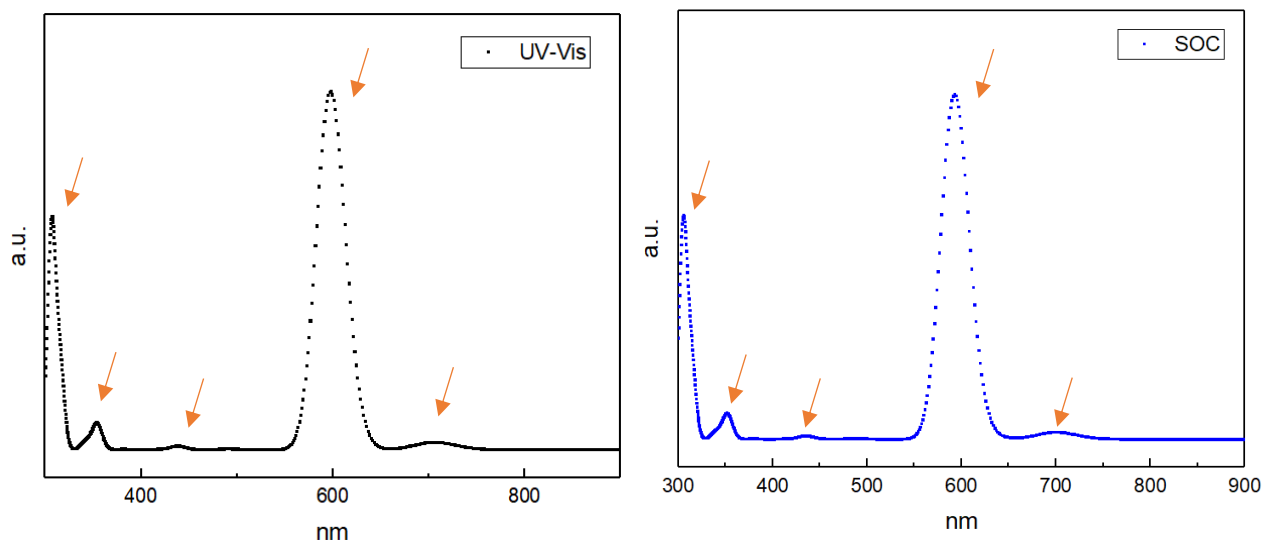


**Figure 4**

UV-Vis and SOC spectra of  $[\text{Co}(\text{DPC})_2]^-$  with 4 hydroxyl groups

There are five peaks observed in the UV-Vis spectra (Figure 4) at 355, 439, 492, 598 and 706 nm.

**Table 10**

Description of the UV-Vis spectrum transitions of  $[\text{Co}(\text{DPC})_2]^-$  with 4 hydroxyl groups

State	Energy (eV)	Wavelength (nm)	Major Contributions	Oscillator Strength
15	4.057	305.6	HOMO-6 $\rightarrow$ LUMO (19.01%) [d-d]	0.2270
9	3.507	353.6	HOMO-1 $\rightarrow$ LUMO+5 (29.25%) HOMO-3 $\rightarrow$ LUMO+5 (22.61%) [d-d]	0.0420
6	2.832	437.8	HOMO-12 $\rightarrow$ LUMO (37.07%) HOMO-4 $\rightarrow$ LUMO+5 (23.43%) [d-d]	0.0057
4	2.076	597.2	HOMO $\rightarrow$ LUMO (87.20%) [ligand to metal or d-d]	0.5696
3	1.757	705.7	HOMO-12 $\rightarrow$ LUMO (34.53%) HOMO-4 $\rightarrow$ LUMO+5 (20.20%) [d-d]	0.0118

**Table 11**

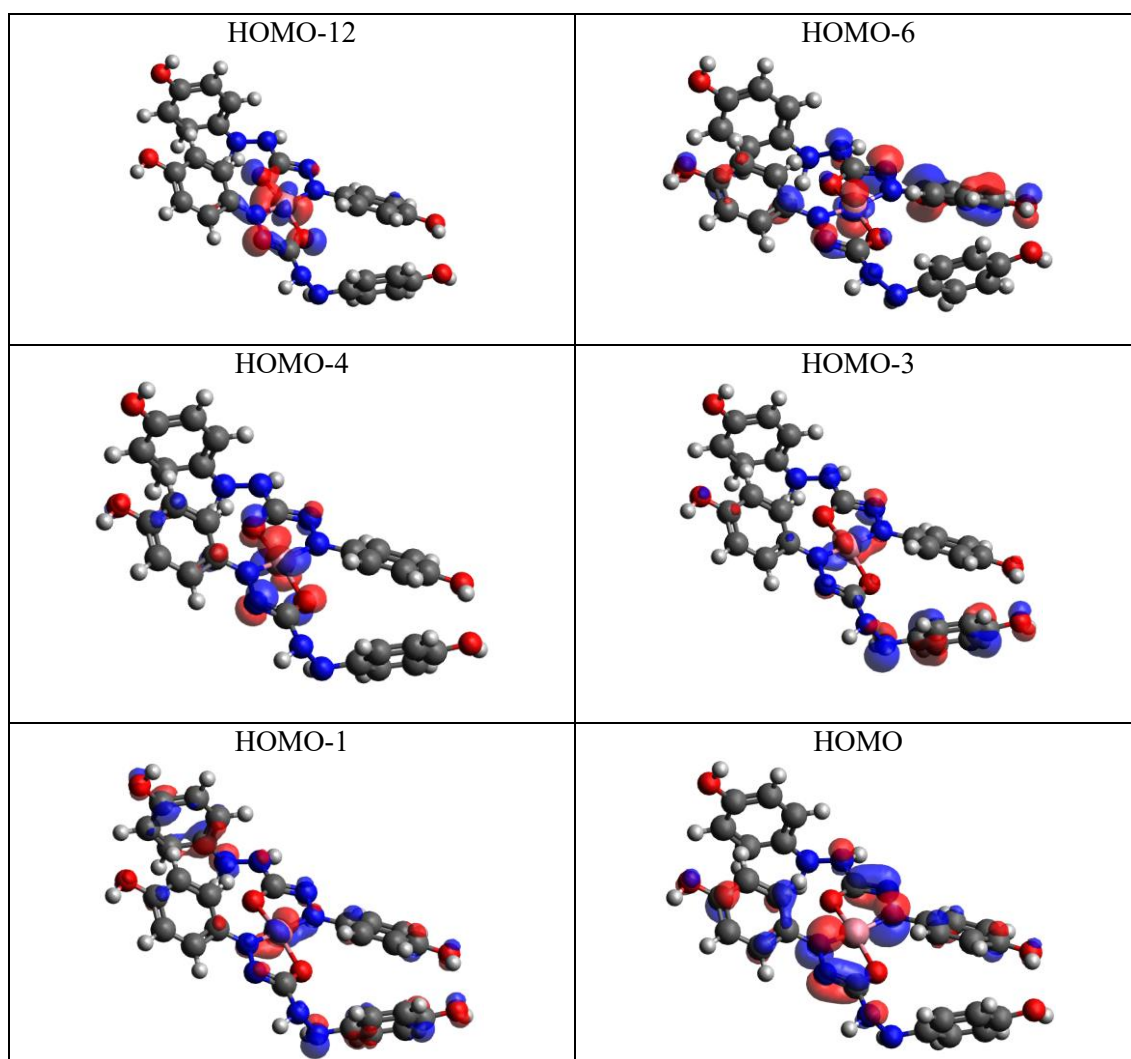
Description of the UV-Vis spectrum transitions of  $[\text{Co}(\text{DPC})_2]^-$  with 4 hydroxyl groups

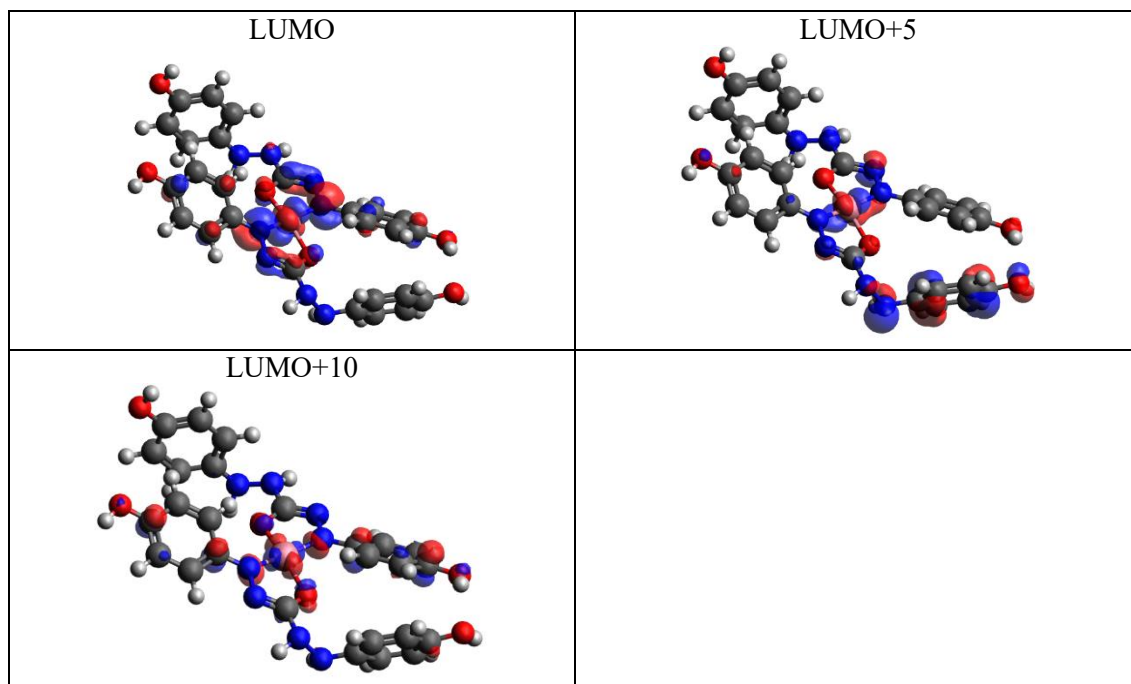
State	Energy (eV)	Wavelength (nm)	Major Contributions	Oscillator Strength
78	4.073	304.3	$S_{15} (M_s:0)$ 99.99%	0.2212
48	3.524	351.8	$S_9 (M_s:0)$ 99.87%	0.0410
33	2.851	434.8	$S_6 (M_s:0)$ 93.38%	0.0054
28	2.092	592.4	$S_4 (M_s:0)$ 99.81%	0.5561
24	1.771	700.00	$S_3 (M_s:0)$ 96.82% $T_8 (M_s:0)$ 2.47%	0.0112
<b>State</b>	<b>Major Contributions</b>			



S <sub>3</sub>	HOMO-12 → LUMO (34.53%) HOMO-4 → LUMO+5 (20.20%)
S <sub>4</sub>	HOMO → LUMO (87.20%)
S <sub>6</sub>	HOMO-12 → LUMO (37.07%) HOMO-4 → LUMO+5 (23.43%)
S <sub>9</sub>	HOMO-1 → LUMO+5 (29.25%) HOMO-3 → LUMO+5 (22.61%)
S <sub>15</sub>	HOMO-6 → LUMO (19.01%)
T <sub>8</sub>	HOMO-12 → LUMO+5 (39.84%) HOMO-12 → LUMO+10 (14.33%) [d-d]

**Table 12**  
Orbitals involved in the transitions of [Co(DPC)<sub>2</sub>]<sup>-</sup> with 4 hydroxyl groups





### I.5 Amine-DPC

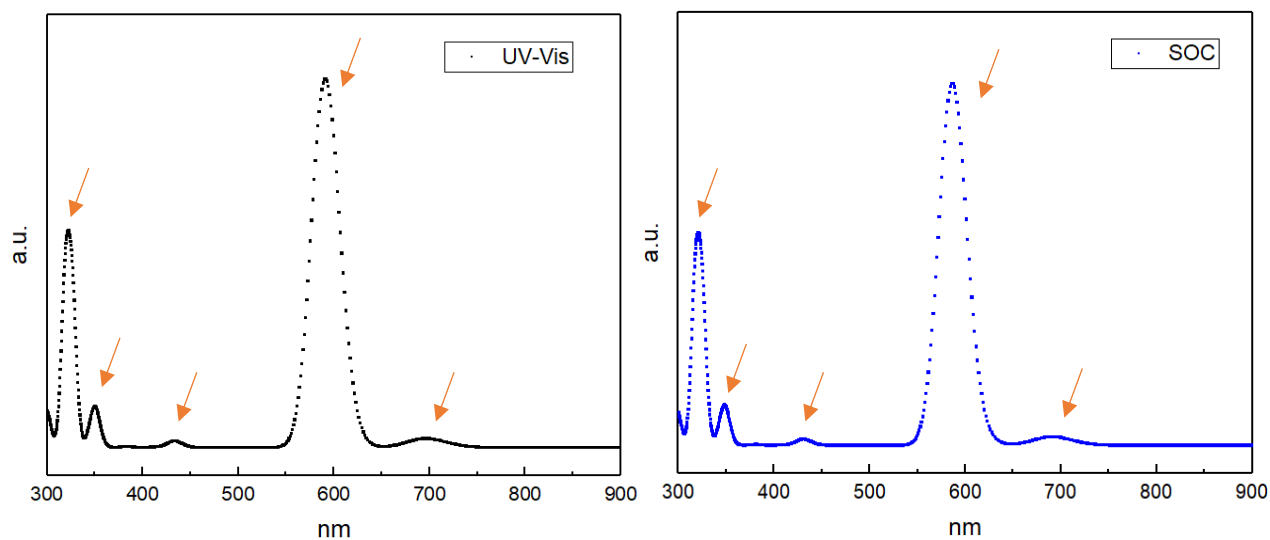


**Figure 5**  
UV-Vis and SOC spectra of  $[\text{Co}(\text{DPC})_2]^-$  with 4 amine groups

There are five peaks observed in the UV-Vis spectra (Figure 5) at 322, 350, 432, 589 and 693 nm.

**Table 13**  
Description of the UV-Vis spectrum transitions of  $[\text{Co}(\text{DPC})_2]^-$  with 4 amine groups

State	Energy (eV)	Wavelength (nm)	Major Contributions	Oscillator Strength
13	3.890	318.8	HOMO-4 $\rightarrow$ LUMO (61.78%) HOMO-2 $\rightarrow$ LUMO (27.27 %) [Ligand to metal]	0.2507
9	3.542	350.0	HOMO-1 $\rightarrow$ LUMO+5 (21.40 %) HOMO-3 $\rightarrow$ LUMO+5 (19.28%) [d-d]	0.0607

6	2.864	432.9	HOMO-12 → LUMO (42.78%) HOMO-5 → LUMO+5 (17.64%) [d-d]	0.0104
4	2.099	590.6	HOMO → LUMO (86.83%) [Ligand to metal or d-d]	0.5904
3	1.782	695.9	HOMO-12 → LUMO (40.69%) HOMO-5 → LUMO+5 (14.91%) [d-d]	0.0142

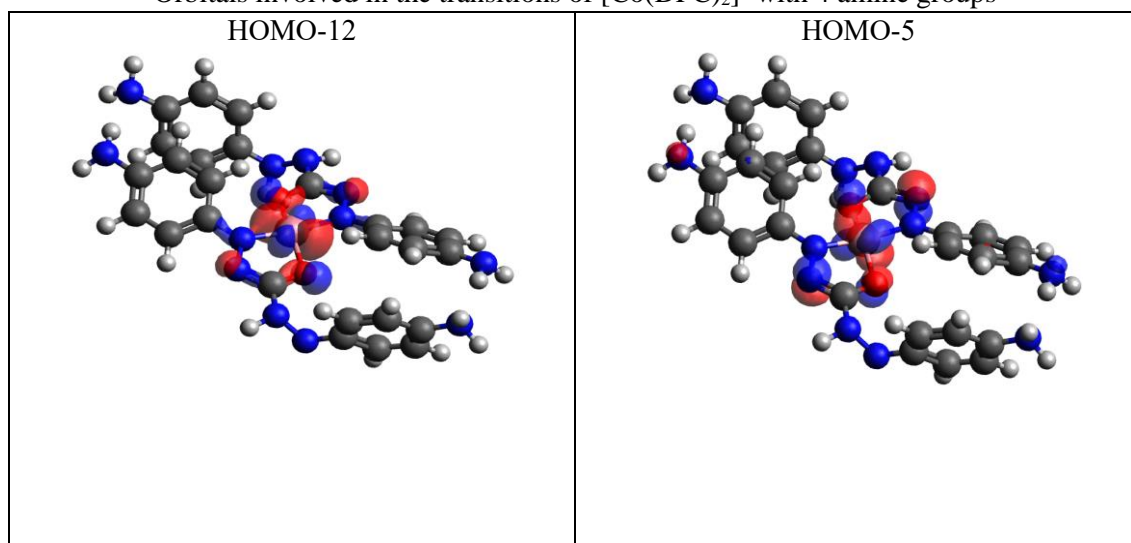
**Table 14**

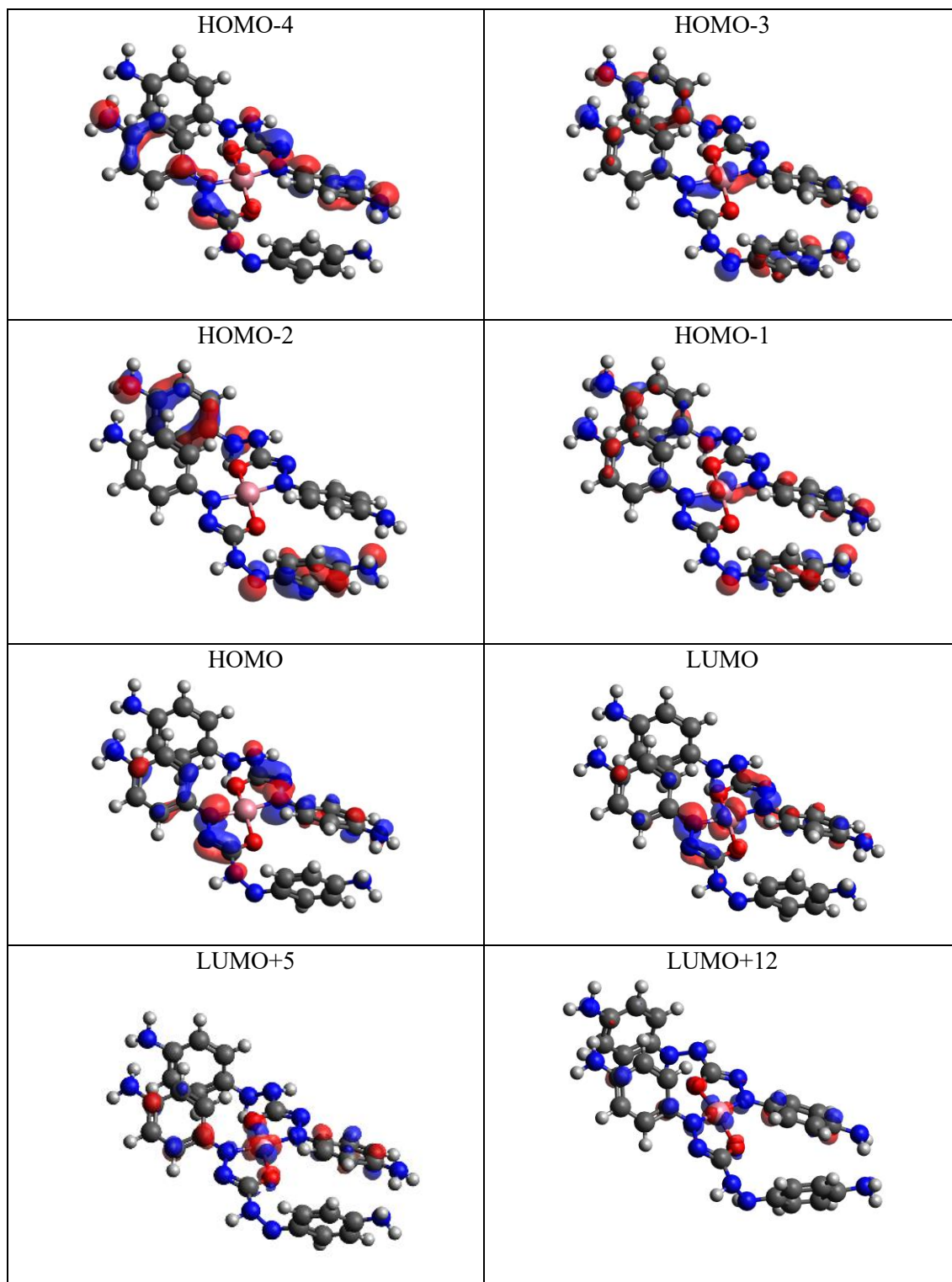
Description of the UV-Vis spectrum transitions of [Co(DPC)<sub>2</sub>]<sup>-</sup> with 4 amine groups

State	Energy (eV)	Wavelength (nm)	Major Contributions	Oscillator Strength
76	3.175	3.905	S <sub>13</sub> (M <sub>s</sub> :0) 99.42%	0.2448
57	3.558	348.4	S <sub>9</sub> (M <sub>s</sub> :0) 99.90%	0.0595
33	2.882	430.2	S <sub>6</sub> (M <sub>s</sub> :0) 98.64%	0.0099
28	2.115	586.2	S <sub>4</sub> (M <sub>s</sub> :0) 99.75%	0.5781
24	1.795	690.6	S <sub>3</sub> (M <sub>s</sub> :0) 97.13% T <sub>8</sub> (M <sub>s</sub> :0) 2.22%	0.0136
State	Major Contributions			
S <sub>3</sub>	HOMO-12 → LUMO (40.69%) HOMO-5 → LUMO+5 (14.91%)			
S <sub>4</sub>	HOMO → LUMO (86.83%)			
S <sub>6</sub>	HOMO-12 → LUMO (42.78%) HOMO-5 → LUMO+5 (17.64%)			
S <sub>9</sub>	HOMO-1 → LUMO+5 (21.40 %) HOMO-3 → LUMO+5 (19.28%)			
S <sub>13</sub>	HOMO-4 → LUMO (61.78%) HOMO-2 → LUMO (27.27 %)			
T <sub>8</sub>	HOMO-12 → LUMO+5 (42.09%) HOMO-12 → LUMO+12 (13.95%) [d-d]			

**Table 15**

Orbitals involved in the transitions of [Co(DPC)<sub>2</sub>]<sup>-</sup> with 4 amine groups





## II. Computational study of $[\text{Co}(\text{DPC})_2]^-$ with different solvents

In all of the cases the complex was simulated and one optimized structure was obtained, considering the singlet multiplicity as the ground state. The resulting complex in all cases shows a square plane geometry. With the optimized structure, the corresponding UV-Vis spectra was calculated, as well as the SOC spectrum. Also, the transitions of the spectra (between 300 and 850 nm) will be described in detail and the orbitals involved in these transitions will be shown as well.

## II.2 Water

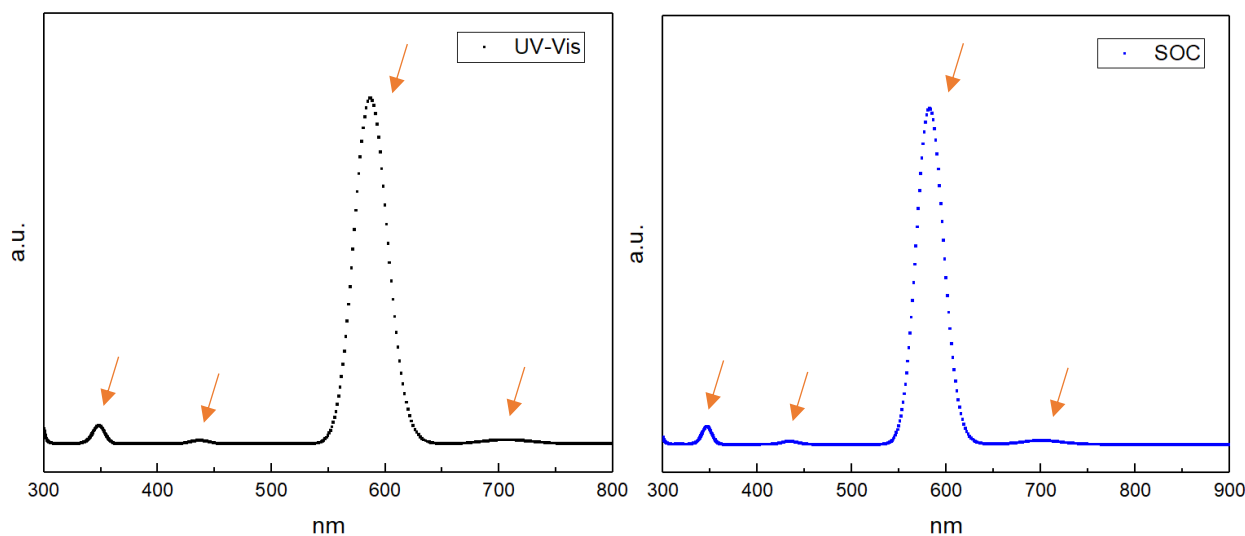


**Figure 6**  
UV-Vis and SOC spectra of  $[\text{Co}(\text{DPC})_2]^-$  in water

There are four peaks observed in the UV-Vis spectra (Figure 6) at 347, 436, 585 and 705 nm.

**Table 16**  
Description of the UV-Vis spectrum transitions of  $[\text{Co}(\text{DPC})_2]^-$  in water

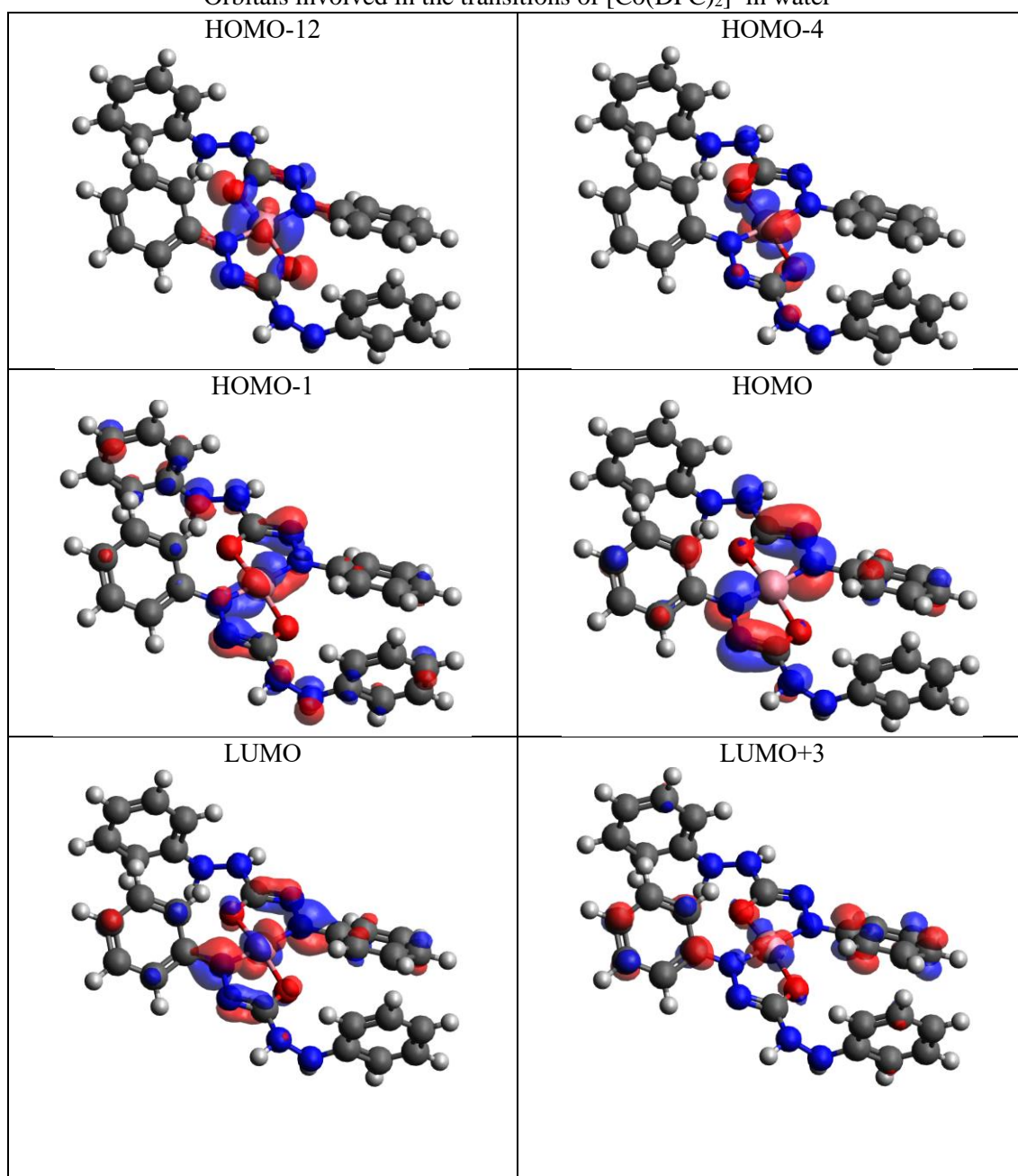
State	Energy (eV)	Wavelength (nm)	Major Contributions	Oscillator Strength
9	3.564	347.9	HOMO-1 $\rightarrow$ LUMO+3 (29.39%) HOMO-1 $\rightarrow$ LUMO+10 (14.24%) [d-d]	0.0294
6	2.840	436.5	HOMO-12 $\rightarrow$ LUMO (41.08%) HOMO-4 $\rightarrow$ LUMO+3 (18.20%) [d-d]	0.0054
4	2.144	586.4	HOMO $\rightarrow$ LUMO (90.28%) [Ligand to metal or d-d]	0.5562
3	1.756	706.0	HOMO-12 $\rightarrow$ LUMO (41.58%) HOMO-4 $\rightarrow$ LUMO+3 (14.72%) [d-d]	0.0066

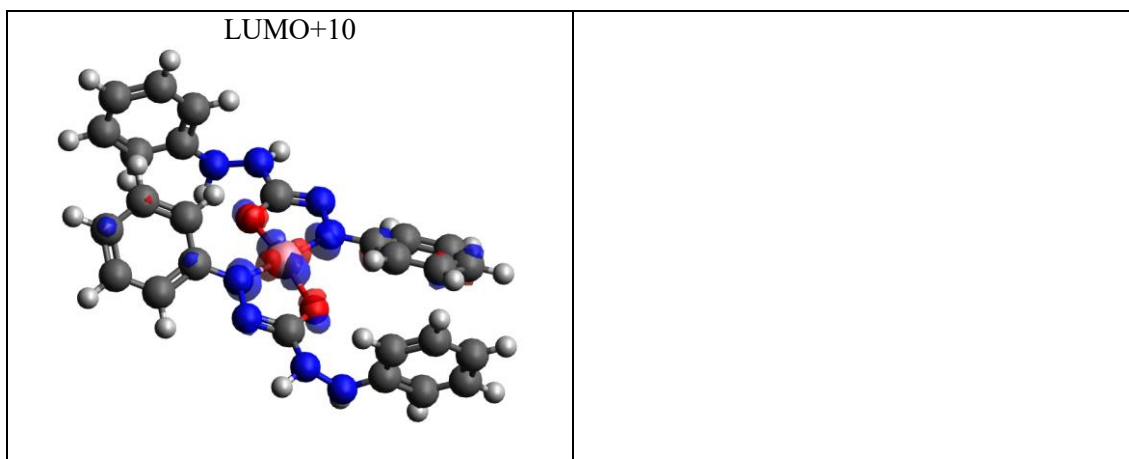
**Table 17**  
Description of the UV-Vis spectrum transitions of  $[\text{Co}(\text{DPC})_2]^-$  in water

State	Energy (eV)	Wavelength (nm)	Major Contributions	Oscillator Strength
42	3.582	346.1	$S_9 (M_s:0)$ 98.54%	0.0286
33	2.862	433.2	$S_6 (M_s:0)$ 93.72% $T_9 (M_s:-1)$ 2.99% $T_9 (M_s:1)$ 2.99%	0.0048
28	2.131	581.8	$S_4 (M_s:0)$ 99.88%	0.5432
24	1.771	699.8	$S_3 (M_s:0)$ 97.50% $T_8 (M_s:0)$ 1.86%	0.0063
<b>State</b>	<b>Major Contributions</b>			
$S_3$	HOMO-12 $\rightarrow$ LUMO (41.58%)			

	HOMO-4 → LUMO+3 (14.72%)
S <sub>4</sub>	HOMO → LUMO (90.28%)
S <sub>6</sub>	HOMO-12 → LUMO (41.08%) HOMO-4 → LUMO+3 (18.20%)
S <sub>9</sub>	HOMO-1 → LUMO+3 (29.39%) HOMO-1 → LUMO+10 (14.24%)
T <sub>8</sub>	HOMO-12 → LUMO+3 (28.75%) HOMO-12 → LUMO+10 (22.18%) [d-d]
T <sub>9</sub>	HOMO-1 → LUMO+3 (27.51%) HOMO-1 → LUMO+10 (15.39%) [d-d]

**Table 18**  
Orbitals involved in the transitions of [Co(DPC)<sub>2</sub>]<sup>-</sup> in water





## II.2 Methanol

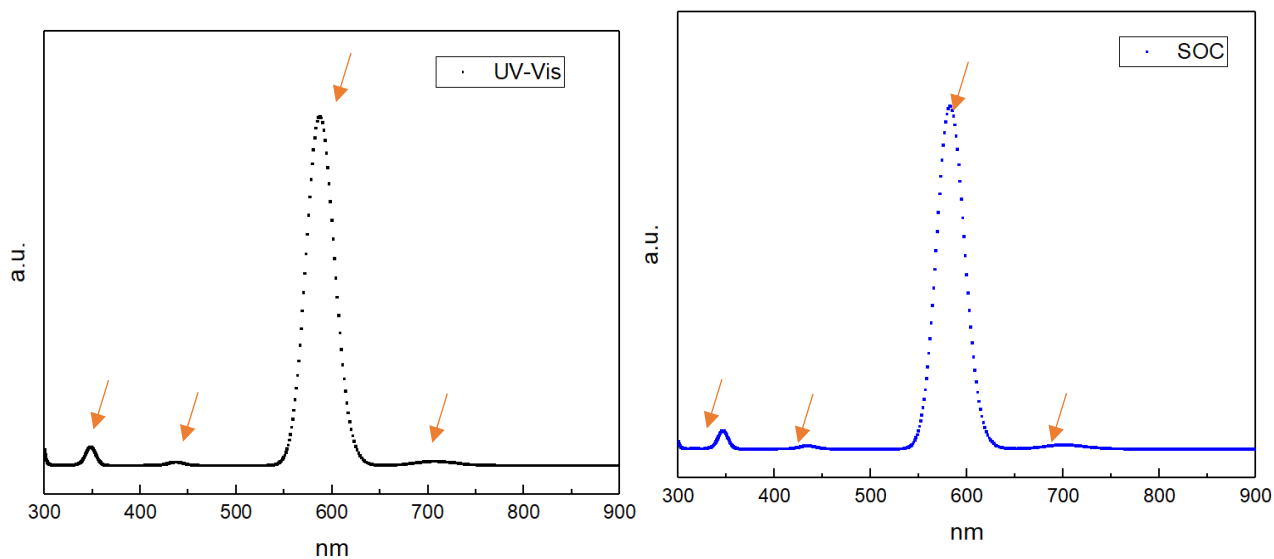


**Figure 7**  
UV-Vis and SOC spectra of  $[\text{Co}(\text{DPC})_2]^-$  in methanol

There are four peaks observed in the UV-Vis spectra (Figure 7) at 347, 436, 585 and 705 nm.

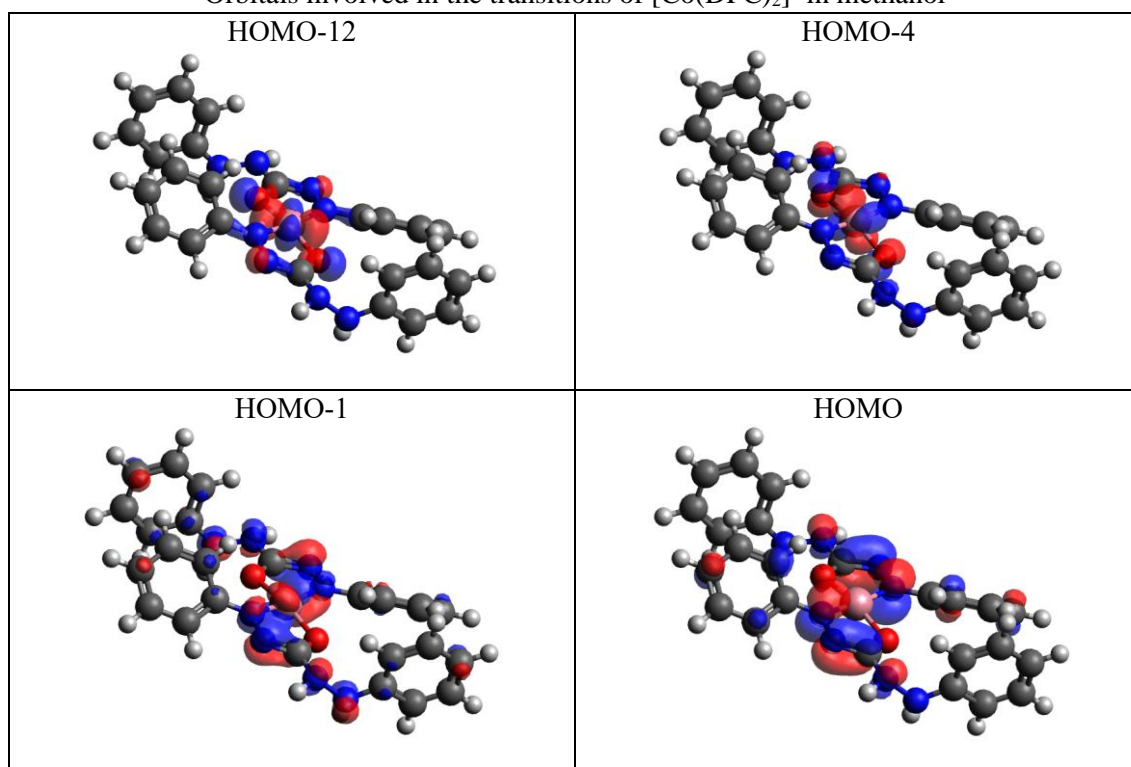
**Table 19**  
Description of the UV-Vis spectrum transitions of  $[\text{Co}(\text{DPC})_2]^-$  in water

State	Energy (eV)	Wavelength (nm)	Major Contributions	Oscillator Strength
9	3.564	347.8	HOMO-1 $\rightarrow$ LUMO+3 (31.84%) HOMO-1 $\rightarrow$ LUMO+10 (15.79%) [d-d]	0.0294
6	2.840	436.6	HOMO-12 $\rightarrow$ LUMO (40.95%) HOMO-4 $\rightarrow$ LUMO+3 (17.89%) [d-d]	0.0053
4	2.113	586.7	HOMO $\rightarrow$ LUMO (90.32%) [Ligand to metal or d-d]	0.5564
3	1.755	706.4	HOMO-12 $\rightarrow$ LUMO (41.63%) HOMO-4 $\rightarrow$ LUMO+3 (14.38%) [d-d]	0.0065

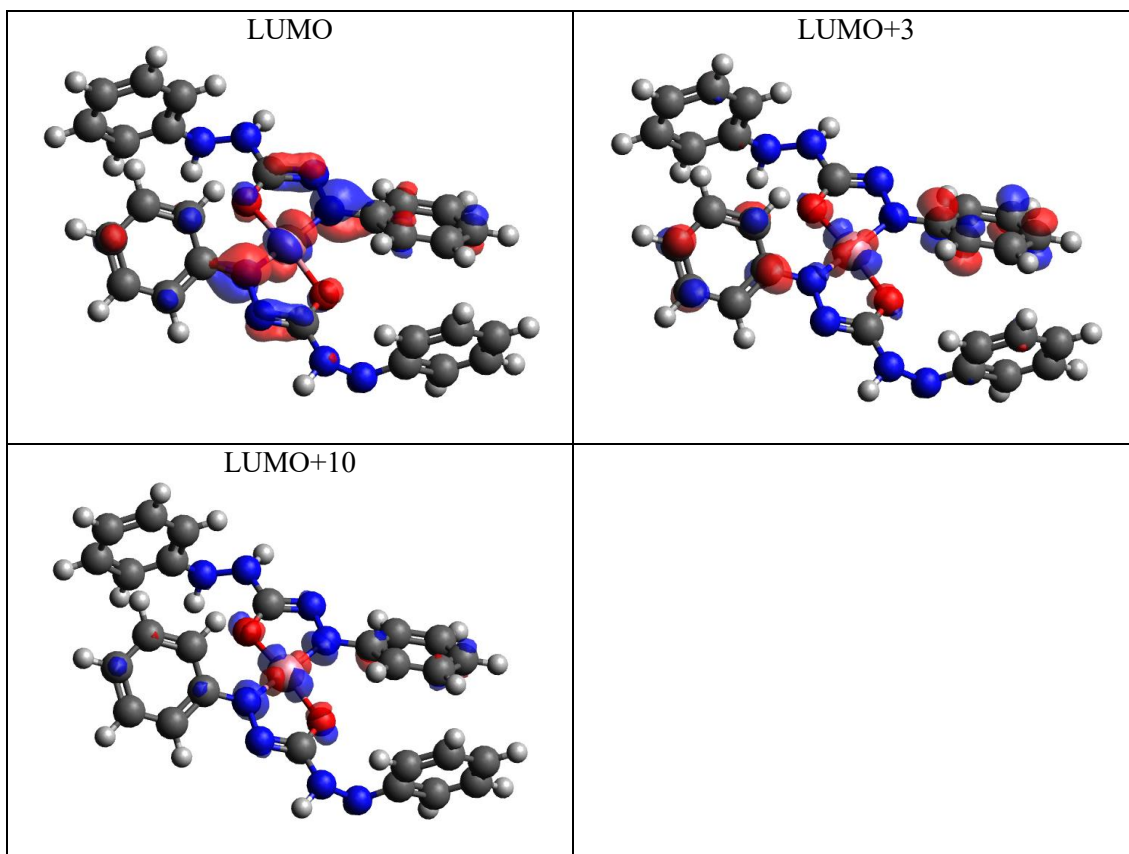
**Table 20**  
Description of the UV-Vis spectrum transitions of  $[\text{Co}(\text{DPC})_2]^-$  in methanol

State	Energy (eV)	Wavelength (nm)	Major Contributions	Oscillator Strength
42	3.582	346.1	S <sub>9</sub> (M <sub>s</sub> :0) 99.00%	0.0287
33	2.861	433.3	S <sub>6</sub> (M <sub>s</sub> :0) 93.44% T <sub>9</sub> (M <sub>s</sub> :-1) 3.12% T <sub>9</sub> (M <sub>s</sub> :1) 3.12%	0.0047
28	2.130	582.0	S <sub>4</sub> (M <sub>s</sub> :0) 99.88%	0.5431
24	1.770	700.2	S <sub>3</sub> (M <sub>s</sub> :0) 97.53% T <sub>8</sub> (M <sub>s</sub> :0) 1.83%	0.0062
State	Major Contributions			
S <sub>3</sub>	HOMO-12 → LUMO (41.63%) HOMO-4 → LUMO+3 (14.38%)			
S <sub>4</sub>	HOMO → LUMO (90.32%)			
S <sub>6</sub>	HOMO-12 → LUMO (40.95%) HOMO-4 → LUMO+3 (17.89%)			
S <sub>9</sub>	HOMO-1 → LUMO+3 (31.84%) HOMO-1 → LUMO+10 (15.79%)			
T <sub>8</sub>	HOMO-12 → LUMO+3 (28.29%) HOMO-12 → LUMO+10 (22.30%) [d-d]			
T <sub>9</sub>	HOMO-1 → LUMO+3 (29.80%) HOMO-1 → LUMO+10 (17.04%) [d-d]			

**Table 21**  
Orbitals involved in the transitions of  $[\text{Co}(\text{DPC})_2]^-$  in methanol







II.3 Hexane

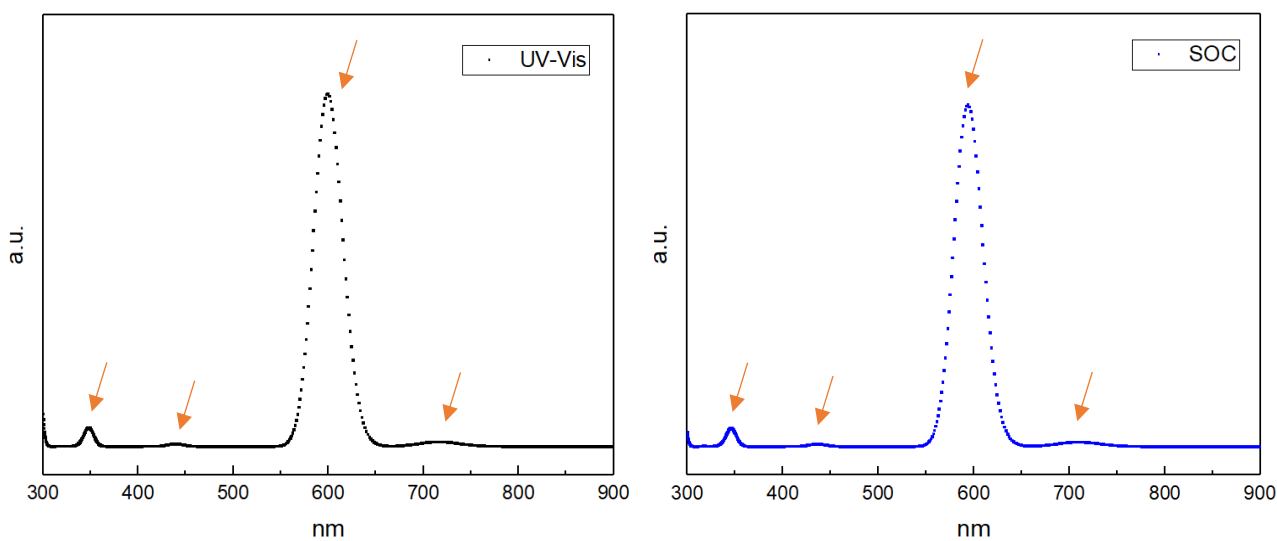


**Figure 8**  
UV-Vis and SOC spectra of  $[\text{Co}(\text{DPC})_2]^-$  in hexane

There are four peaks observed in the UV-Vis spectra (Figure 8) at 347, 436, 598 and 715 nm.

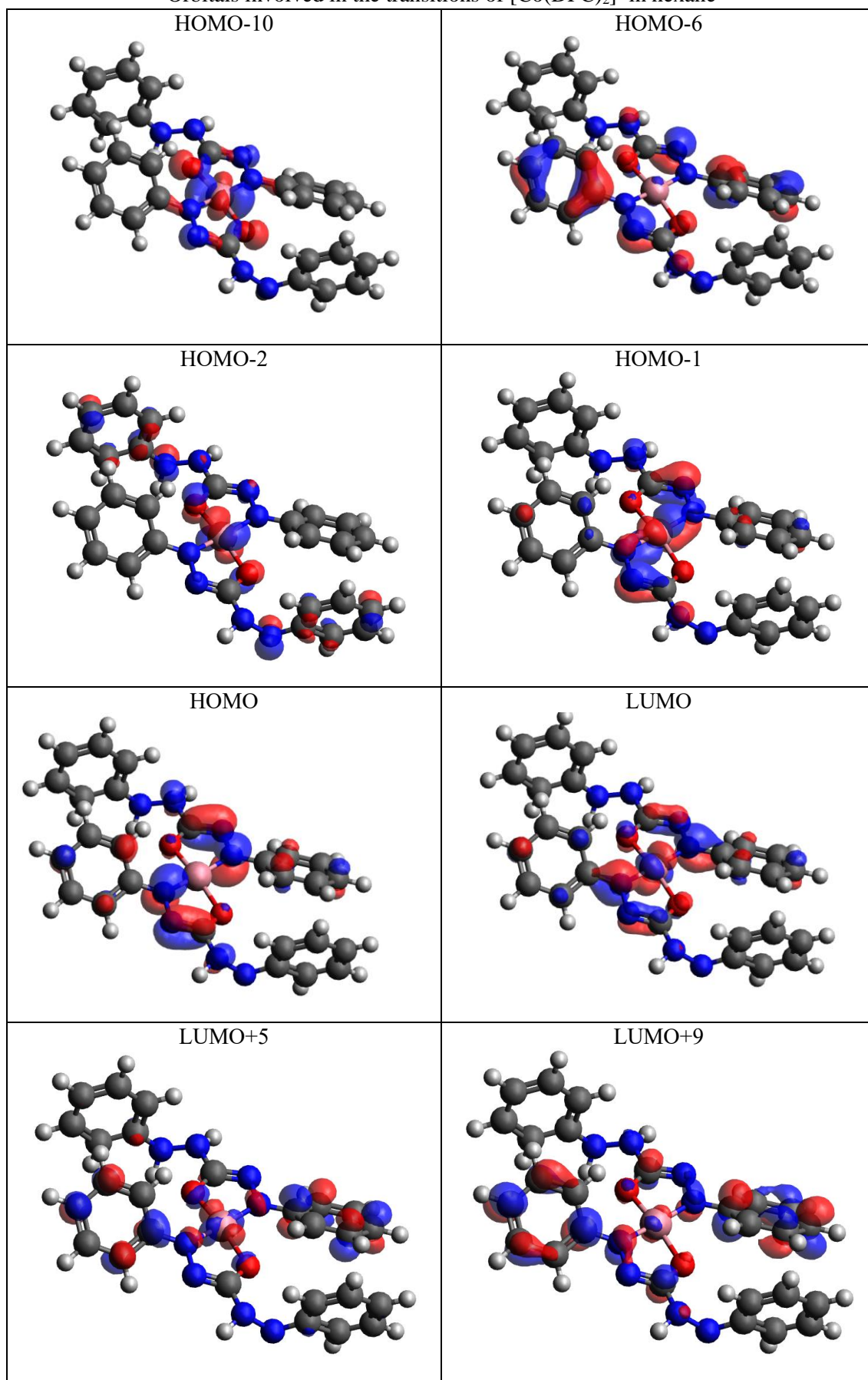
**Table 22**Description of the UV-Vis spectrum transitions of [Co(DPC)<sub>2</sub>]<sup>-</sup> in hexane

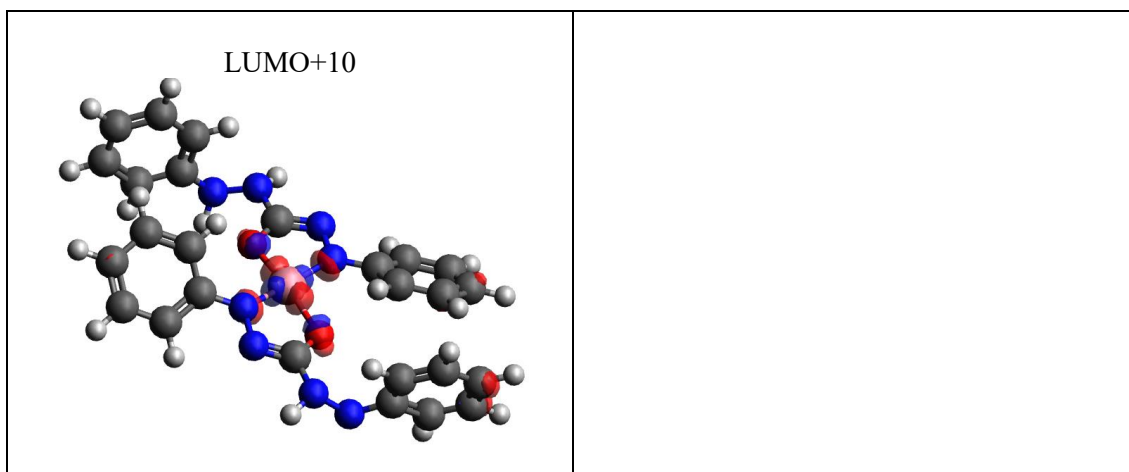
State	Energy (eV)	Wavelength (nm)	Major Contributions	Oscillator Strength
9	3.565	347.8	HOMO-1 → LUMO+5 (41.81%) HOMO-1 → LUMO+10 (18.35%) [d-d]	0.0301
6	2.825	438.8	HOMO-10 → LUMO (38.46%) HOMO-2 → LUMO+5 (13.28%) [d-d]	0.0042
4	2.070	599.0	HOMO → LUMO (90.59%) [Ligand to metal or d-d]	0.5649
3	1.732	715.8	HOMO-10 → LUMO (41.77%) HOMO-2 → LUMO+5 (10.21%) [d-d]	0.0074

**Table 23**Description of the UV-Vis spectrum transitions of [Co(DPC)<sub>2</sub>]<sup>-</sup> in hexane

State	Energy (eV)	Wavelength (nm)	Major Contributions	Oscillator Strength
42	3.584	345.8	S <sub>9</sub> (M <sub>s</sub> :0) 97.43% T <sub>12</sub> (M <sub>s</sub> :-1) 1.21% T <sub>12</sub> (M <sub>s</sub> :1) 1.21%	0.0284
33	2.851	434.9	S <sub>6</sub> (M <sub>s</sub> :0) 86.16% T <sub>9</sub> (M <sub>s</sub> :-1) 6.59% T <sub>9</sub> (M <sub>s</sub> :1) 6.59%	0.0033
28	2.809	593.5	S <sub>4</sub> (M <sub>s</sub> :0) 99.76%	0.5457
24	1.750	708.4	S <sub>3</sub> (M <sub>s</sub> :0) 97.98% T <sub>8</sub> (M <sub>s</sub> :0) 1.41%	0.0071
State	Major Contributions			
S <sub>3</sub>	HOMO-10 → LUMO (41.77%) HOMO-2 → LUMO+5 (10.21%)			
S <sub>4</sub>	HOMO → LUMO (90.59%)			
S <sub>6</sub>	HOMO-10 → LUMO (38.46%) HOMO-2 → LUMO+5 (13.28%)			
S <sub>9</sub>	HOMO-1 → LUMO+5 (41.81%) HOMO-1 → LUMO+10 (18.35%)			
T <sub>8</sub>	HOMO-10 → LUMO+5 (29.06%) HOMO-10 → LUMO+10 (18.21%)			
T <sub>9</sub>	HOMO-1 → LUMO+5 (39.61%) HOMO-1 → LUMO+10 (19.26%) [d-d]			
T <sub>12</sub>	HOMO-6 → LUMO (51.36%) [Ligand to metal or d-d] HOMO → LUMO+9 (19.61%) [Ligand to ligand or d-d]			

**Table 24**  
Orbitals involved in the transitions of  $[\text{Co}(\text{DPC})_2]^-$  in hexane





### III. Computational study of *trans,trans,trans*-[Pt(N<sub>3</sub>)<sub>2</sub>(OH)<sub>2</sub>(Py)(MA)]

The complex [Pt(N<sub>3</sub>)<sub>2</sub>(OH)<sub>2</sub>(Py)(MA)] was simulated and one optimized structure was obtained, considering the singlet multiplicity as the ground state. In the complex, Platinum has an oxidation state of 4+, the azide ligand has a charge -1 as well as the hydroxyl groups, and the pyridine as well as the methylamine don't have charge. The complex has an octahedral geometry. In the complex, the pyridine is bonded to the complex by the nitrogen, as well as the methylamine. With the optimized structure, the corresponding UV-Vis spectra was calculated, as well as the SOC spectrum. The optimized structures as well as their corresponding spectra are shown in Figures 9-10. Also, the transitions of the spectra (between 300 and 850 nm) will be described in detail and the orbitals involved in these transitions will be shown as well (Tables 25-27).

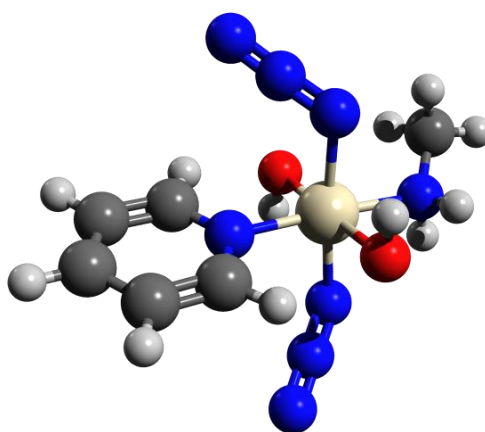


**Figure 9**  
Optimized structure of [Pt(N<sub>3</sub>)<sub>2</sub>(OH)<sub>2</sub>(Py)(MA)]

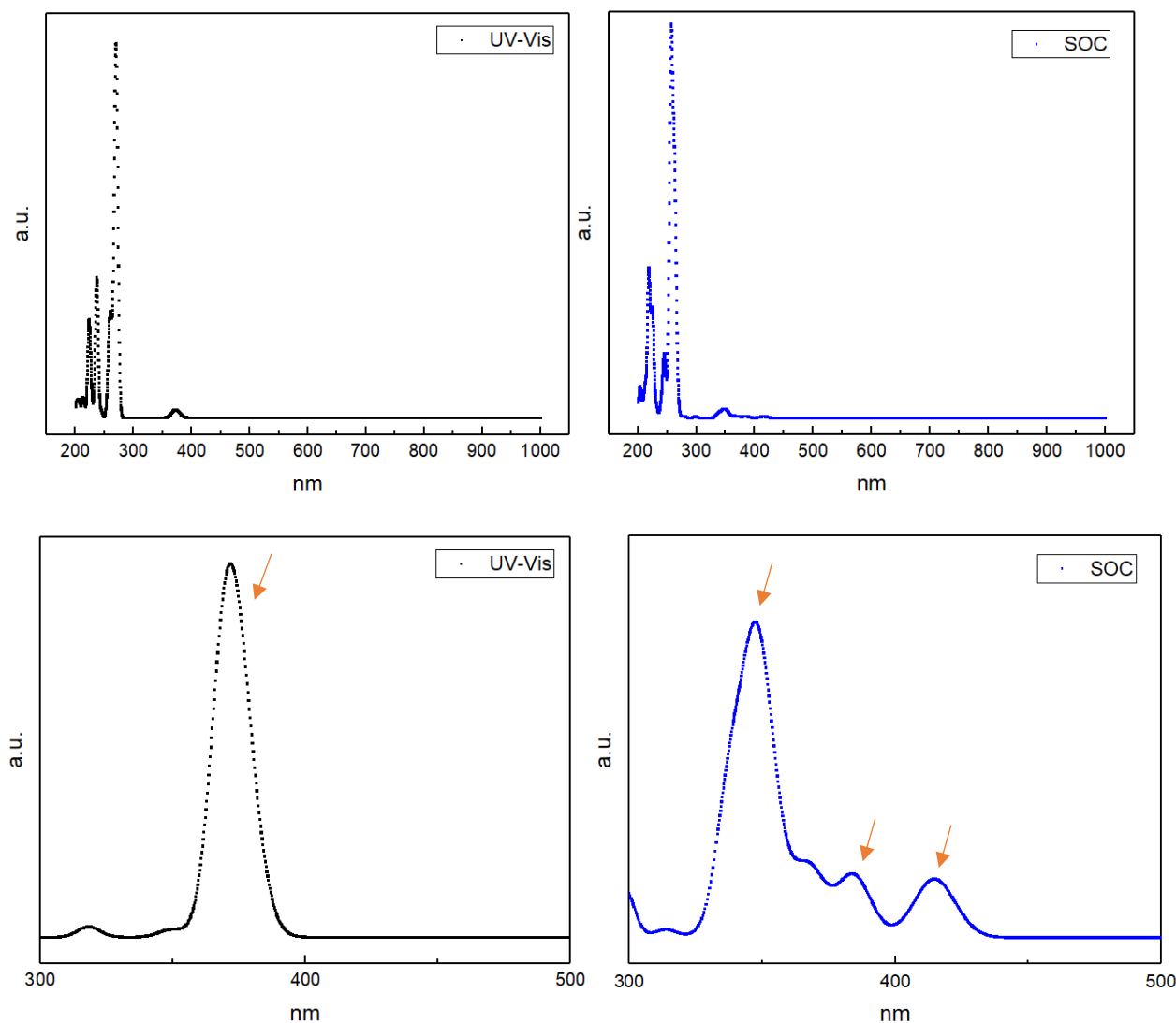


**Figure 10**

UV-Vis and SOC spectra of  $[\text{Pt}(\text{N}_3)_2(\text{OH})_2(\text{Py})(\text{MA})]$

There is 1 peak in the UV-Vis spectrum (Figure 10) at 371 nm. The fact that there is 1 peak suggests that  $\text{Pt}^{3+}$  ( $d^6$  species) favors high spin (1 transition expected).

**Table 25**

Description of the UV-Vis spectrum transitions of  $[\text{Pt}(\text{N}_3)_2(\text{OH})_2(\text{Py})(\text{MA})]$

State	Energy (eV)	Wavelength (nm)	Major Contributions	Oscillator Strength
2	3.351	370	HOMO-1 $\rightarrow$ LUMO (73.65%) HOMO $\rightarrow$ LUMO (14.58%) [d-d]	0.00511

**Table 26**

Description of the SOC spectrum transitions of  $[\text{Pt}(\text{N}_3)_2(\text{OH})_2(\text{Py})(\text{MA})]$

State	Energy (eV)	Wavelength (nm)	Major Contributions	Oscillator Strength
13	3.558	348.5	$S_1 (M_s:0)$ 59.64%	0.00285
6	3.226	384.2	$T_2 (M_s:0)$ 40.15%	0.00104

			T <sub>1</sub> (M <sub>s</sub> :-1) 15.26% T <sub>1</sub> (M <sub>s</sub> :-1) 15.26%	
2	2.986	415.1	T <sub>2</sub> (M <sub>s</sub> :0) 27.18% T <sub>1</sub> (M <sub>s</sub> :-1) 26.78% T <sub>1</sub> (M <sub>s</sub> :1) 26.78%	0.00089
<b>State</b>	<b>Major Contributions</b>			
S <sub>1</sub>	HOMO → LUMO (74.42%) HOMO-1 → LUMO (15.14%)			
T <sub>1</sub>	HOMO → LUMO (84.47%) [d-d]			
T <sub>2</sub>	HOMO-1 → LUMO (84.10%) [d-d]			

**Table 27**  
Orbitals involved in the transitions of [Pt(N<sub>3</sub>)<sub>2</sub>(OH)<sub>2</sub>(Py)(MA)]

